NASA
CR
820
v.13
c.1

NASA CONTRACTOR REPORT

NASA CR-832

N.A.S.A. C.R.
0099737
TECH LIBRARY KAFB, NM
LOAN COPY: RETURN TO
AFWL (WLIL-2)
KIRTLAND AFB, N MEX

ANALYSIS AND DESIGN OF SPACE VEHICLE FLIGHT CONTROL SYSTEMS

VOLUME XIII - ADAPTIVE CONTROL

by Arthur L. Greensite

Prepared by
GENERAL DYNAMICS CORPORATION
San Diego, Calif.
for George C. Marshall Space Flight Center

NATIONAL AERONAUTICS AND SPACE ADMINISTRATION • WASHINGTON, D. C. • AUGUST 1967

TECH LIBRARY KAFB, NM

0099737

NASA CR-832

ANALYSIS AND DESIGN OF SPACE VEHICLE FLIGHT CONTROL SYSTEMS

VOLUME XIII - ADAPTIVE CONTROL

By Arthur L. Greensite

Distribution of this report is provided in the interest of information exchange. Responsibility for the contents resides in the author or organization that prepared it.

Issued by Originator as Report No. GDC-DDE67-002

Prepared under Contract No. NAS 8-11494 by
GENERAL DYNAMICS CONVAIR
A DIVISION OF GENERAL DYNAMICS CORPORATION
San Diego, Calif.

for George C. Marshall Space Flight Center

NATIONAL AERONAUTICS AND SPACE ADMINISTRATION

For sale by the Clearinghouse for Federal Scientific and Technical Information
Springfield, Virginia 22151 – CFSTI price $3.00

FOREWORD

This report was prepared under NASA Contract NAS 8-11494 and is one of a series intended to illustrate methods used for the design and analysis of space vehicle flight control systems. Below is a complete list of the reports in the series:

Volume I	Short Period Dynamics
Volume II	Trajectory Equations
Volume III	Linear Systems
Volume IV	Nonlinear Systems
Volume V	Sensitivity Theory
Volume VI	Stochastic Effects
Volume VII	Attitude Control During Launch
Volume VIII	Rendezvous and Docking
Volume IX	Optimization Methods
Volume X	Man in the Loop
Volume XI	Component Dynamics
Volume XII	Attitude Control in Space
Volume XIII	Adaptive Control
Volume XIV	Load Relief
Volume XV	Elastic Body Equations
Volume XVI	Abort

The work was conducted under the direction of Clyde D. Baker, Billy G. Davis and Fred W. Swift, Aero-Astro Dynamics Laboratory, George C. Marshall Space Flight Center. The General Dynamics Convair program was conducted under the direction of Arthur L. Greensite.

TABLE OF CONTENTS

Section		Page
1	STATEMENT OF THE PROBLEM	1
2	STATE OF THE ART	3
3	RECOMMENDED PROCEDURES	5
	3.1 Model Reference Techniques	5
	3.1.1 Whitaker (MIT) System	5
	3.1.2 Tutt and Waymeyer System	12
	3.2 Virtual Slope Methods	17
	3.2.1 Gyro Blending	18
	3.2.2 Phasor Cancellation	20
	3.3 Digital Adaptive Filter	25
	3.4 Notch Filter Methods	48
	3.4.1 Spectral Identification Filter	48
	3.4.2 Adaptive Tracking Filter	54
	3.5 Frequency-Independent Signal Processing	66
4	REFERENCES	73
APPENDIX	VEHICLE DYNAMICS	77

LIST OF ILLUSTRATIONS

Figure	Title	Page
1	Simplified Functional Diagram of a Model-Reference Adaptive Flight Control System	6
2	MIT Adaptive Control System	9
3	Response Characteristics of MIT Adaptive System	12
4	Model Reference Adaptive System	13
5	Alternate Model Configuration	14
6	Command Response with $\mu_\alpha^* = 15\%$ Less Than μ_α	14
7	Command Response with $\mu_\alpha^* = 15\%$ Greater Than μ_α	14
8	Rate Response to Step Disturbance	15
9	Model Reference Adaptive System with Disturbance Sensing	16
10	Comparison of Response to Wind Inputs	17
11	Gyro Blender Adaptive Control System	19
12	Detail of Gyro Blender Operation	19
13	Phasor Cancellation Adaptive Control System	21
14	Frequency Response Characteristics of Bandpass Filter	21
15	Detail of Adaptive Controller	22
16	Analog Computer Trace, Initially Unstable Bending Mode	23
17	Effect of Variation in Integrator Gain, k	24
18	Analog Computer Trace, Response to Random Disturbance	25
19	Schematic of Digital Adaptive Filter	30
20	Application of Digital Adaptive Filter to Launch Vehicle Autopilot	32
21	Basic Configuration for Signal Decomposition by Digital Filtering	34
22	Basic Transient Response to One-Degree Step Attitude Command	35
23	Block Diagram of Vehicle Control System with the Digital Adaptive Filter and Secondary Linear Filter	36
24	Basic Transient Response as in Figure 22 But Control Transferred to Secondary Filters at t = 1.96 Sec	38

LIST OF ILLUSTRATIONS, Contd

Figure	Title	Page
25	Basic Transient Response as in Figure 22, But with Applied Step	39
26	Transient Response as in Figure 25, But Digital Filter Replaced by Unity Gain	40
27	Control System Error Response to a Unit Step Input	42
28	Response to a Unit Step Input (Bending Mode Added)	43
29	Response to an Alternating Step Input with a Half-Period of 25 Samples	44
30	Response to an Alternating Step Input with a Half-Period of 18 Samples	44
31	Response to an Atlernating Step Input with a Half-Period of 12 Samples	45
32	Control System Response to a Ramp Command Input	45
33	Control System Response with Variation in Sampling Rate Per Rigid Body Cycle	46
34	Control System Response with Body Bending Frequency Equal to Rigid Body Frequency	46
35	Spectral Identification Adaptive Control System	49
36	Typical Input to Spectral Filter	50
37	Truncated f(t) Curve	50
38	Frequency Sensor Principle of Operation	55
39	A Practical Frequency Tracker	56
40	An Adaptive Tracking Notch Filter	58
41	Schematic of Adaptive Tracking Notch Filter	59
42	Typical Operation of Adaptive Tracking Filter	60
43	Schematic of Adaptive Tracking Filter	61
44	Frequency Response of Lag-Lead Filter, Eq. (65)	62
45	Frequency Response of Notch Filter, Eq. (66)	63
46	Reference/Input Signal Transfer Functions	64
47	Operation of Various Types of Demodulators	65
48	Control System Utilizing Adaptive Tracking Filters	67

LIST OF ILLUSTRATIONS, Contd

Figure	Title	Page
49	Block Diagram of System for Processing Attitude and Attitude Rate Signals	70
A1	Vehicle Geometry	78
A2	Sign Convention for Bending Parameters	79
A3	Typical Normalized Mode Shapes	80

1. STATEMENT OF THE PROBLEM

It has been said that to define adaptive control is to invite an argument. Indeed the phrase is fraught with emotional overtones both for those to whom it represents a potential (if not present) panacea, and for those to whom adaptive control is at best an ambiguous aspiration having no cohesive structure within which a sound unified theory can be formulated.

Within the context of the present monograph, which is limited to adaptive control of space launch vehicles, the term adaptive control will be applied in a limited sense. It is generally agreed that adaptive control as a design philosophy enters the picture when a control system cannot be adequately designed a priori to cope with a changing or unknown environment. There are two fundamental aspects to this problem: identification and control function manipulation. The adaptive control of space launch vehicles exhibits both of these features.

The question of adaptive control for a launch vehicle autopilot must begin with a discussion of the problems of conventional control.

The optimum design of a space launch vehicle, from an overall performance point of view, maximizes payload and minimizes structural weight. Minimum structural weight results in increased flexibility (i.e., the ability of the vehicle to bend), which in turn has an adverse effect on the attitude control system.

The purpose of the attitude control system is to determine and maintain the direction of vehicle travel. A boost vehicle is similar to a long rod that bends in two ways when forces are placed upon it. The first is a steady-state bend equivalent to the sag in a rod when it is supported horizontally at both ends. The second is an oscillatory bend by the rod if a weight is dropped on it. This oscillatory bending tends to die out unless it is continually forced and excited as in the case of the control system continually applying forces to the vehicle. The system must be designed so that it does not increase bending beyond safety margins. The vehicle attitude sensor, rigidly attached to the vehicle, also measures bending at the sensor location. The attitude control forces computed from the sensor output are thus partially determined by the bending magnitude at the sensor. Factors depending upon the relative bending direction at the sensor locations and the attitude control force point, plus delays in computing the attitude control force magnitude from the sensor output, determine whether the applied force increases or decreases any bending that may exist. The effects of computational delays are directly dependent upon the oscillatory frequency of the bending.

A normal control system for a flexible vehicle does not allow high frequencies to pass through to the force point, thus eliminating the reinforcing of high-frequency oscillatory bending modes. Computational delays are so designed that the low-frequency

oscillatory bending modes are suppressed by the control forces rather than reinforced. However, with very large and very flexible vehicles a normal control system design may be inadequate. For very flexible vehicles the bending oscillatory frequencies become low enough that even the higher modes cannot be filtered out without detrimental effects upon attitude control. With large vehicles it is impossible to predetermine the bending oscillatory frequency to the accuracy required to adjust the computational delays in a manner to guarantee control.

A detailed quantitative discussion of these factors is contained in Ref. 1. The main problems from a controls point of view may be summarized as follows:

a. Bending mode frequencies are not known with sufficient precision.

b. Bending mode properties vary with flight time.

c. The lowest bending mode frequency may be of the same order of magnitude as the control frequency.

Many schemes have been devised to cope with these problems. They have been called "adaptive" since the control system parameters vary (adapt) as a function of flight environment. A discussion of these concepts forms the subject matter for the present monograph.

2. STATE OF THE ART

A discussion of adaptive control cannot proceed without at least a tentative definition. One widely accepted is that an adaptive control system can monitor its own performance, evaluate the effectiveness of its response, and then modify its parameters automatically to achieve desired performance. When applied to a launch vehicle autopilot this implies that the adaptive control system will identify an unstable bending mode frequency, and activate some suitable compensation device to stabilize the system. This compensation may take the form of cancellation, phase stabilization, or gain stabilization. The cancellation technique, as typified by the model-reference or virtual slope methods, for example, makes the sensor output behave as if the sensor were located on an antinode (point of zero bending mode slope). Phase and gain stabilization techniques depend on an accurate identification of the bending mode frequency since these modes are highly tuned (very low relative damping factor). In some cases signal shaping by conventional filtering is inadequate since the signals to be separated do not have a sufficiently large frequency separation. The digital adaptive filter and frequency-independent signal processing techniques have been developed to cope with this problem.

One thing is certain. Adaptive control has not suffered from a lack of attention in the literature. Neither has Air Force or NASA funding been lacking for pursuing investigations of particular concepts. Yet today, some ten years after adaptive control began to be studied intensively, very few adaptive systems have reached the flight test stage (these mainly on aircraft), and none are operational. A partial answer is that so-called conventional methods have been refined considerably, and the point at which adaptive control becomes mandatory has never been clearly defined. There is a considerable (and understandable) reservation in committing oneself to complicated and exotic control schemes where multimillion dollar vehicles are concerned if their need has not been clearly established.

At present, conventional and straightforward control methods appear adequate. However, if past experience is any indication, one will assuredly be confronted with problems that strain the capabilities of current technologies. When this occurs, advanced schemes presently in the "drawing board" stage will be evaluated under actual operating conditions and thus serve both to refine and enlarge these concepts presently called "adaptive control."

3. RECOMMENDED PROCEDURES

The following paragraphs describe the major bending mode adaptive techniques. They also provide a critical evaluation of the virtues and limitations of each type. To date, none of these schemes has been flight tested, although many of them have been thoroughly simulated (via computer) with varying degrees of complexity. Consequently, while different Government agencies and aerospace contractors have their preferences, there is no universal agreement that any one type represents a definitive solution to the problem.

At present, conventional linear techniques seem to be adequate for the current generation of booster vehicles[2]. The methods presented here are therefore to be interpreted as possible solutions if and when more advanced vehicles exhibit bending control problems that cannot be resolved by today's methods.

In order to simplify the presentation, and provide a common framework for analysis and comparison of the different methods, each will be discussed with reference to the mathematical model described in the Appendix.

3.1 MODEL-REFERENCE TECHNIQUES

The basic idea of employing a model to obtain improved system response is apparently due to Lang and Ham[3]. However, in its original version this was merely a disguised high-gain system in which prefiltering together with high open-loop gain were used to achieve relatively invariant response in the presence of parameter variations. The methodology may nevertheless be applied in different ways in order to satisfy prescribed objectives. Two particular extensions of this philosophy to the bending mode problem are described next.

3.1.1 Whitaker (MIT) System

The model-reference adaptive control concept was originally proposed and investigated at the MIT Instrumentation Laboratory. It was evolved to enable design of a control system that could adjust its own controllable parameters in the presence of changing or poorly defined operating characteristics. The underlying philosophy has been to provide a control system that will meet system specifications provided its variable parameters can be adjusted to proper values. The function of the adaptive system is then that of providing the proper parameter values.

Figure 1 is a functional diagram of a general model-reference adaptive flight control system. The system specifications are incorporated into a reference model that receives the same commands as the actual system. A response error signal is obtained by comparing the response of the model to that of the system. The

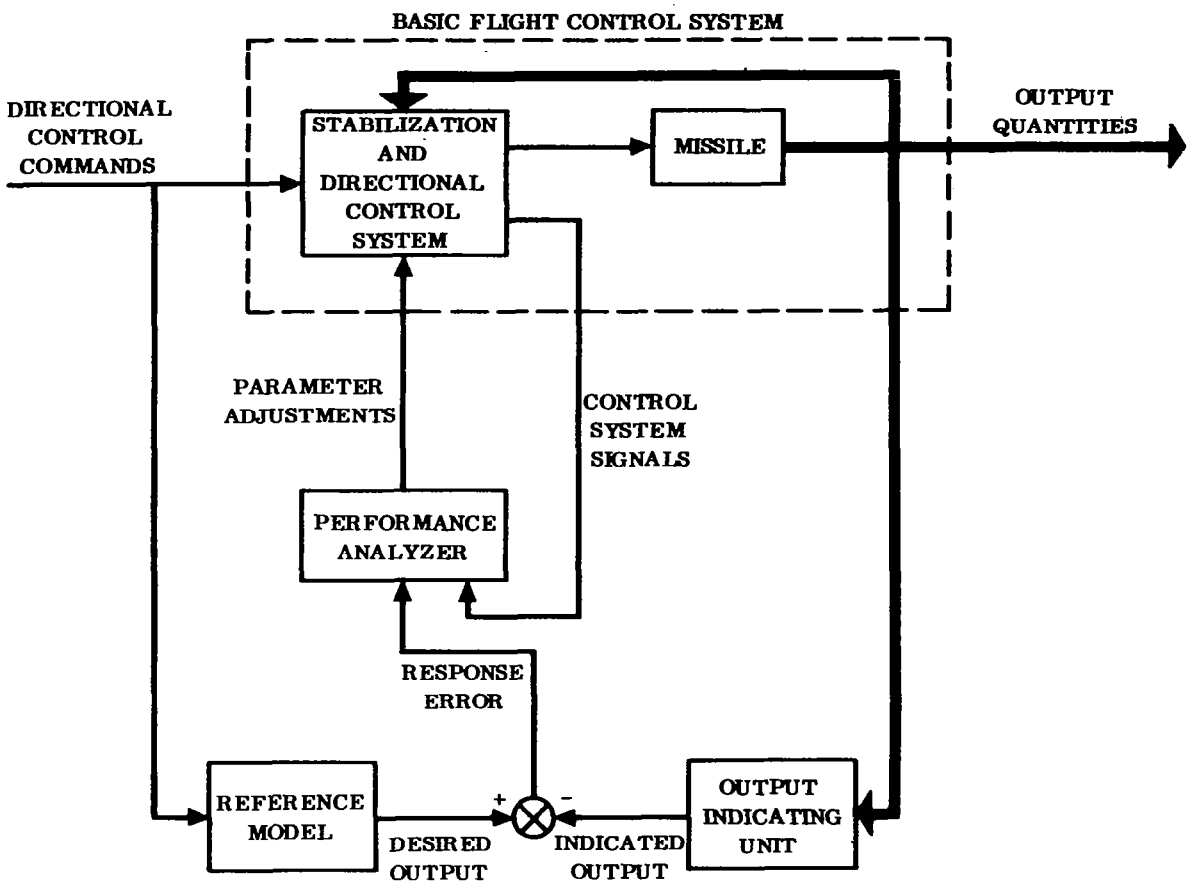

Figure 1. Simplified Functional Diagram of a Model-Reference Adaptive Flight Control System

controllable parameters are adjusted so that the integral-squared error between system and model outputs is minimized. The index of performance is then the integral-squared response error, and the criterion for successful adaptation is that the integral-squared error (ISE) be the minimum value obtainable with the parameter variation provided.

$$\int (E)^2 \, dt = \text{minimum} \tag{1}$$

At the desired operating point the slope of the ISE as a function of the variable parameters P_n is zero, or

$$\frac{\partial^n}{\partial P_1, \partial P_2, \cdots, \partial P_n} \left(\int (E)^2 \, dt \right) = 0 \tag{2}$$

If the limits of integration are independent of P_n and the integral of the partial derivative of the function exists, the partial differentiation may be carried out under the integral sign, resulting in the error quantity

$$(EQ)_{P_n} = \frac{\partial}{\partial P_n}\left(\int (E)^2\, dt\right) = \int \frac{\partial (E)^2}{\partial P_n}\, dt = 2\int \left(\frac{\partial E}{\partial P_n}\right) E\, dt$$

$$= \int W_E\,(t)\,(E)\, dt \tag{3}$$

The error quantity is the integral of the error weighted by a function such that the error quantity is indicative of the state of the system. The sign and magnitude of the error quantity indicates the direction and amount that the variable parameter should be changed. A simple mechanization results if the change of the parameter is made proportional to the error quantity. The weighted error is then proportional to a time rate of change of the parameter which will result in setting the parameter to the desired operating point. The integration of Eq. (3) may then be carried out in the parameter adjustment device.

The weighting function is determined by performing a straightforward partial differentiation of the differential equation for the error as a function of the input quantities, or by considering the change in the parameter as a disturbance entering the system after the parameter. The error weighting function can be generated by taking the signal at the input to the variable parameter and feeding it through a filter having the same performance function as the system, cascaded with a filter that is the reciprocal of some of the forward path components. It is not possible to obtain a signal that exactly satisfies the equations since the ill-defined or unknown characteristics of the system is what leads to the requirement for the adaptive system. An approximation to Eq. (3) is obtained by substitution of the performance function of the model for the performance function of the system. In cases where a system model does not exist explicitly, Eq. (3) may be approximated by using an approximation for the dynamic characteristics of the optimum system.

The validity of this approximation depends upon the accuracy of the approximation of the system by the model and the weighting function filter. In the neighborhood of optimum response, this approximation is good. For system parameter settings far removed from optimum the approximation is poor; however, if the algebraic sign of the weighting function is correct, proper system operation is obtained. Even though the weighted error has the incorrect sign instantaneously, satisfactory results are obtained if the error quantity has the proper sign over the evaluation period. The derivation of these equations is based on the assumption of the constant coefficient linear system. When the parameters are varied during the response to input signals, these equations are in error by perturbation terms.

Because of the nonlinear nature of the system, operation can best be studied by analog simulation. Simulation is also required to evaluate the use of the approximate dynamics in the weighting function filter. It is to be expected that the operating state selected by the adaptive system will not be the optimum operating state predicted by the exact Eq. (2), but will have some error due to the approximations. It has been found that these errors are usually small and the characteristics of the weighting function filter usually are not critical.

In applying the above concepts to the elastic vehicle control problem, we must begin by defining two quantities:

a. The performance index.

b. The parameter(s) to be varied.

In order to provide the adaptive capability, it is also necessary to define a model that incorporates the system specifications and to obtain a response error that is indicative of the state of the system. The most desirable situation would be elimination of the bending, in which case the "model" is zero and the response error is the bending itself. Thus we may take as a performance index,

$$\text{P.I.} = \int \left[q^{(1)}\right]^2 dt \tag{4}$$

where $q^{(1)}$ is the generalized coordinate of the first bending mode.† The control system to be described is then adaptive only with respect to this mode.

We must now choose the parameter to be varied in order to minimize Eq. (4). For this purpose, Kezer[4] takes the "effective bending" sensed by the rate gyros. Such a signal may be obtained, for example, by taking the difference between the outputs from two gyros located at different positions along the vehicle; thus

$$\left(\dot{\theta}_R + \sigma_{GR}^{(1)}\,\dot{q}^{(1)}\right) - \left(\dot{\theta}_R + \sigma_{GF}^{(1)}\,\dot{q}^{(1)}\right) = \sigma_E^{(1)}\,\dot{q}^{(1)}$$

The quantity $\sigma_E^{(1)}$ is selected as the parameter to be varied in order to minimize Eq. (4). Proper operation of the system then requires that

$$\frac{\partial}{\partial \sigma_E^{(1)}} \int \left[q^{(1)}\right]^2 dt = \int \frac{\partial}{\partial \sigma_E^{(1)}} \left[q^{(1)}\right]^2 dt$$

$$= 2\int q^{(1)} \left(\frac{\partial q^{(1)}}{\partial \sigma_E^{(1)}}\right) dt = 0 \tag{5}$$

†The nomenclature used in the following discussion is defined in the Appendix.

The system is now made adaptive by setting the rate of change of $\sigma_G^{(1)}$ proportional to

$$q^{(1)}\left(\frac{\partial \dot{q}^{(1)}}{\partial \sigma_E^{(1)}}\right) \tag{6}$$

To do this we must have available both $q^{(1)}$ and $\partial q^{(1)}/\partial \sigma_E^{(1)}$. The latter may be determined directly from the equations of motion of the system. Referring to Fig. 2 and the Appendix, we have†

$$\left(s^2 - \mu_\alpha\right)\theta_R = \mu_c\,\delta \tag{7}$$

$$\left(s^2 + 2\xi_1\omega_1 s + \omega_1^2\right)q^{(1)} = -\frac{T_c}{\mathfrak{M}_1}\,\delta \tag{8}$$

$$\left(s + K_c\right)\delta = K_c\,\delta_c \tag{9}$$

$$\delta_c = K_A\left(\theta_c - \theta_F\right) \tag{10}$$

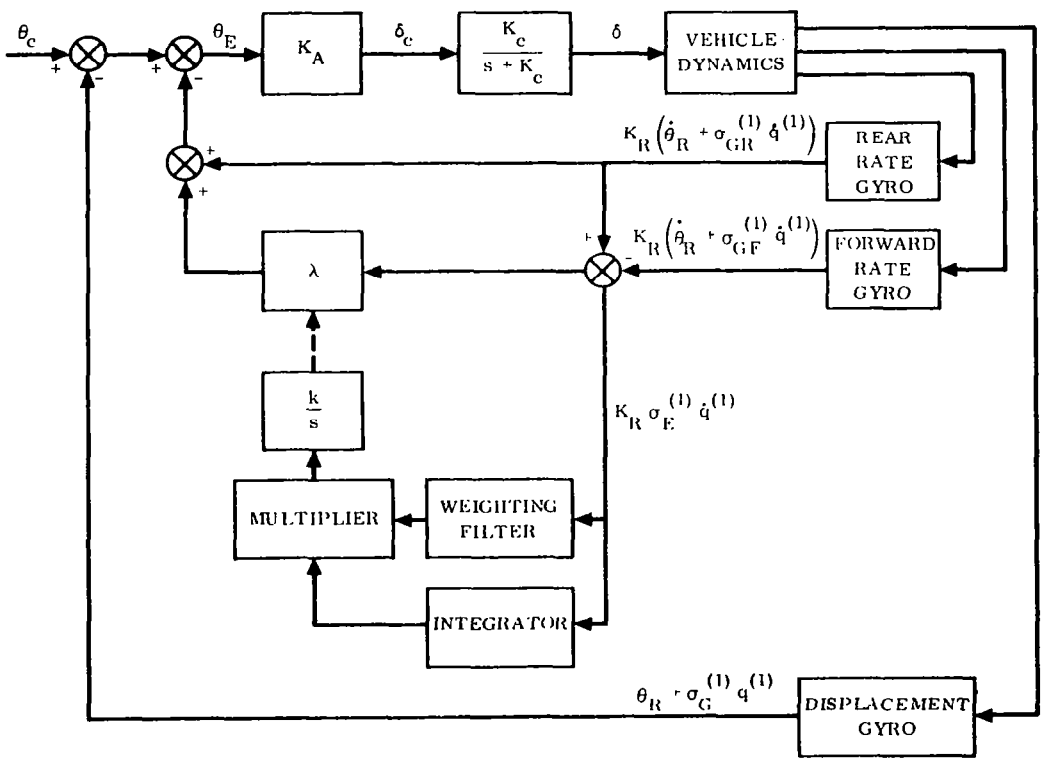

Figure 2. MIT Adaptive Control System

†It is assumed that $K_I \approx 0$ and $\alpha \approx \theta$.

$$\theta_F = \theta_R + \sigma_G^{(1)} q^{(1)} + K_R\left(\dot{\theta}_R + \sigma_{GR}^{(1)} q^{(1)}\right)$$

$$+ K_R\left[\left(\dot{\theta}_R + \sigma_{GR}^{(1)} \dot{q}^{(1)}\right) - \left(\dot{\theta}_R + \sigma_{GF}^{(1)} \dot{q}^{(1)}\right)\right]$$

$$= \left(K_R s + 1\right)\left(\theta_R + \sigma_G^{(1)} q^{(1)}\right) + K_R s \sigma_E^{(1)} q^{(1)} \tag{11}$$

where

$$\sigma_E^{(1)} = \sigma_{GR}^{(1)} - \sigma_{GF}^{(1)}$$

and

$$\sigma_{GR}^{(1)} = \sigma_G^{(1)}$$

From Eqs. (7) through (11), we find that $q^{(1)}$ is related to θ_c by

$$G_0(s)\, q^{(1)} = -\frac{K_A K_c T_c}{\mathfrak{M}_1}\left(s^2 - \mu_\alpha\right)\theta_c \tag{12}$$

where

$$G_0(s) = \left[\left(s^2 - \mu_\alpha\right)\left(s + K_c\right) + K_A K_c \mu_c \left(K_R s + 1\right)\right]\left(s^2 + 2\xi_1 \omega_1 s + \omega_1^2\right)$$

$$- \frac{K_A K_c T_c}{\mathfrak{M}_1}\left[K_R s\left(\sigma_G^{(1)} + \sigma_E^{(1)}\right) + \sigma_G^{(1)}\right]\left(s^2 - \mu_\alpha\right) \tag{13}$$

Taking the partial derivative of Eq. (12) with respect to $\sigma_E^{(1)}$, we find

$$G_0(s)\frac{\partial q^{(1)}}{\partial \sigma_E^{(1)}} - \frac{K_A K_c K_R T_c}{\mathfrak{M}_1}\left(s^2 - \mu_\alpha\right) s\, q^{(1)} = 0$$

or

$$\frac{\partial q^{(1)}}{\partial \sigma_E^{(1)}} = \frac{K_A K_c K_R T_c \left(s^2 - \mu_\alpha\right)}{\mathfrak{M}_1 G_0(s)} \tag{14}$$

If the transfer function for the weighting filter is taken as

$$G_w(s) = \frac{K_A K_c T_c \left(s^2 - \mu_\alpha\right)}{\mathfrak{M}_1 G_0(s)} \tag{15}$$

and if the input is $K_R \sigma_E^{(1)} \dot{q}^{(1)}$, we see that the output of the weighting filter is the quantity

$$\sigma_E^{(1)} \left(\frac{\partial q^{(1)}}{\partial \sigma_E^{(1)}}\right) \tag{16}$$

Furthermore, the output of the integrator is

$$K_R \sigma_E^{(1)} q^{(1)} \tag{17}$$

and it follows that the multiplier output is

$$K_R \left[\sigma_E^{(1)}\right]^2 \left(\frac{\partial q^{(1)}}{\partial \sigma_E^{(1)}}\right) q^{(1)} \tag{18}$$

i.e., proportional to the error quantity, Eq. (6). This signal is used to adjust the sign and magnitude of the gain λ. A steady-state value is achieved when the multiplier output is zero, which indicates that the first bending mode signal has been essentially eliminated from the "blended" rate gyro feedback.

Some typical results of a computer simulation for this system are shown in Fig. 3. The input θ_c was a square pulse in each of the three cases shown. In the first case, with the adaptive loop open, it is apparent that the bending mode signal is poorly damped. The improvement in response for the next two cases (where the adaptive system is employed) is quite evident.

Remark: The MIT adaptive system is an elegant and conceptually sound approach to the bending mode problem, and has an obvious appeal to the theoretically inclined. The system is fast acting, and acts on either common or disturbance inputs with equal effectiveness. Studies have shown that the multiplier may be replaced by a relay, and that the integrator (for generating $q^{(1)}$) may be replaced by a low pass filter. It is thus relatively simple to mechanize.

On the other hand, the scheme is effective only when one bending mode is significant and well separated in frequency from the other modes.

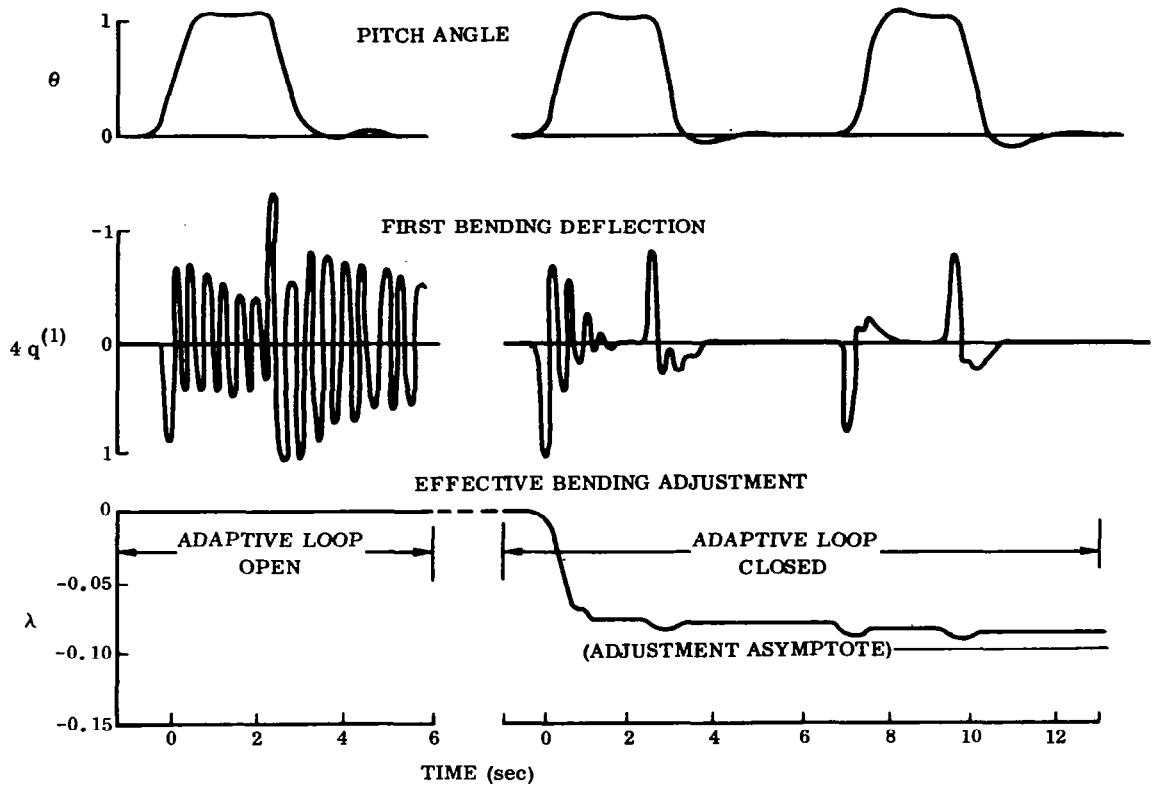

Figure 3. Response Characteristics of MIT Adaptive System

It should be noted also that the weighting filter is of necessity an approximation since, as is apparent from Eqs. (15) and (13), some estimate is necessary for the $\mathfrak{M}_1$, $\sigma^{(1)}$ and ω_1 values that are not known; hence the need for adaptive control. Furthermore, the quantities μ_c and μ_α are time varying, and various higher-order dynamic effects are neglected. These factors are not usually crucial, however; it means essentially that the error quantity, Eq. (6), will not attain a zero value. Adaptive control is still exhibited in the sense that corrections are applied (by varying λ in Fig. 2) to reduce the error. How well this is done is a function of how well the weighting filter approximates the "optimum" filter.

3.1.2 Tutt and Waymeyer System

A "brute force" approach to the problem of separating rigid body from bending mode signals is by using passive low pass linear filters on the rate and displacement gyro outputs. It is well known that this approach results in an unacceptable deterioration in rigid body response. In order to recover rigid body motion signals, one could conceivably employ predicted attitude and rate information from a model of the

rigid body dynamics of the vehicle. Such a scheme is shown in Fig. 4. The engine angle signal δ is fed to a model of the rigid body dynamics, which requires a knowledge of the control and aerodynamic moment effectiveness, μ_c^* and μ_α^*, respectively (asterisks denote "model" parameters). The attitude rate output from the model, $\dot{\theta}_M$, is then multiplied by K_R, the rate gyro gain, fed through a high pass filter, and summed with the actual rate gyro output after the latter was fed through a low pass filter. This sum is used as the rate feedback to the system. Thus the rate gyro information is heavily filtered to reject bending mode signals, and a "clean" rigid body rate signal is obtained from a model of the rigid body dynamics. A similar procedure is applied to the attitude displacement information.

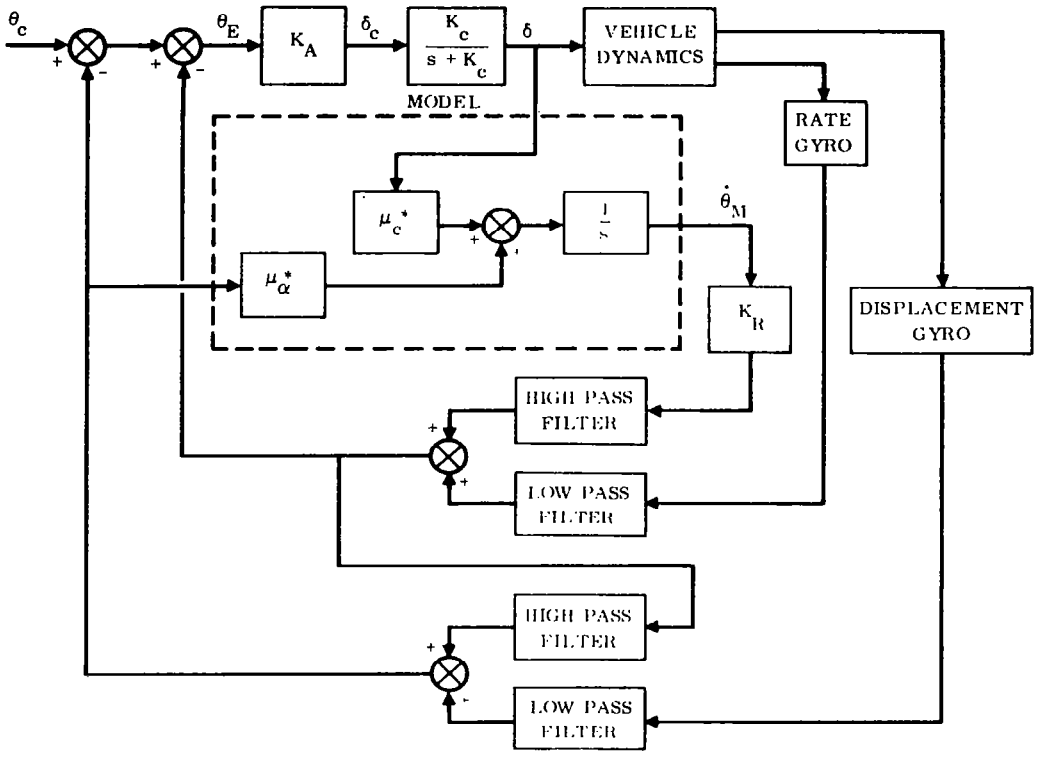

Figure 4. Model Reference Adaptive System

In accordance with this control philosophy it would appear that one could generate "model" attitude and rate information from a configuration of the form shown in Fig. 5. However, it is not possible for μ_α^* to operate only on computed information, since a closed-loop pole-zero pair would appear in the right-half s-plane, and these would cancel only if $\mu_\alpha^* = \mu_\alpha$ exactly. Therefore the configuration shown in Fig. 4 is used where μ_α^* is acted upon by a combination of computed and actual body attitudes.

A crucial factor in the model reference approach is the required accuracy in μ_c^* and μ_α^*, of which the latter is the more critical. Computer traces for attitude rate in

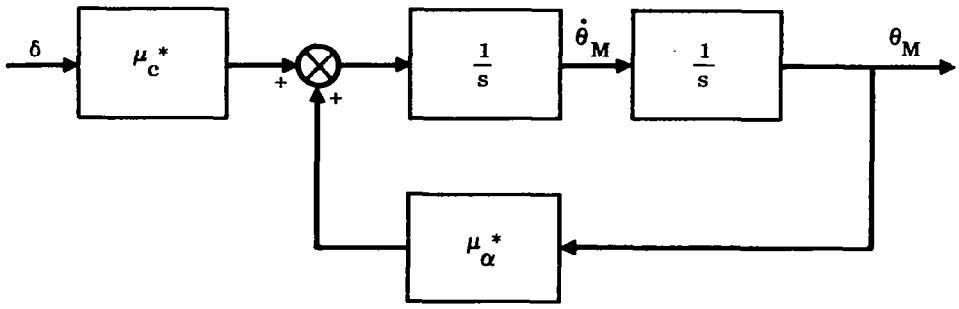

Figure 5. Alternate Model Configuration

response to step input commands in θ_c are shown in Figs. 6 and 7 for μ_α* 15% less than and 15% greater than μ_α, respectively. These traces indicate (and analytical studies verify) that the tolerance on μ_α* (with respect to μ_α) should be heavily weighted toward the positive ($\mu_\alpha^* > \mu_\alpha$).

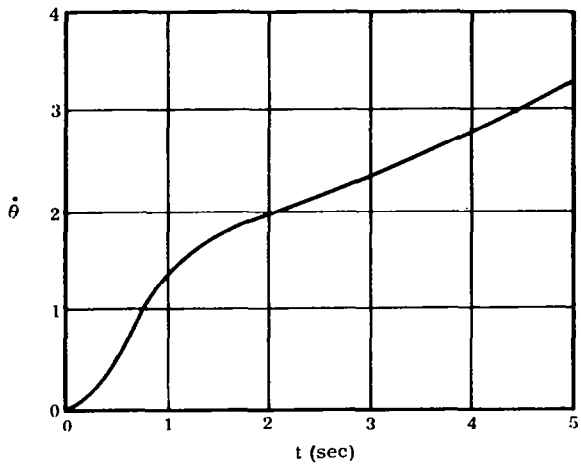

Figure 6. Command Response with μ_α^* = 15% Less Than μ_α

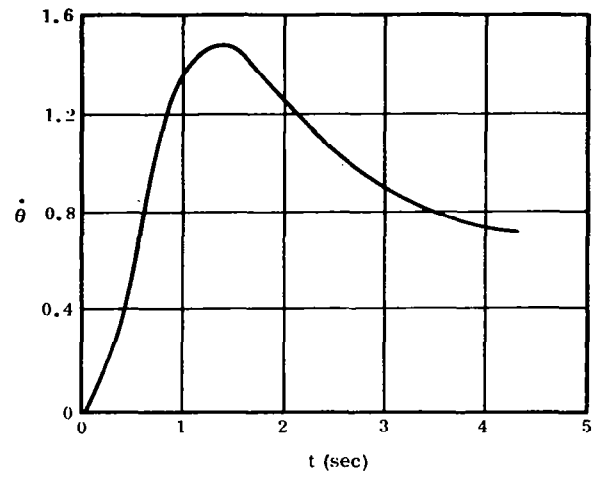

Figure 7. Command Response with μ_α^* = 15% Greater Than μ_α

In Fig. 8 are shown the rate response traoes due to a step wind disturbance for both model feedback and conventional systems, each with the same system parameters. The very poor response for the model feedback system was to be expected since actual body motion is not generated solely by engine deflection. In the configuration of Fig. 4 the engine responds only to the heavily filtered real body loop.

Since for a realistic launch vehicle the wind inputs are often the predominant inputs to the system, the model-reference configuration of Fig. 4 is clearly inadequate. Various modifications are proposed by Tutt and Waymeyer[5], of which all are based essentially on some form of angle-of-attack sensing. The problem is to obtain some sort of disturbance information without re-introducing the bending previously rejected.

To do this we may adopt the same control philosophy used in the attitude and rate loops; namely to use an actual value and a "model reference" value for angle of attack, which is combined and used as an additional feedback loop for the control system. The system would then take the form shown in Fig. 9. The schematic for the α model is derived from Eqs. (A1) and (A2) of the Appendix with

$$N'_{\delta} = \frac{T_c}{m\,U_0} \qquad N_{\alpha} = \frac{L_{\alpha}}{m\,U_0}$$

$$\alpha_M = \frac{w}{U_0}$$

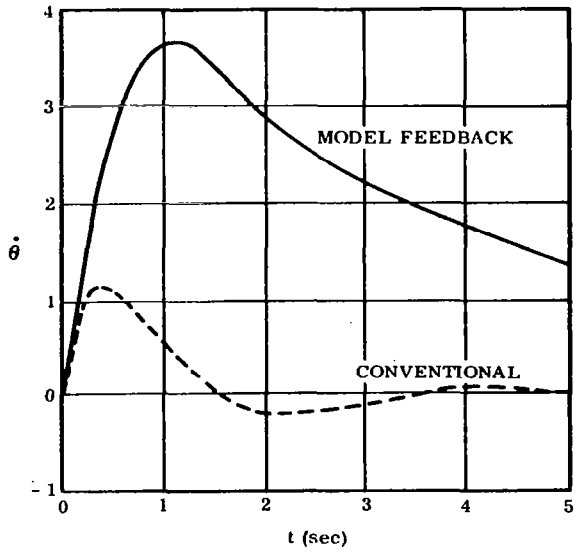

Figure 8. Rate Response to Step Disturbance

The degree of improvement in disturbance response for a typical case is shown in Fig. 10, in which are superimposed the responses for systems denoted as conventional, model feedback, and model feedback with α sensing. Use of α sensing thus yields a significant improvement. Whether this improvement is good enough is something to be determined for the specific mission considered.

Remark: The model reference system is very effective when certain rather stringent requirements are satisfied. First the rigid body parameters (mass, moment of inertia, center-of-gravity location, aerodynamic properties) must be accurately known as a function of flight time. Second, and more important, disturbance effects must be minimal. In other words the vehicle motion must be derived primarily from command inputs. This condition is obviously not satisfied for ballistic booster vehicles, and various additional complexities must be introduced in the control system to take account of disturbance inputs.

It may be noted in passing that if the rigid body model is accurate, one may dispense with the rate gyro entirely.

Many aspects of the model reference control scheme require further investigation. A basic element of the system is the rigid body model, and it is necessary to determine the sensitivity of the system performance to variations in the rigid body "model" parameters. In a realistic system the "model" is essentially a filter with nonstationary parameters. For both analytical and pragmatic reasons this is an undesirable situation, and it would be important to determine if gain switching at preselected intervals

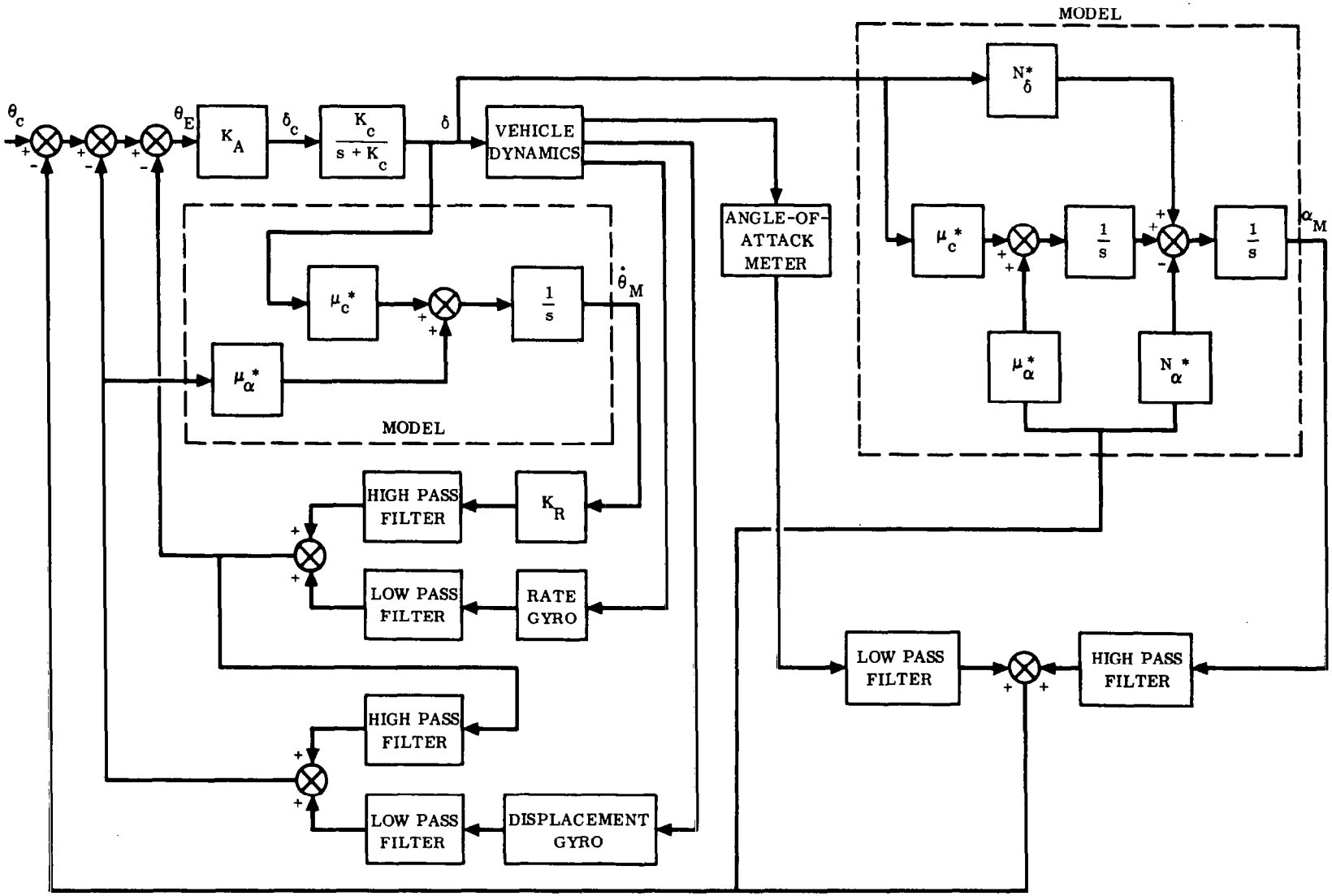

Figure 9. Model Reference Adaptive System with Disturbance Sensing

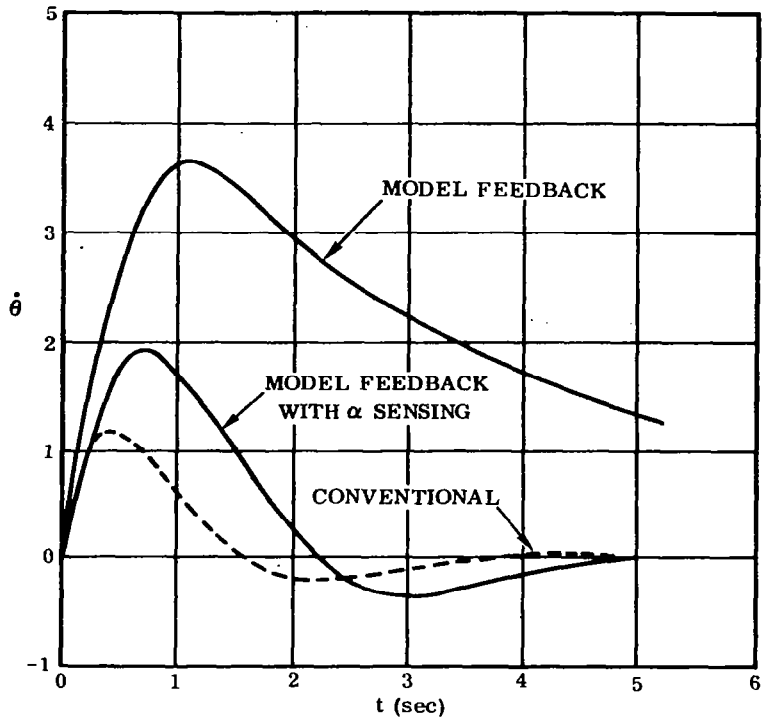

Figure 10. Comparison of Response to Wind Inputs

could replace continuous variations in μ_c* and μ_α*. Another open question at present is the choice of break frequencies in the high and low pass filters. This must obviously be decided for each specific vehicle and depends primarily on the frequency separation between rigid body and first bending mode signals. When these are in fairly close proximity, the effectiveness of the model reference scheme appears marginal.

It has also been argued that the model reference scheme is not an adaptive system at all. Since the control configuration is predetermined and there is neither identification of system parameters nor their control as a function of environment, it is not reasonable to claim that this system is adaptive. However, this could motivate an involved digression in semantics, and we must resist the temptation to pursue it further.

3.2 VIRTUAL SLOPE METHODS

If the vehicle bending modes were known precisely, then a simple means of suppressing bending mode signals for a particular mode would be to locate the gyros on an antinode (point of zero slope) for that mode. However, even if the bending mode data were known precisely as a function of flight time, the antinode location (and other bending mode data) varies with time so that one specific location for the

gyro is not satisfactory throughout the flight regime. Conceptually, one may visualize a gyro moving along the vehicle such that it constantly tracks the desired antinode. This is obviously a fanciful notion, but it is possible to formulate a control scheme that effectively performs this function by other means. Two methods of achieving this are described next.

3.2.1 Gyro Blending

The essential idea for the gyro blending scheme is motivated by the following considerations. Suppose that two rate gyros located at different points along the vehicle are used. The output of the rear rate gyro is†

$$K_R\left(\dot{\theta}_R + \sum_i \sigma_{GR}^{(i)}\,\dot{q}^{(i)}\right) \tag{19}$$

and similarly for the forward rate gyro; viz.

$$K_R\left(\dot{\theta}_R + \sum_i \sigma_{GF}^{(i)}\,\dot{q}^{(i)}\right) \tag{20}$$

If it is assumed that the only significant bending mode is i=1, we may proceed as follows. Multiply Eq. (19) by some number K, and multiply Eq. (20) by (K-1). Adding the result, we have

$$K_R\,\dot{\theta}_R + K_R\left[(1 - K)\,\sigma_{GR}^{(1)} + K\,\sigma_{GF}^{(1)}\right]\dot{q}^{(1)} \tag{21}$$

In order to obtain a signal free of bending mode information, we see that K must satisfy the relation

$$(1 - K)\,\sigma_{GR}^{(1)} + K\,\sigma_{GF}^{(1)} = 0 \tag{22}$$

Under suitable conditions this operation may be made automatic, and the resulting control system configuration has the general form shown in Fig. 11. It remains to investigate the means whereby K is made to satisfy Eq. (22) automatically.

Referring to Fig. 12, which shows the blender operation in detail, suppose that the rate gyro signals attenuated by (1-K) and K respectively, are passed through bandpass filters designed to reject all signals outside the anticipated frequency range of the first bending mode. The signal appearing at the input of the integrator is then

†See the Appendix for definitions of nomenclature.

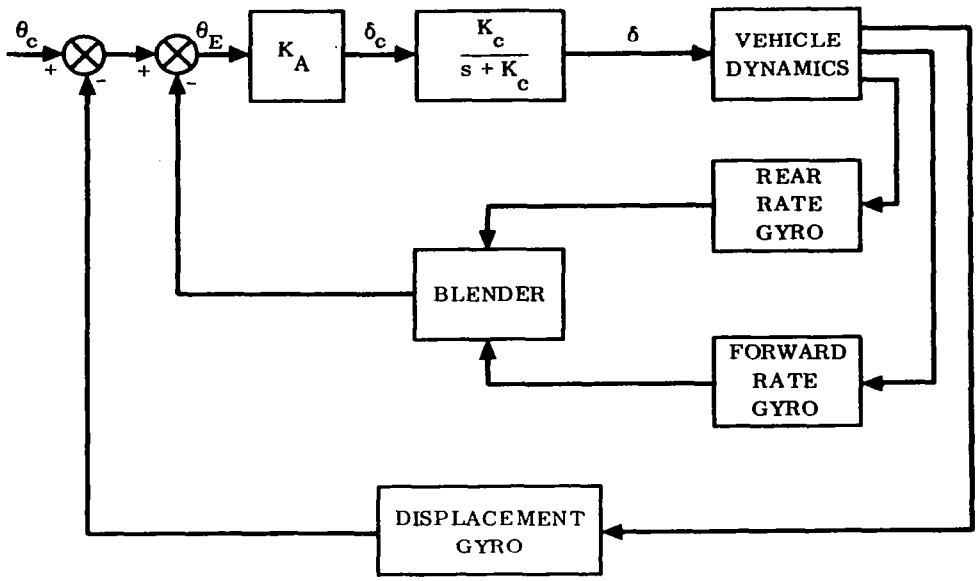

Figure 11. Gyro Blender Adaptive Control System

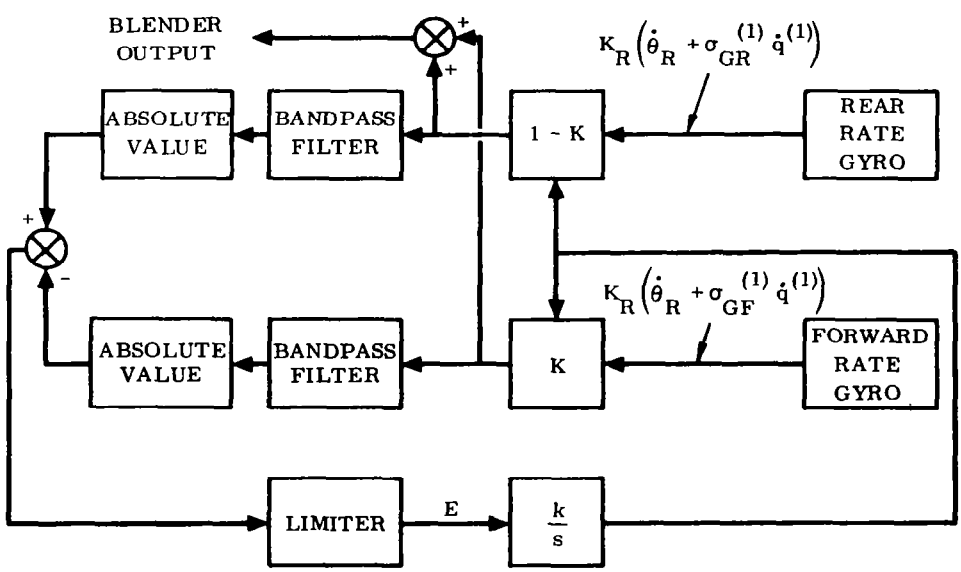

Figure 12. Detail of Gyro Blender Operation

$$\dot{E} = \left|(1 - K)\,\sigma_{GR}^{(1)}\,\dot{q}^{(1)}\right| - \left|K\,\sigma_{GF}^{(1)}\,\dot{q}^{(1)}\right|$$

It is apparent that a steady-state condition (E=0) is reached when K satisfies Eq. (22), which is precisely the condition required for the blender output to be free of bending mode signals.

Since K, which is a potentiometer setting between zero and one, must always be positive, a fundamental requirement for proper operation of this system is that the mode slopes at the two gyro locations be of opposite sign at all times.

Remark: This scheme is workable only if there is assurance that certain prescribed conditions are satisfied. First of all this method requires that the bending mode slopes at the gyro locations always be of opposite sign. Usually this condition prevails only for the first bending mode. Furthermore, effective operation of the bandpass filters requires that there be a moderate frequency separation between rigid body mode and bending mode signals on the one hand, and between first bending mode and other dynamic modes of the system on the other. If this condition does not prevail, the integrator will not null properly, the correct value of K will not be established, and the rate feedback signal will therefore contain bending mode information.

3.2.2 Phasor Cancellation

As in the previous system, the aim of the phasor cancellation concept is to yield a feedback signal free of bending mode signals by an operation that effectively locates the gyros at an antinode. The essential idea may best be described by examining the Fourier decomposition of the feedback signal; viz.

$$\theta_F' = \sum_{i=0}^{n} E_i \sin\left(\omega_i t + \psi_i\right) \tag{23}$$

Each of the terms on the right-hand side of this equation is a phasor, $\bar{E}_i$, with amplitude E_i and phase angle ψ_i. We may associate $\bar{E}_0$ with the rigid body mode and the $\bar{E}_i$ with the bending modes. It will again be assumed that only the first bending mode is significant.

The adaptive system described here generates a phasor whose amplitude and phase angle are identical to E_1, and subtracts this from the feedback control signal, thereby giving a signal free of first bending mode information. The method is illustrated schematically in Fig. 13. In Fig. 14 are shown the frequency response characteristics of the adjustable bandpass filter. To analyze the operation of the system, assume that ω_F is equal to ω_1, the first bending mode frequency. Then the output of the adjustable bandpass filter is a signal whose amplitude and phase are equal to that

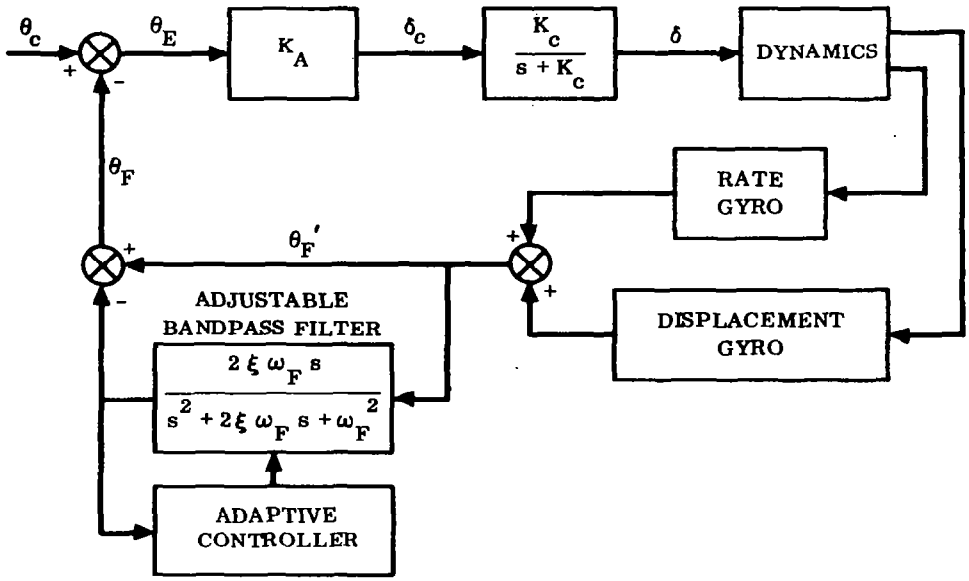

Figure 13. Phasor Cancellation Adaptive Control System

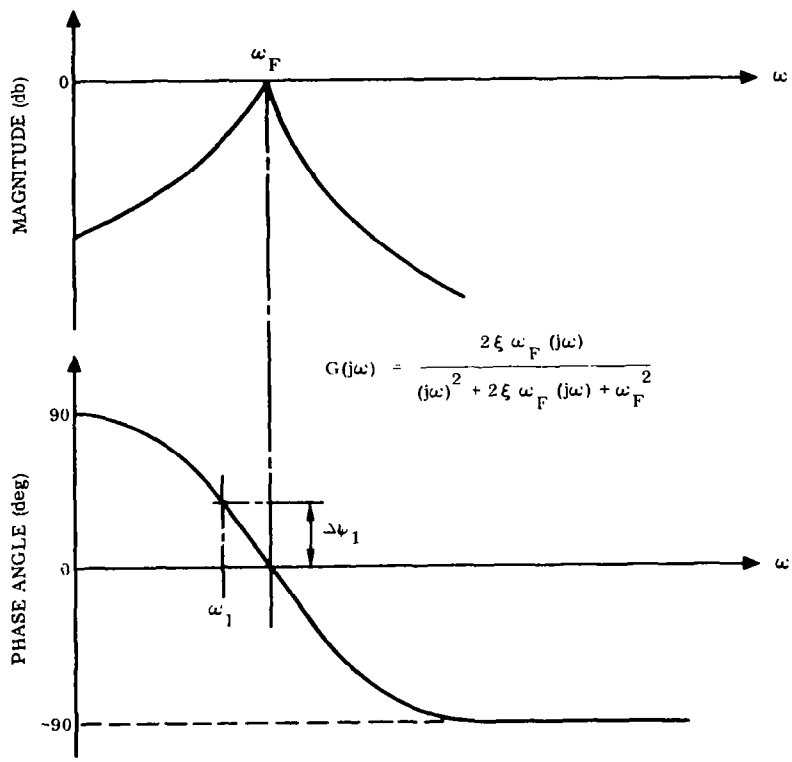

Figure 14. Frequency Response Characteristics of Bandpass Filter

of the first bending mode signal, with all other frequencies sharply attenuated. Therefore subtracting this from θ_F' gives a signal essentially free of first bending mode information.

The function of the adaptive controller is to track the bending mode frequency and set ω_F equal to ω_1 at all times. This may be accomplished in the manner shown in Fig. 15. In general ω_F will not be equal to ω_1 which means that the bending phasor, after passing through the adjustable bandpass filter, will incur a phase shift, $\Delta\psi_1$ (see Fig. 14). This signal, after then passing through the secondary bandpass filter, will incur another phase shift approximately equal to $\Delta\psi_1$ if ω_F is not too far from ω_1 (this means essentially that ω_1 is such that operation is along the nearly linear portion of the phase shift curve in Fig. 14). Thus $\Delta\psi_1$ is a measure of the deviation of ω_F from ω_1.

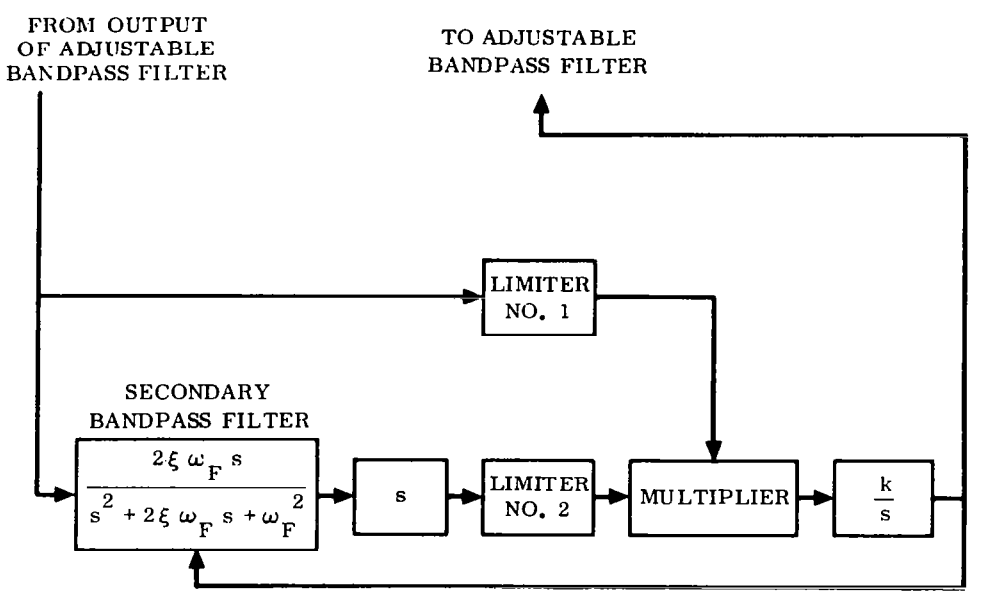

Figure 15. Detail of Adaptive Controller

Now the outputs from limiters No. 1 and No. 2 are

$$A \sin \omega_1 t$$

and

$$A \cos\left(\omega_1 t + \Delta\psi_1\right)$$

respectively. The amplitude A is constant due to the limiters.

The output of the multiplier is then

$$A^2 \sin \omega_1 t \cos\left(\omega_1 t + \Delta\psi_1\right)$$

If $\Delta\psi_1$ is small such that $\sin \Delta\psi_1 \approx \Delta\psi_1$, this last relation may be written as

$$\frac{A^2}{2}\left[-\Delta\psi_1 + \sin\left(2\,\omega_1 t + \Delta\psi_1\right)\right]$$

The second term, which is a phasor of twice the bending mode frequency, is sharply attenuated by the integrator. Thus the output of the multiplier is essentially proportional to $\Delta\psi_1$. The integrator output adjusts ω_F in both bandpass filters in such a way as to drive $\Delta\psi_1$ to zero; that is, until $\omega_F = \omega_1$.

The results of an analog computer simulation of this system are shown in Fig. 16.

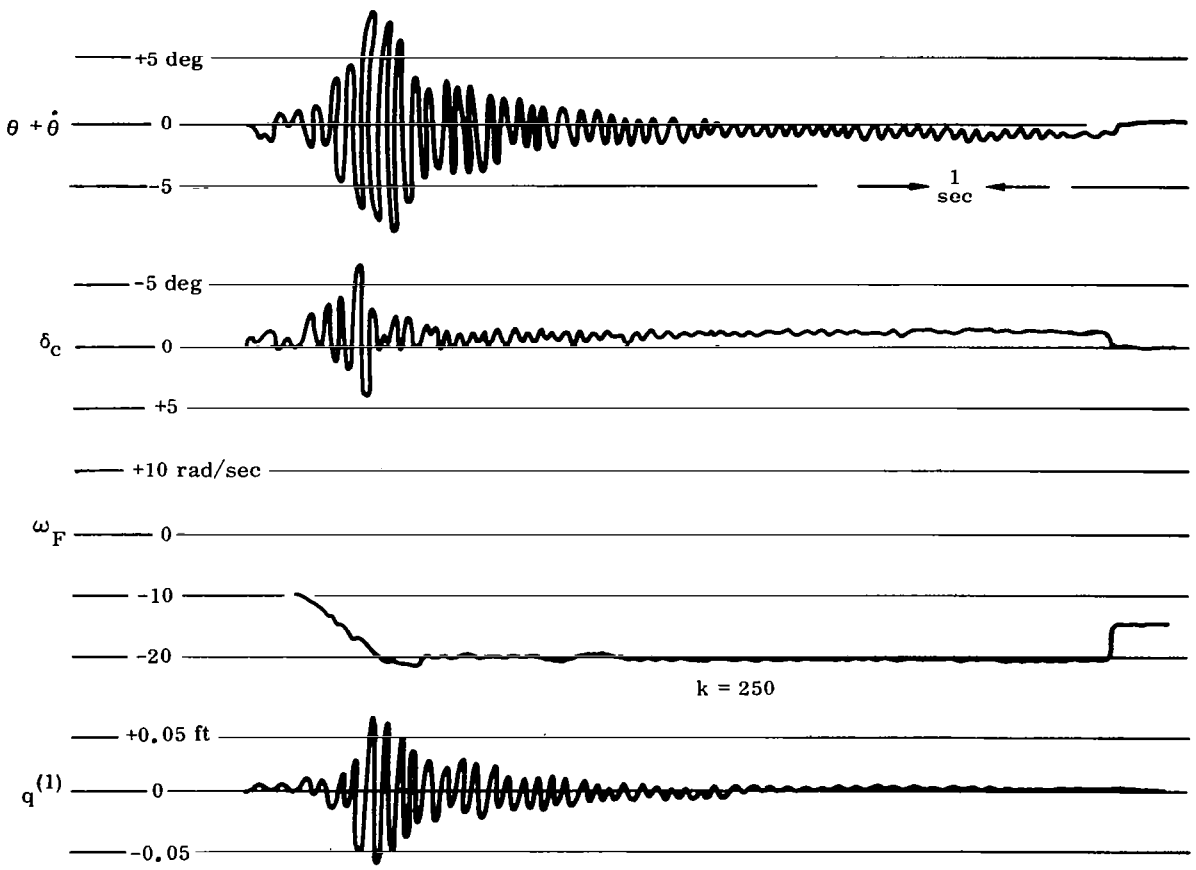

Figure 16. Analog Computer Trace, Initially Unstable Bending Mode

The filter was tuned to 10 rad/sec with the bending frequency at 23 rad/sec. (This simulates a bending frequency increase of greater than 100% in a step fashion. The bending was excited by a one-degree surface command.) The ω_F trace clearly demonstrates the tuning action. Referring to the trace of the bending mode, $q^{(1)}$, it can be seen that the bending is unstable with the filter not tuned to the bending frequency. The bending magnitude reached a maximum peak of ±0.09 foot while the filter was being tuned to the bending frequency. The filter output then canceled the bending oscillation sensed by the rate gyro and displacement gyro.

The double bending frequency component of the multiplier output is seen impressed on the ω_F trace. This term is greatly attenuated and does not present a problem.

The effect of varying the integrator gain, k, is shown in Fig 17. With k set at 400, the adaptive loop was marginally stable. In the lower trace, with k set at 150, the adaptive loop gain was too low, and consequently the tuning action was sluggish with considerable overshoot. The value of k = 250 used in the traces of Fig. 16 represents a compromise value, and results in a filter "lock on" time of approximately three seconds.

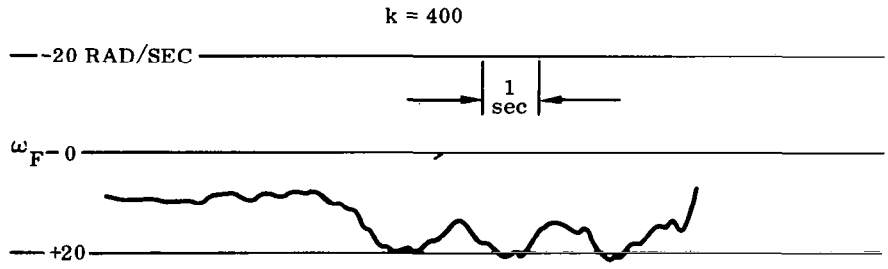

a. High Adaptive Loop Gain

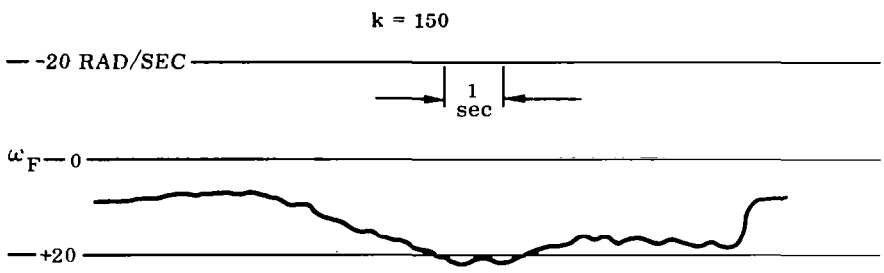

b. Low Adaptive Loop Gain

Figure 17. Effect of Variation in Integrator Gain, k

The operation of the filter when the vehicle is exposed to a random disturbance such as α gusts is shown in Figure 18. White noise was introduced into the α equation to simulate gust disturbances. The filter was offset to 10 rad/sec, and the bending frequency was 22 rad/sec. The filter tunes to the bending frequency and cancels the bending signal to prevent an unstable condition.

Remark: The phasor cancellation scheme exhibits excellent bending mode suppression characteristics when only one bending mode is significant. However, its performance deteriorates sharply when the bending mode frequency is very near the rigid body frequency. This results from the tendency of the filter to attenuate the short-period control frequencies as well as the bending mode components.

3.3 DIGITAL ADAPTIVE FILTER

As has been pointed out repeatedly, the essential problem in autopilot control of launch vehicles is the fact that signals reflecting the structural vibrations appear at the input to the control actuator. In many cases the phase relationships are such that the feedback loops amplify the magnitudes of these signals leading to catastrophic

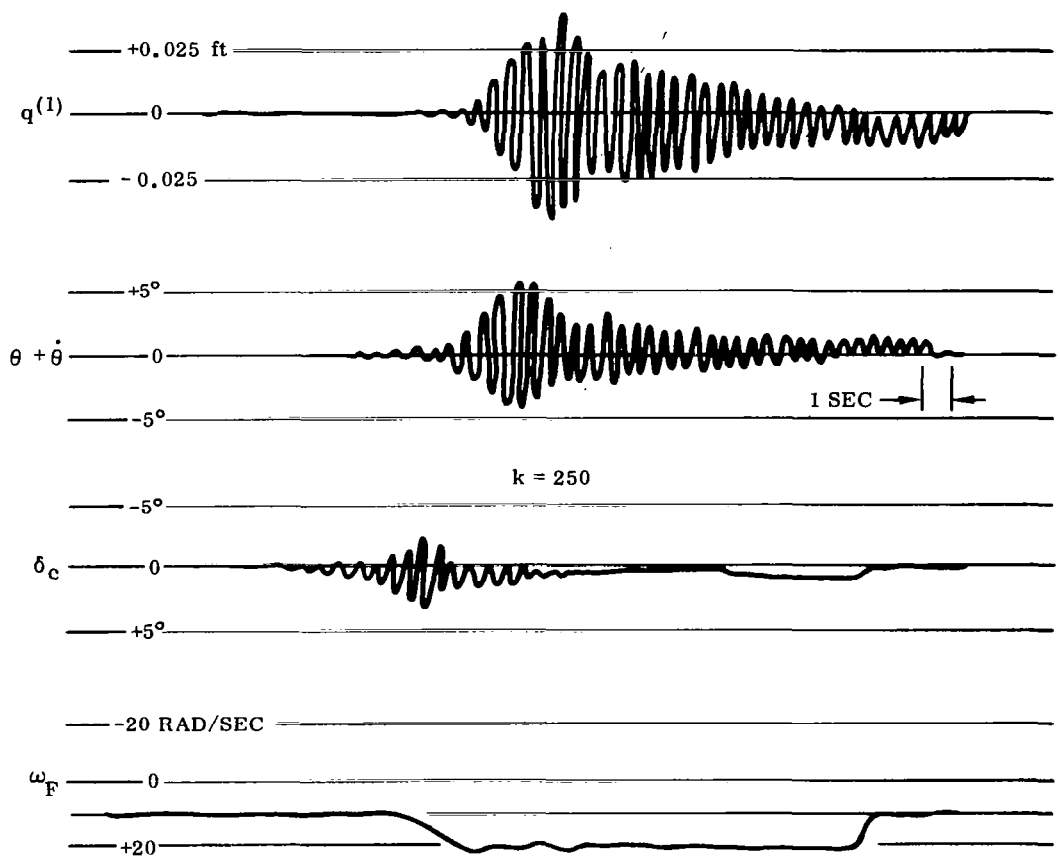

Figure 18. Analog Computer Trace, Response to Random Disturbance

instability. Because of the fact that the bending and rigid body (control) frequencies are not well separated, conventional passive filtering is not always effective. This is in a sense intuitively apparent since if there are no sharp distinguishing features between two groups of objects, the separation cannot be sharp; in short there is a large "grey" area.

As long as one thinks in terms of separating signals on a frequency basis alone, this dilemma remains. However, in a launch vehicle control system the bending and control frequencies, while in close proximity in a frequency sense, are usually widely separated in relative damping factor. Typically a control mode has $\xi = 0.6$ to 0.8 while for the bending mode $\xi = 0.005$ to 0.02. This fact forms the basis for an elegant and sophisticated scheme due to Zaborsky[6,7] which he termed Digital Adaptive Filtering.

The main idea involves identifying the dynamic modes in a given signal, after which the signal may be decomposed and expressed as a sum of individual modes. The effectiveness of this procedure requires that these modes be well separated in the s-plane; frequency characteristics, as such, play no unique role. After the signal decomposition has been accomplished, only predetermined modes may be passed on to the control system with the result that there is theoretically perfect suppression of undesired modes.

The crucial elements in this technique are the identification and decomposition features. It is appropriate, therefore, to motivate the discussion by considering the general aspects of this problem.

We assume that the transfer function for the system under consideration has the form

$$\left.\begin{aligned} \frac{V(s)}{U(s)} &= G(s) \\ &= \frac{\sum_{i=0}^{k} a_i s^i}{\sum_{i=0}^{n} b_i s^i} \\ &= K \frac{\prod_{i=0}^{k} (s - z_i)}{\prod_{i=1}^{n} (s - p_i)} \end{aligned}\right\} \quad (24)$$

The output v(t) and its first (n-1) derivatives have the initial values

$$\frac{d^i v(t)}{d t^i} = v^{(i)}(o)$$

$$i = 0, 1, 2, \cdots, (n-1)$$

One may then write the Laplace transform of the output as

$$V(s) = \left[\frac{\sum_{i=0}^{k} a_i s^i}{\sum_{i=0}^{n} b_i s^i}\right] U(s) + \frac{\sum_{i=0}^{n-1} v^{(i)}(o) \sum_{j=i+1}^{n} b_j s^{j-i-1}}{\sum_{i=0}^{n} b_i s^i} \tag{25}$$

The system input is written as

$$u(t) = \sum_{i=0}^{h} R_i t^i \tag{26}$$

or

$$U(s) = \sum_{i=0}^{h} \frac{i!\, R_i}{s^{i+1}} \tag{27}$$

Substituting this into Eq. (25) and taking a partial fraction expansion, we find

$$V(s) = \sum_{x=1}^{n-g} \frac{K_x}{s - p_x} + \sum_{w=1}^{g+h+1} \frac{D_w}{s^w} \tag{28}$$

where g is the order of the singularity of G(s) at s=0.

If there are y real poles and n-g-y complex poles, then the inverse Laplace transform of Eq. (28) becomes

$$v(t) = \sum_{x=1}^{y} K_x \epsilon^{p_x t} + \sum_{x=y+1}^{n-g} 2\,|K_x|\, \epsilon^{-\alpha_x t} \cos\left(\beta_x t + \angle K_x\right)$$

$$+ \sum_{w=1}^{g+h+1} \frac{D_w t^{w-1}}{(w-1)!} \tag{29}$$

Here the second summation extends over the complex poles in the upper half s-plane. For present purposes it is presumed that the form of v(t) as shown by Eq. (29) is known. However, the parameters

$$K_x \text{ and } p_x \qquad x = 1, 2, \cdots, y$$

$$\left.\begin{array}{l} K_x = |K_x| \angle K_x \\ \\ \text{and } p_x = -\alpha_x + i\beta_x \end{array}\right\} \quad x = (y+1), \cdots, (n-g)$$

$$D_w \qquad w = 1, 2, \cdots, (g+h+1)$$

are unknown. As shown above, these constitute a total of (2n-g+h+1) parameters.† In order to identify these, we may take a total of (2n-g+h+1) measurements of v(t), thereby giving the proper number of equations that in principle may be solved for the above unknowns.

A more feasible procedure from a practical point of view is to identify these parameters by means of a least-squares procedure.

Suppose for example we observe the M values (where $M > 2n - g + h + 1$)

$$v_m\left(t_{N-M+1}\right)$$

$$v_m\left(t_{N-M+2}\right)$$

$$\vdots$$

$$v_m\left(t_N\right)$$

and define the quantity

$$F\left(t_{N-M+1}\right) = W(i)\left[v_m\left(t_{N-M+i}\right) - v\left(t_{N-M+i}\right)\right] \tag{30}$$

where W(i) is an optional weighting factor. For example it might be desired to weigh recent measurements more heavily than others. Then the condition for a least-squares fit becomes

$$\underset{p_x,\, K_x,\, D_w}{\text{Min}} \sum_{i=1}^{M} F^2\left(t_{N-M+i}\right) \tag{31}$$

†One may without loss of generality assume that $b_n=1$ in Eq. (24) in which case the number of unknown parameters becomes 2n-g+h.

This leads to the (2n-g+h+1) equations

$$\frac{\partial}{\partial p_x} (\bar{F} \cdot \bar{F}) = 0 \qquad x = 1, 2, \cdots, (n-g) \tag{33}$$

$$\frac{\partial}{\partial K_x} (\bar{F} \cdot \bar{F}) = 0 \qquad x = 1, 2, \cdots, (n-g) \tag{34}$$

$$\frac{\partial}{\partial D_w} (\bar{F} \cdot \bar{F}) = 0 \qquad w = 1, 2, \cdots, (g+h+1) \tag{35}$$

the solution of which yields the (2n-g+h+1) unknown parameters, p_x, K_x, D_w.

However, the set of equations (33) - (35) is nonlinear, and their solution, even by computer, is a formidable task. We may take the point of view that identification is periodically repeated at judiciously selected intervals such that approximate values for p_x, K_x, and D_w are known. In this case we write

$$\begin{aligned} p_x &= p_{xN} + \Delta p_x \\ K_x &= K_{xN} + \Delta K_x \\ D_w &= D_{wN} + \Delta D_w \end{aligned} \tag{36}$$

where the p_{xN}, K_{xN}, D_{wN} are initial estimates and the $\Delta(\ )$ quantities are assumed small. The value of v(t) at some generic time t_k is then given by

$$v\left(t_k\right) = v^*\left(t_k\right) + \sum_x \frac{\partial}{\partial p_x} v^*\left(t_k\right) \Delta p_x + \sum_x \frac{\partial}{\partial K_x} v^*\left(t_K\right) \Delta K_x + \sum_w \frac{\partial}{\partial D_w} v^*\left(t_k\right) \Delta D_w \tag{37}$$

where the asterisk signifies that the nominal (subscript N) parameters are used. Using (36) and (37), the set of equations (33) - (35) are linear and may be solved for Δp_x, ΔK_x, and ΔD_w, thereby determining updated values for p_x, K_x, and D_w.

Once the present values of p_x, K_x, and D_w are known, Eq. (29) completely determines the signal v(t). Furthermore, Eq. (29) determines this signal as a sum of its individual components. Any component or any group of components can then be

separated from the signal v(t) by computing in real time a partial sum which includes only the desired components. This separation of the signal components can best be done on a digital computer. The output of the digital computation can then be converted, in line, to an "analog" form and used to replace the actual v(t) for the purposes of control. By this process it is possible to restrict the composition of the control signal to only the desired modes of response; for example, the rigid body modes of a missile. All other modes, such as the elastic modes, can be filtered out simply by leaving them out of the summation of Eq. (29) as carried out on the computer. Clearly this filtering operation should be effective for filtering any modes for which the roots of the characteristic equation, p_x, are separated by a large distance in the s-plane. It is not required that the frequencies be different; only the total distance counts. In fact, two modes of the same frequency are effectively filtered if their damping is quite different.

The digital instrumentation of the operation described in the preceding section is sketched in Fig. 19. An analog-to-digital converter samples and digitizes the measured continuous signal v(t) every T seconds. The present sample is v(NT) where N is the total number of samples from the beginning of the operation. A fixed number M of the most recent samples is stored in the digital computer. When a new sample arrives, it is put at the first address, the other samples are shifted to the left by one place, and the oldest sample in the memory is dropped. An equal number of samples produced by the computer which represents the present fitted curve is stored in the

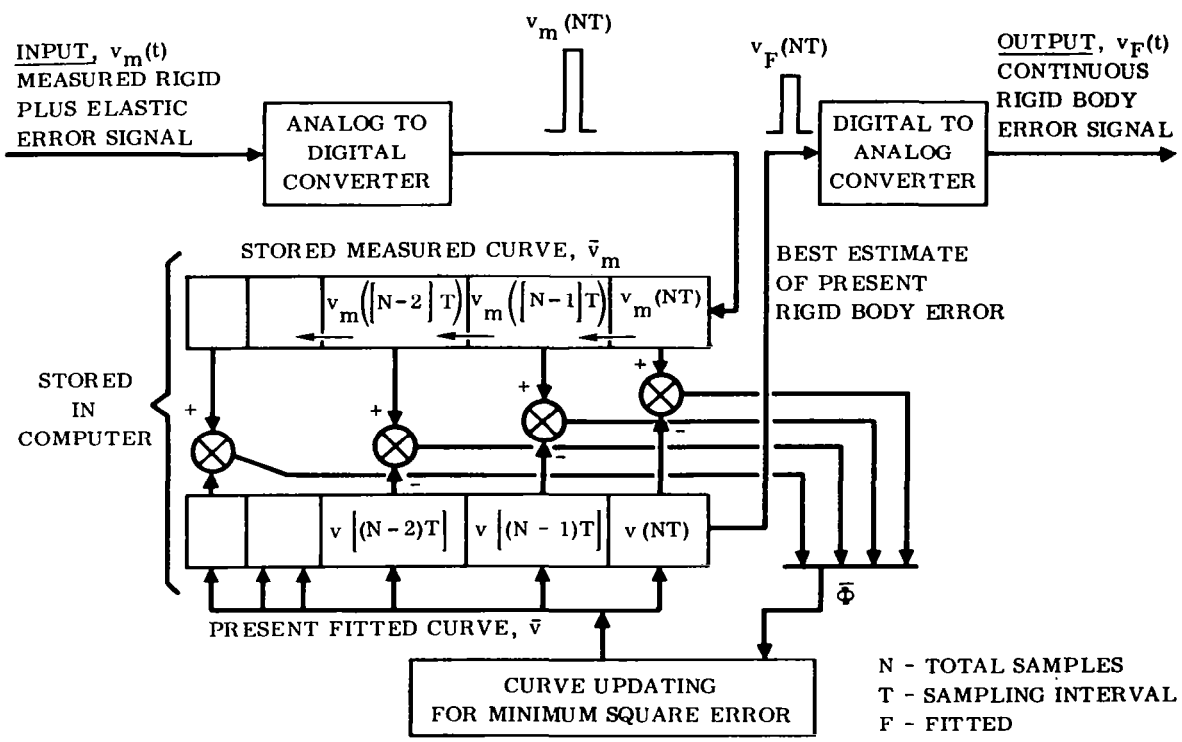

Figure 19. Schematic of Digital Adaptive Filter

block below. These latter samples are computed from the present best estimates of the parameters p_x, K_x, and D_w (denoted by p_{xN}, K_{xN}, and D_{wN}) and jointly represent the sampled form over the last $\tau = MT$ seconds of the v(t) or $v(t; p_x, K_x, D_w)$ signal of Eq. (29) through (37). The difference of signals v(t) and $v_m(t)$ over the last $\tau = MT$ seconds,

$$\Phi(t) = v(t) - v_m(t) \tag{38}$$

is used to determine through an inversion of Eqs. (33) - (35) the new estimate p_{xN+1}, K_{xN+1}, and D_{wN+1} by Eq. (36). More precisely, the operation is digital, involving the sampled form of $\Phi(t)$, the difference of the samples in the two blocks of Fig. 19. These sets of samples can be represented as vectors or column matrices:

$$\bar{\Phi} = \bar{v} - \bar{v}_m \tag{39}$$

with coordinates

$$\begin{aligned} \Phi_i &= \Phi\left[(N - M + i)T\right] \\ &= v\left[(N - M + i)\,T\right] \\ &\quad - v_m\left[(N - M + i)\,T\right] \end{aligned} \tag{40}$$

Naturally, Eqs. (33) - (35) are also set up and inverted in a discrete and digital version. Once the new estimate p_{xN+1}, K_{xN+1}, and D_{wN+1} is obtained by the computer from the discrete versions of Eqs. (33) - (35) and (36), then the updated samples $v\left[(N-M+i)T\right]$ for the lower memory block in Fig. 19 can be obtained from Eq. (29) and the digital computer is ready to take in the next sample of $v_m(NT)$ and repeat the outlined cycle. Simultaneously the computer has also obtained such a partial sum of Eq. (29) that consists of those modes only which comprise the desired filtered signal $v_f(NT)$. This latter is fed through a digital-to-analog converter directly to the control system and the airframe. Note that, ideally, this operation completely suppresses the undesirable components of the signal; the filtering is perfect.

The application of the above ideas to a typical launch vehicle autopilot is shown in Fig. 20.

While the complete signal decomposition and digital filtering process can be successfully instrumented with high-speed airborne computers, it undoubtedly puts considerable demands on the computer. Thus the process should be simplified.

This simplification can be achieved if the plant output signal v(t) contains a predominant desired mode or modes that are damped at a much faster rate (approximately $\xi = 0.7$) than those signal components to be suppressed (approximately $\xi = 0.005$).

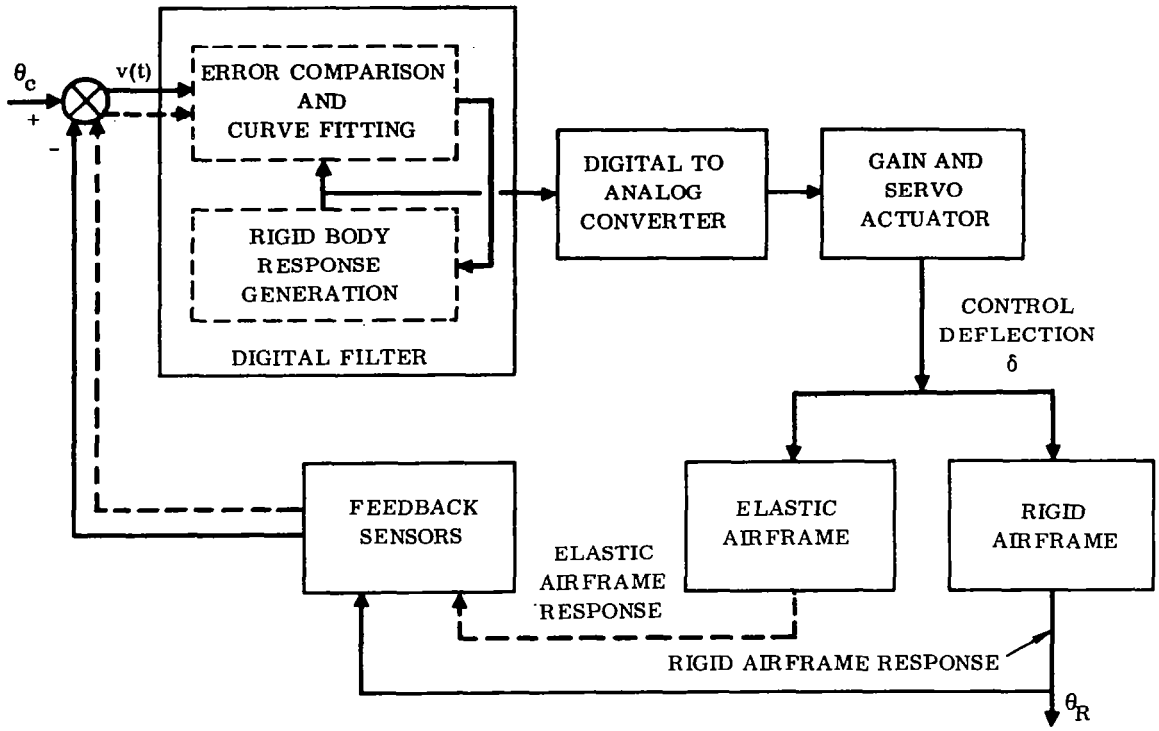

Figure 20. Application of Digital Adaptive Filter to Launch Vehicle Autopilot

Let it be assumed that $p_{1,2} = -\alpha \pm j\beta$ represents a damped oscillatory (rigid body) mode that comprises $v'(t)$, the desired part of the input signal. Then from (29)

$$v'(t) = 2\,|K_1|\,\epsilon^{-\alpha t}\cos\left(\beta t + \angle K_1\right) \tag{41}$$

$$= A\,\epsilon^{-\alpha t}\cos\beta t + B\,\epsilon^{-\alpha t}\sin\beta t$$

where the constants A and B replace $|K_1|$ and $\angle K_1$. The total input signal is

$$v(t) = v'(t) + v''(t) \tag{42}$$

where $v''(t)$ denotes the undesired portion of $v(t)$.

Assuming that (41) represents the predominant portion of $v(t)$, the problem reduces to one of identifying A, B, α, and β by suitable measurements and computer computations.† This operation is to be performed each time a sample is received; the updated values are available by the time the next sample arrives. It has been found,

†Actually it can be shown that the desired portion of $v(t)$ can be readily identified even if the undesired portion, $v''(t)$, is not negligible, providing that the relative damping of the latter is small compared to $v'(t)$. See Ref. 14.

however, that α and β change very slowly and may be estimated at more widely separated intervals than A and B. Accordingly we will describe in detail the estimation procedures for A and B (α and β assumed known and invariant) only. The four-parameter estimation procedure is identical in principle, involving merely a more complicated "bookkeeping."

From Eqs. (37) and (41) we have

$$v'(t) \approx v(t) = A_N \epsilon^{-\alpha t} \cos \beta t + B_N \epsilon^{-\alpha t} \sin \beta t + \left(\epsilon^{-\alpha t} \cos \beta t\right) \Delta A + \left(\epsilon^{-\alpha t} \sin \beta t\right) \Delta B \tag{43}$$

where A_N and B_N are the current estimates of A and B respectively. Suppose we have available M measurements, denoted by the vector

$$\bar{v}_m = \begin{bmatrix} v_m\left(t_{N-M+1}\right) \\ v_m\left(t_{N-M+2}\right) \\ \vdots \\ v_m\left(t_N\right) \end{bmatrix} \tag{44}$$

In the present case the set of equations (33) - (35) becomes

$$\frac{\partial}{\partial(\Delta A)} \sum_{i=1}^{M} F^2\left(t_{N-M+i}\right) = 0 \tag{45}$$

$$\frac{\partial}{\partial(\Delta B)} \sum_{i=1}^{M} F^2\left(t_{N-M+i}\right) = 0 \tag{46}$$

These two equations, which are linear in ΔA and ΔB, may be readily solved for ΔA and ΔB, giving the new estimate

$$A_{N+1} = A_N + \Delta A \tag{47}$$

$$B_{N+1} = B_N + \Delta B \tag{48}$$

When the next measurement, $v_m(t_{N+1})$, becomes available, the process is repeated using the new estimates above and the measurements, $v_m(t_{N-M+2})$, $v_m(t_{N-M+3})$, $\cdots$, $v_m(t_{N+1})$.

In a typical launch vehicle application of the form shown in Fig. 20, v(t) is the total error signal, containing the rigid body, bending, and other modes. The digital filter output consists essentially of the rigid body portion of v(t) as shown in Eq. (41). Subtracting this from the total command error results in a signal that consists essentially of the signal components associated with the elastic oscillations.

It is then feasible to close the loop for the v_r signal through a compensating network, as shown in Fig. 21, that is designed for optimum rigid body response while excluding for the purpose of this design the elastic poles and zeros from G(s). Conversely the loop is closed for v_e through a compensation designed for optimum damping at the bending modes while disregarding for this design the rigid body poles and zeros in G(s). If the v_e control branch is omitted, the bending modes will oscillate open loop and attenuate with the small structural damping. In this latter case the digital filter simply prevents closed-loop excitation of the bending modes which might make them unstable.

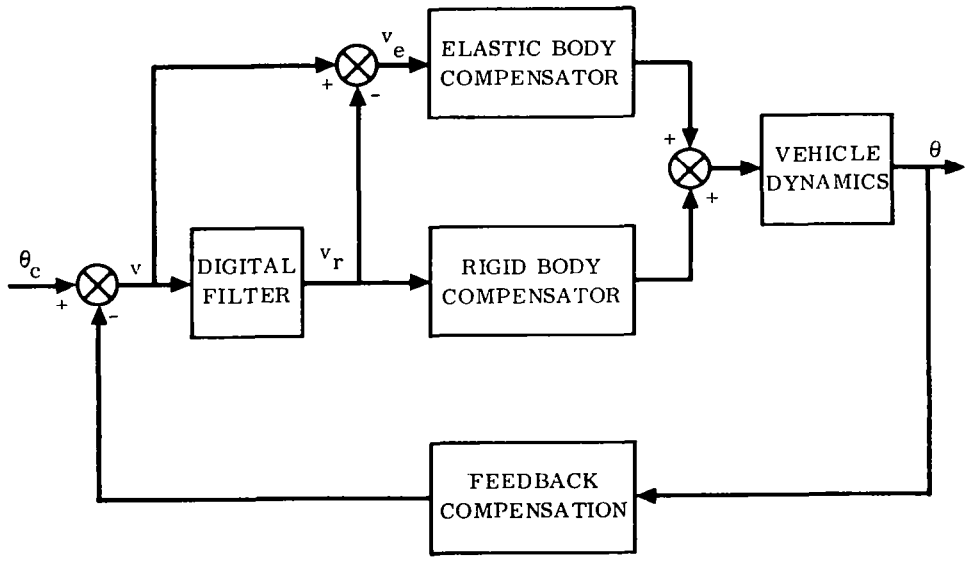

Figure 21. Basic Configuration for Signal Decomposition by Digital Filtering

The operation of a typical launch vehicle autopilot employing the configuration of Fig. 20 is shown in Fig. 22, which illustrates the response to a one-degree step command. It is apparent that there is firm control of the vehicle as long as there is a component in the error corresponding to the predominant rigid body modes; that is, as long as there is a transient. As the transient signal dies out, however, the digital

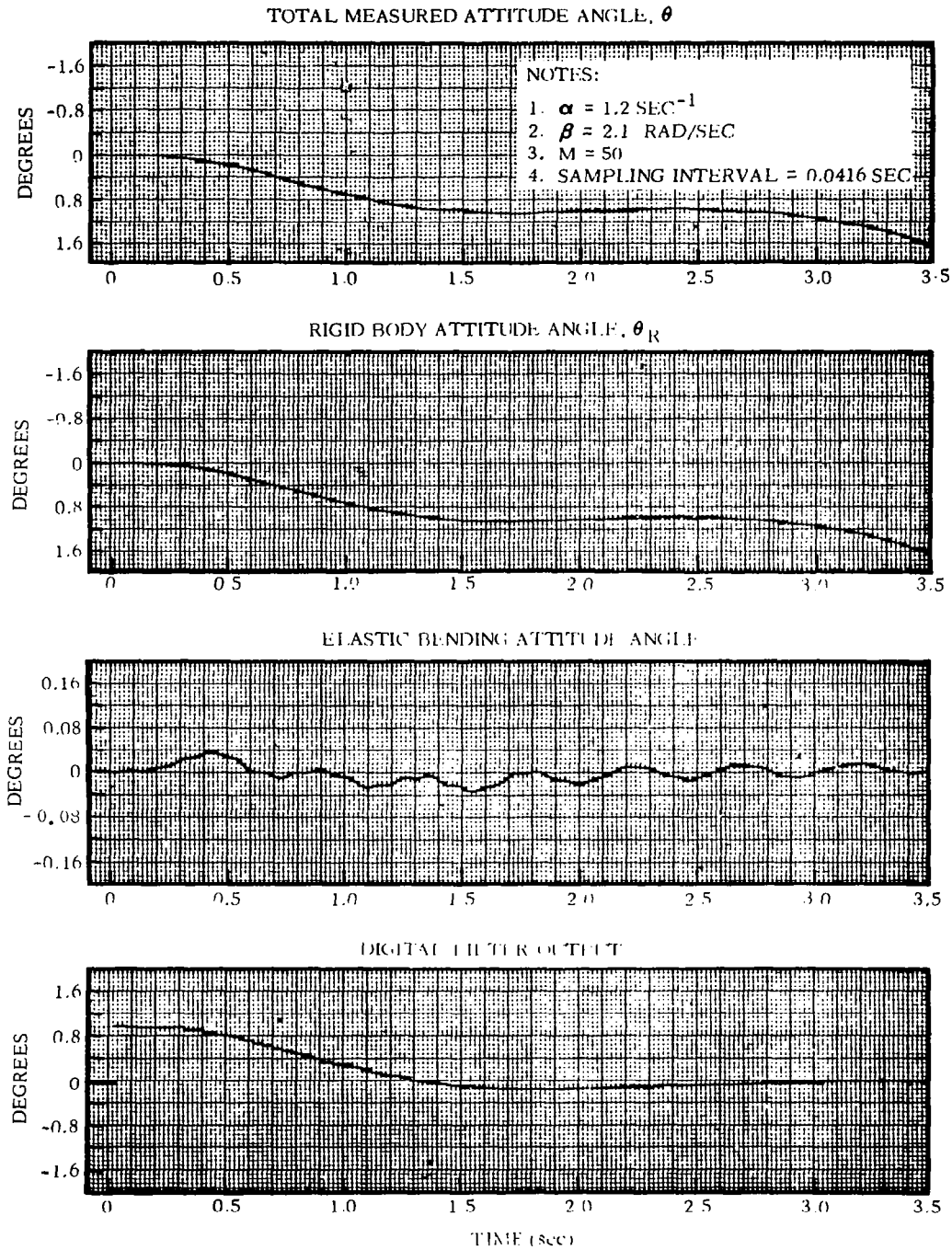

Figure 22. Basic Transient Response to One-Degree Step Attitude Command

filter output fades out and the control loop for the airframe opens. This loss of control is especially objectionable when the airframe is aerodynamically unstable.

This feature represents the major problem in the application of the digital adaptive filter to launch vehicle control systems. The difficulty is that the digital adaptive filter in effect closes the loop for the rigid body transient response but keeps the loop open for the body elastic oscillations and all other signals. This open-loop operation is the desired condition as far as the body elastic oscillation is concerned. However, there are desired signals, such as guidance commands and feedback signals resulting from wind shear, that must be transmitted just as the rigid body transients are transmitted. The frequency band of these signals is usually significantly lower than the frequency of the rigid body transient. In order for the control system to respond to these desired signals, the signal rejected by the digital adaptive filter (residual) may be passed through a secondary filter as illustrated in Fig. 23. This filter will have a low cutoff frequency so that it will adequately pass slowly varying command signals yet suppress the elastic oscillations. Analysis indicates that a conventional linear filter may be suitable for this secondary filtering operation. The combination of the digital adaptive filter and secondary filter will then transmit the desired component of the total error signal but will reject body bending oscillations.

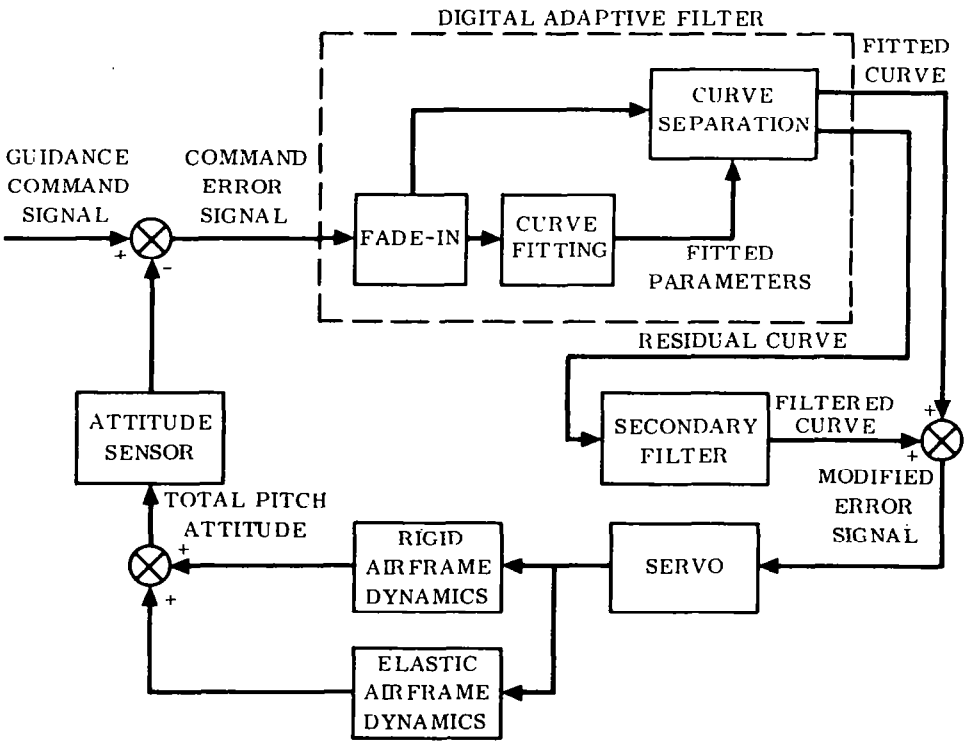

Figure 23. Block Diagram of Vehicle Control System with the Digital Adaptive Filter and Secondary Linear Filter

With a secondary filter added in the manner shown in Fig. 23, the system whose response is illustrated in Fig. 22 now exhibits the response shown in Fig. 24. It is apparent that there is no longer any loss of control. For best operation the secondary filter is cut in when the digital filter output reaches a predetermined level (at approximately 2 seconds in Fig. 24). This cut-in time is not critical; there would be similar results with a ±50% tolerance on this value.

The response shown in Fig. 24 combines the speed and accuracy of the digital filter control shown in Fig. 22 with the steady-state stability of the secondary filter. A small-amplitude residual oscillation with the low predominant frequency of the sluggish secondary filter can be observed in Fig. 24 but the overall response is still nearly ideal.

In Figs. 22 and 24 the system, including the bending modes, was initially at rest at time $t = 0$ when the step input was applied. Fig. 25 shows the system response when the three bending modes are already oscillating with a rather high amplitude at the time of applying the step input command. It can be observed in Fig. 25 that the digital filter output curve regains its clear damped sinusoidal form after the first quarter cycle, although in the total error, $v(t) = 1 - \theta(t)$, the rigid body mode is nearly swamped by the presence of the elastic oscillations. During the first quarter cycle of approximately 0.5 second the input data are insufficient for positive identification of the rigid body mode; consequently some of the bending signal component is seen in the digital filter output during this period. Comparison of the digital filter output in Figs. 22 and 24 reveals that the presence of body bending oscillations does not cause significant deterioration in the rigid body response. The bending modes still oscillate essentially with open-loop frequency and damping. Different amplitude selections of the initial bending oscillations will have varying effects on the late part of the system response but the transient remains essentially unaffected as long as the bending amplitude does not much exceed half the amplitude of the step command.

What would happen in the case shown in Fig. 25 if no digital filtering were incorporated in the control system is revealed by Fig. 26. Comparison of Figs. 25 and 26 makes it possible to appreciate the effect of the digital filter with signal decomposition in stabilizing the bending modes.

Instead of using a secondary filter, another possible solution to the loss-of-control problem can be the periodic restarting of the fitting process. This simply consists of periodically resetting the length of the fitting interval to $M = 1$ sample in the computer. Then the computer raises this number one sample at a time until M_{max}, the ultimate length of the fitting interval, is reached. Such restarting will assure the continuous supply of small transients because there always will be some small error at the instant of restart. This initial error is then eliminated by the control action. The resulting sequence of successive small transients will assure continued stability. It also assures the step-wise following of any continuous control signals θ_c that may be

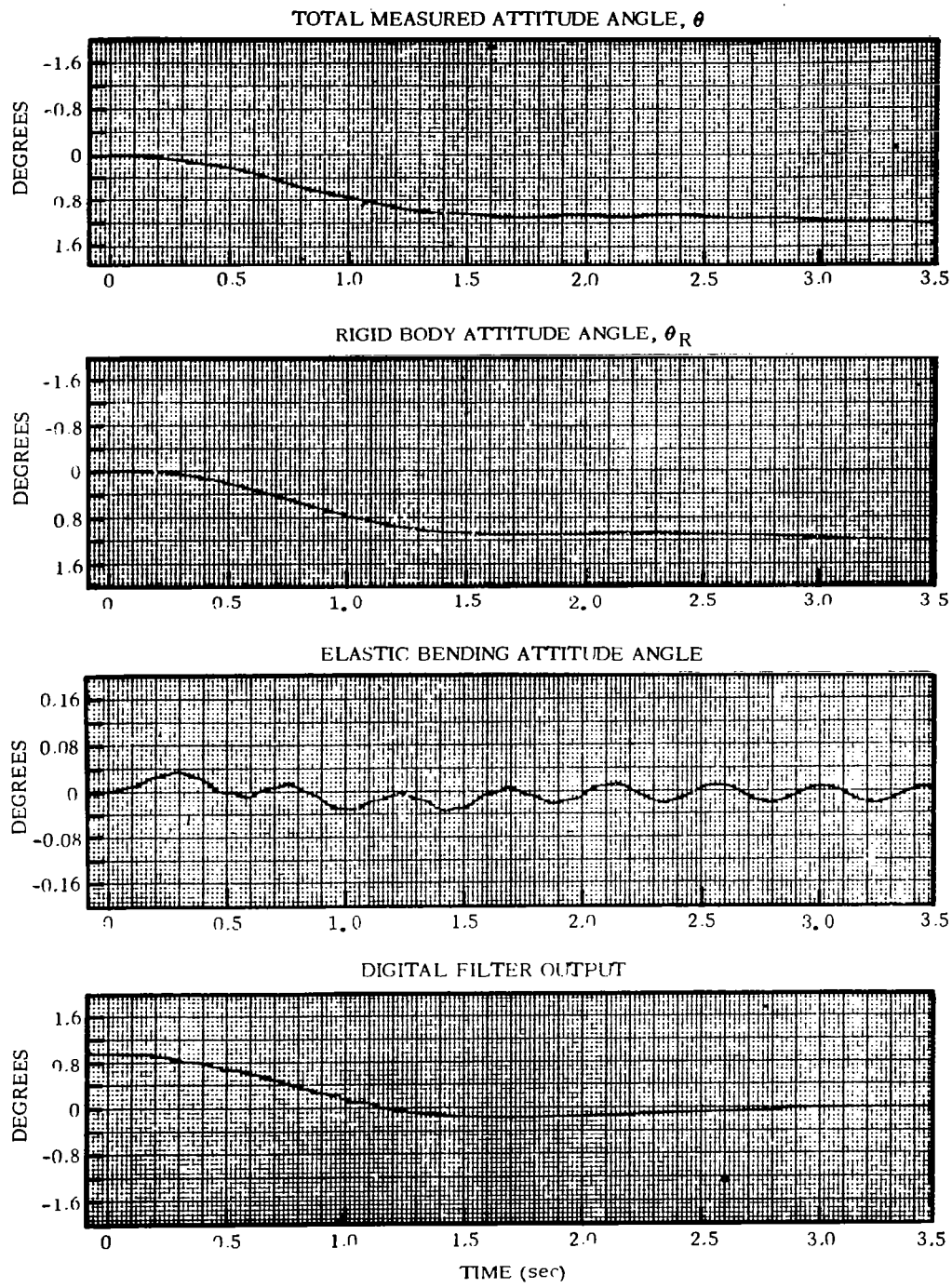

Figure 24. Basic Transient Response as in Figure 22 But Control Transferred to Secondary Filters at t = 1.96 Sec

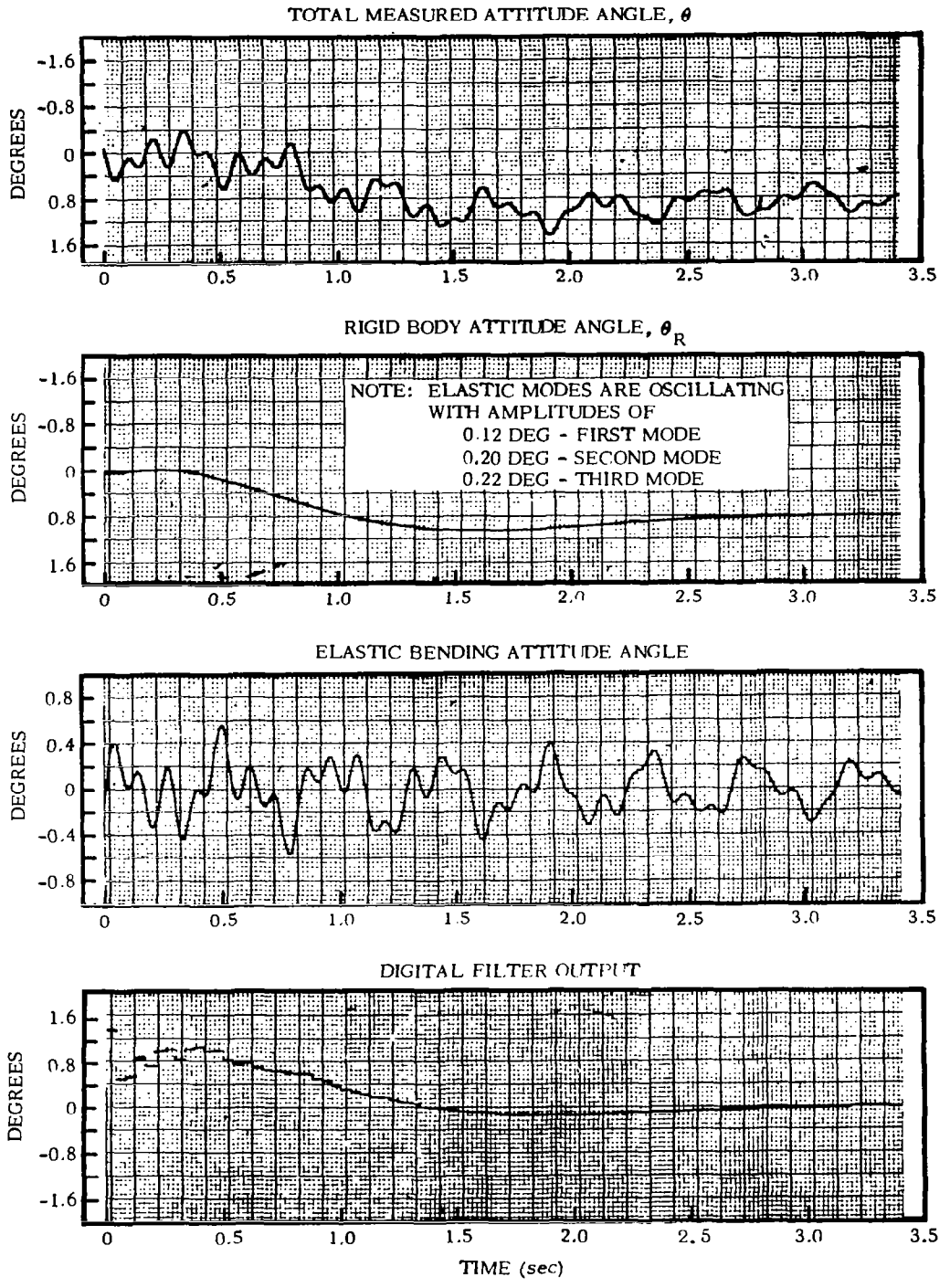

Figure 25. Basic Transient Response as in Figure 22, But with Applied Step

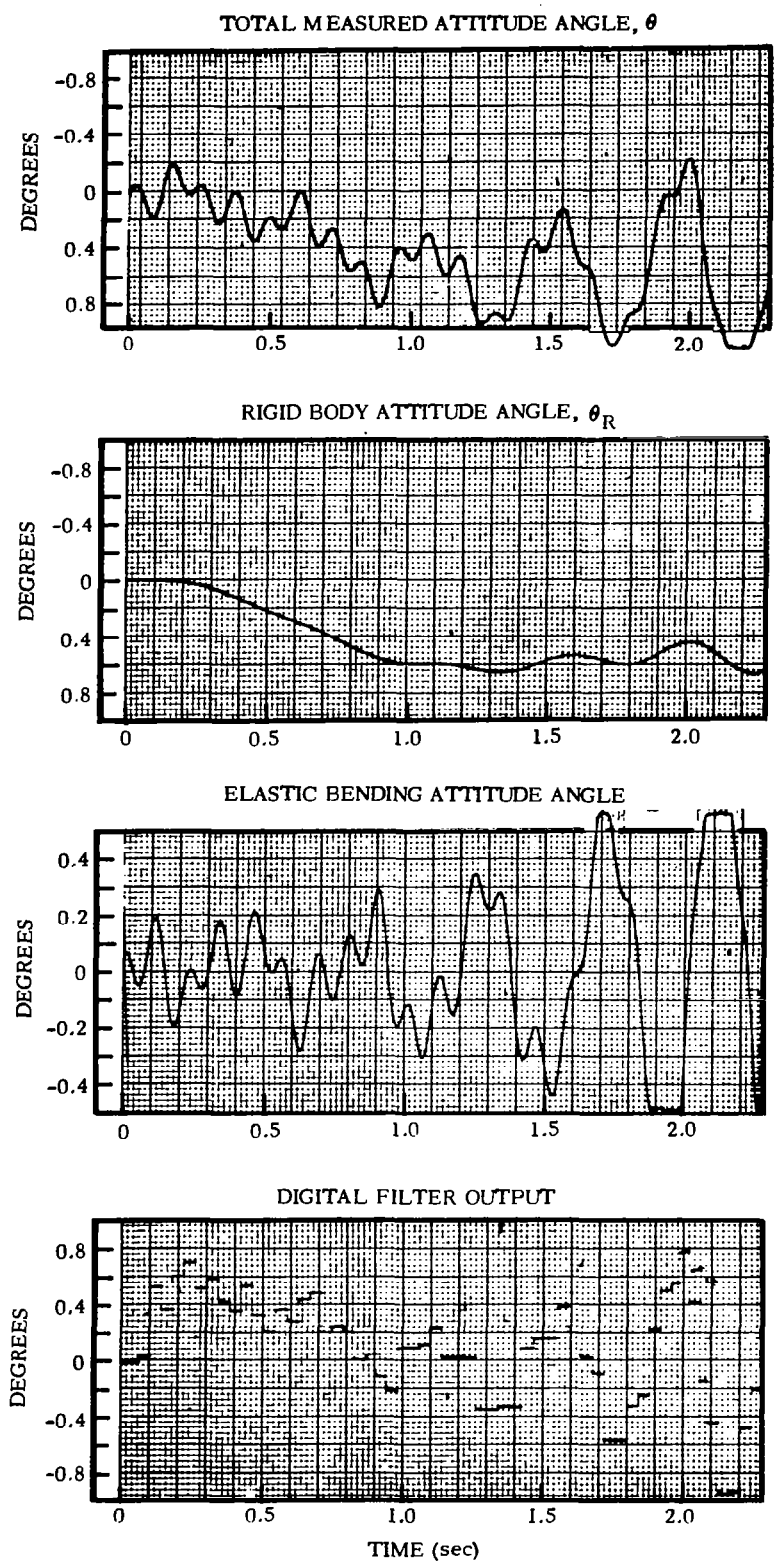

Figure 26. Transient Response as in Figure 25, But Digital Filter Replaced by Unity Gain

present. Discontinuities in the command θ_c or its lower derivatives must be monitored. Such discontinuities mark the start of new transients and should occasion the switching to $M = 1$ and the ensuing development of a new fitting cycle.

The discussion in the preceding paragraphs assumes that the length of the fitting interval is stationary; that is, the length of fitting interval does not change from one sample to the next. This type of operation is only justified if the entire fitting interval is filled with a single branch of a transient. Consequently the length of the fitting interval must be made variable when new transients start. Immediately after the start of a new transient, the fitting interval will be only one sample. Then the fitting interval will gradually increase until it reaches the length of the desired stationary fitting interval. This transition is referred to as the fade-in period.

Two problems arise in conjunction with the fade-in period: 1) it is necessary to somehow identify the start of a new transient branch and 2) the quality of curve fitting during the fade-in period must be investigated.

For a detailed discussion of this, we must refer the reader to Zaborsky's report[6].

The performance of the Digital Adaptive Filter in a launch vehicle control system was extensively investigated via computer simulation[6]. Some of the results are shown in Figs. 27 through 34. The control configuration is as shown in Fig. 23 where the secondary filter is a simple first-order lag with a cutoff frequency equal to one-fourth of the lowest rigid body frequency. The sampling interval in the Digital Adaptive Filter was normalized to unity when the number of samples per closed-loop rigid body cycle is equal to 25.

Fig. 27 illustrates the system response to a unit step input when the vehicle is completely rigid (no bending modes). Curve fitting in the digital computer is based on two parameters, A and B. The response consists of an almost pure second-order sinusoid. It is easy to see that this case is handled smoothly and effectively by the Digital Adaptive Filter. The amplitudes, A and B, decay to zero, of course, as the error signal approaches zero.

The same case with one bending mode added is shown in Fig. 28. The rigid body is still controlled in a well-damped second-order mode while the bending mode operates essentially open loop with a slight structural damping, as shown by the command error signal curve. Note that the rigid body control remains tight and stable even when the bending oscillation greatly exceeds the rigid body component.

The response to an alternating step input is shown in Figs. 29 through 31. The time period between successive step inputs was varied from 100% to 50% of the closed-loop rigid body period. An elastic mode oscillation of twice the closed-loop rigid body

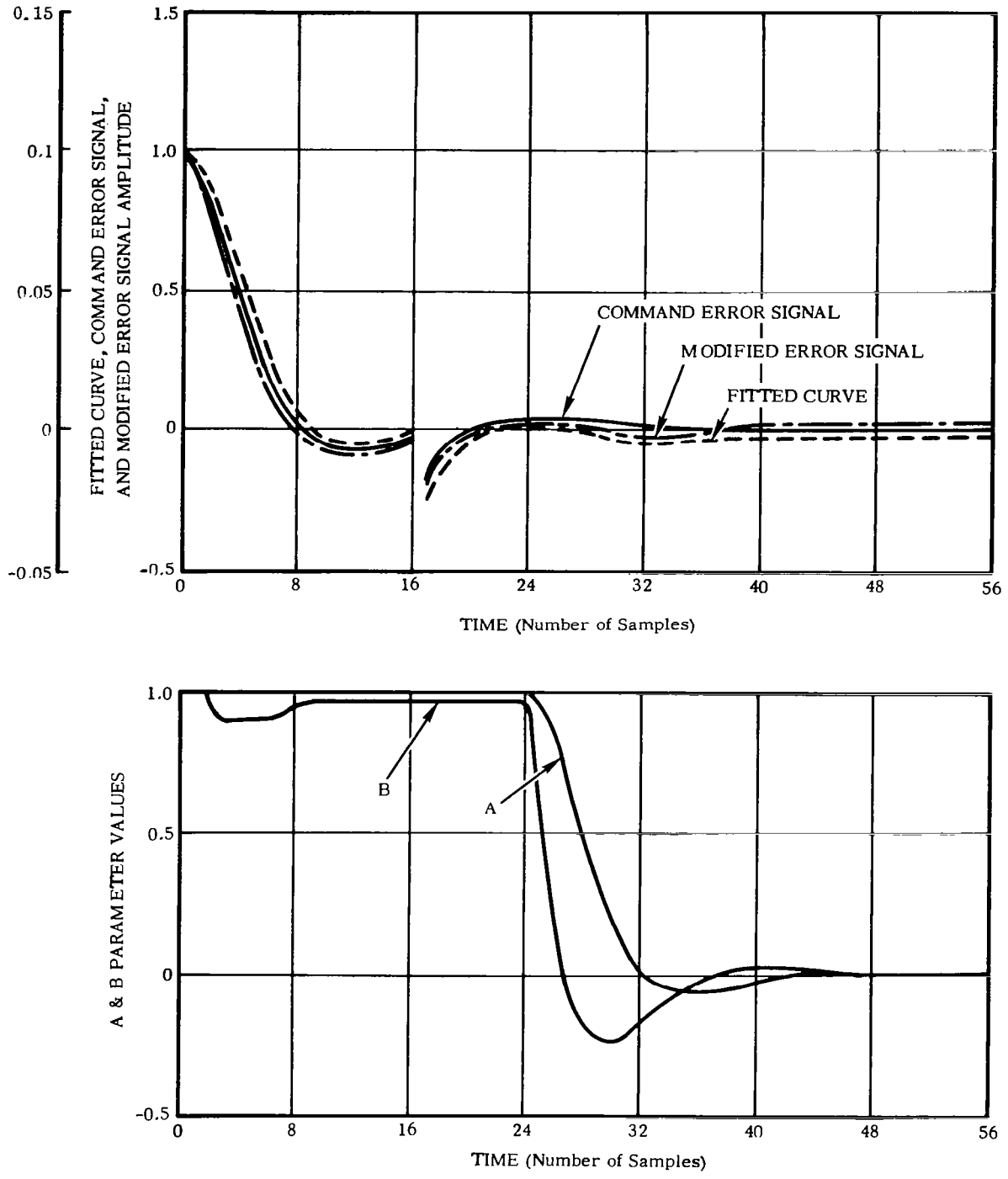

Figure 27. Control System Error Response to a Unit Step Input

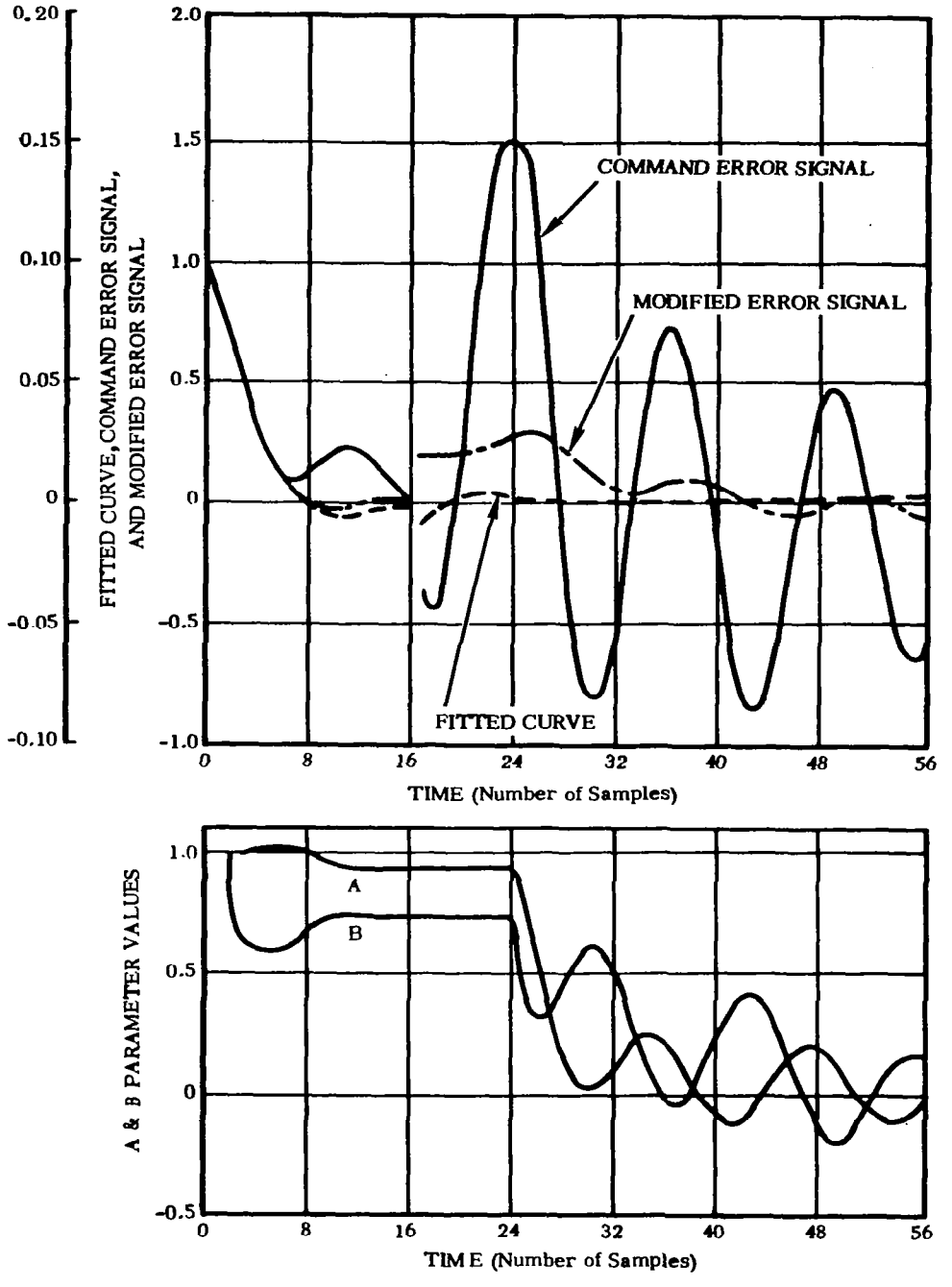

Figure 28. Response to a Unit Step Input (Bending Mode Added)

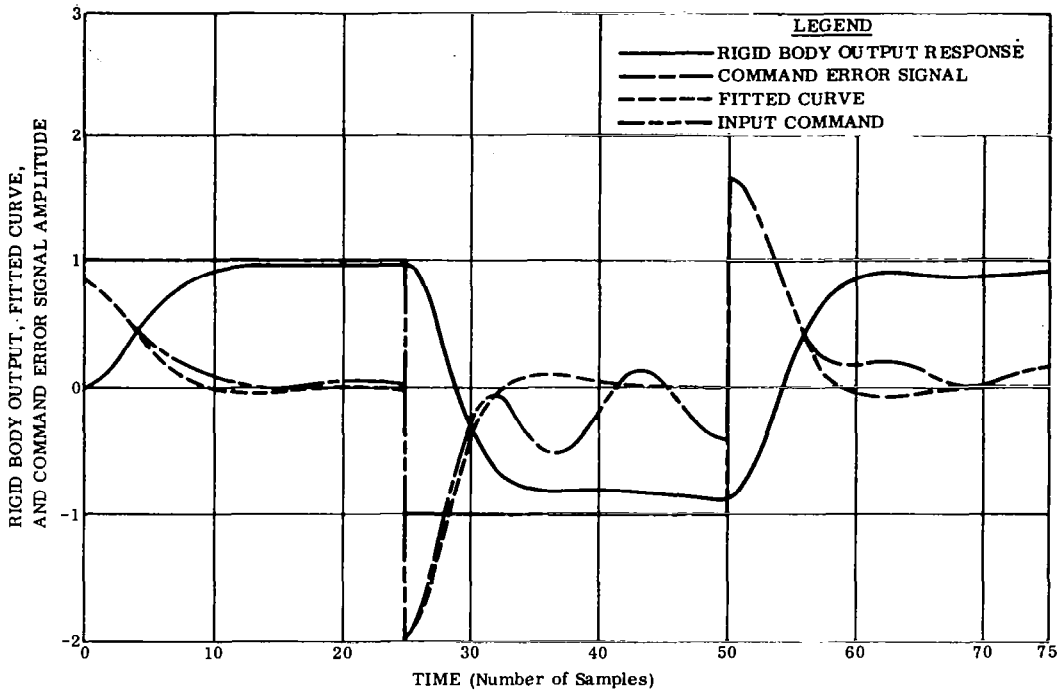

Figure 29. Response to an Alternating Step Input with a Half-Period of 25 Samples

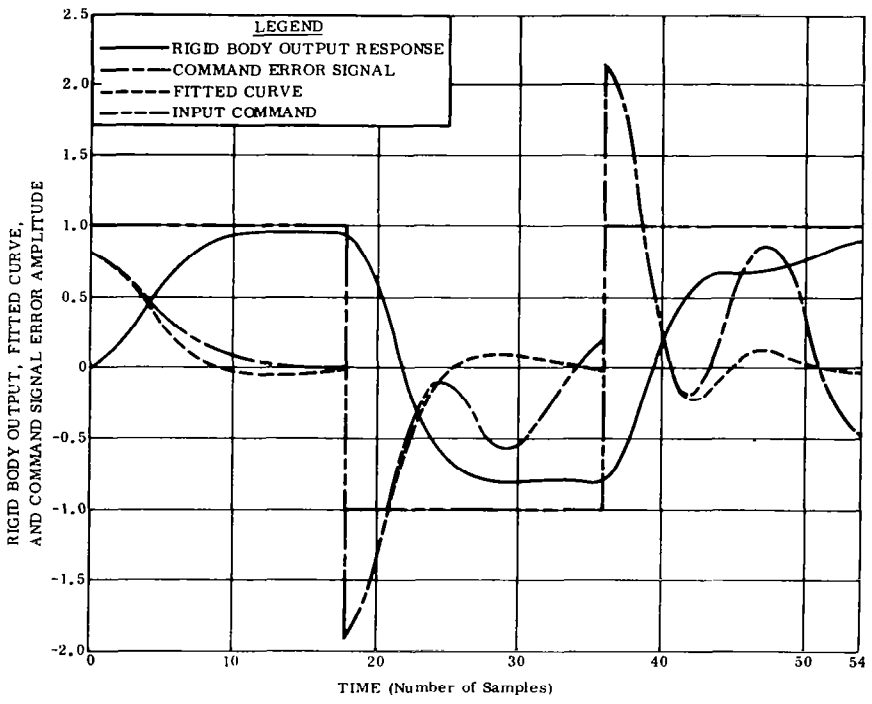

Figure 30. Response to an Alternating Step Input with a Half-Period of 18 Samples

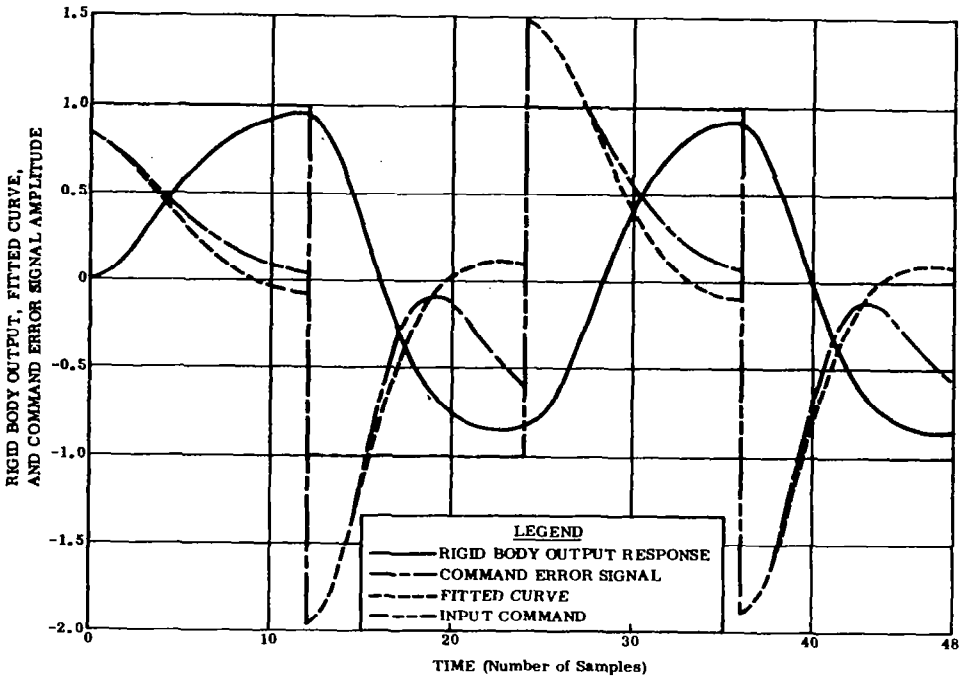

Figure 31. Response to an Alternating Step Input with a Half-Period of 12 Samples

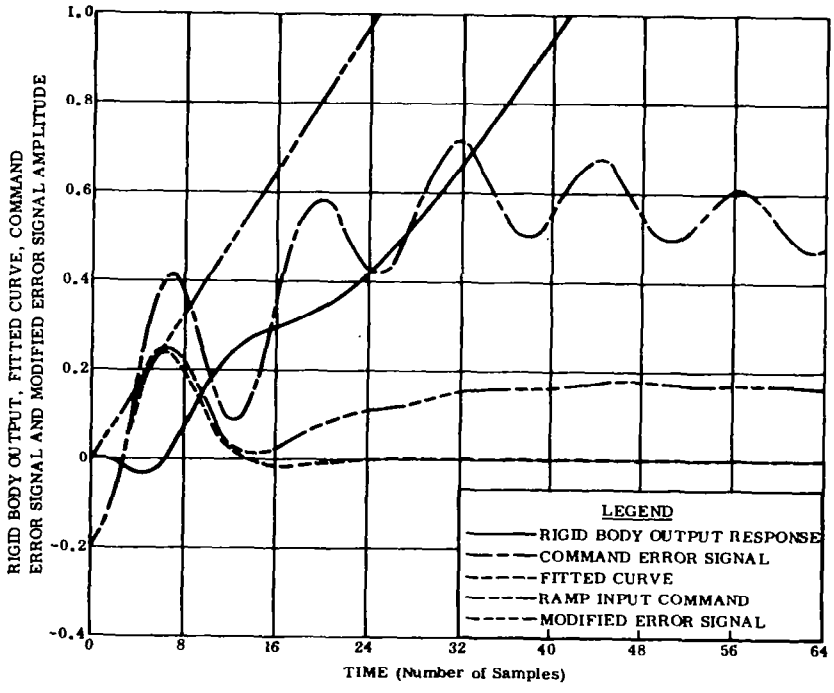

Figure 32. Control System Response to a Ramp Command Input

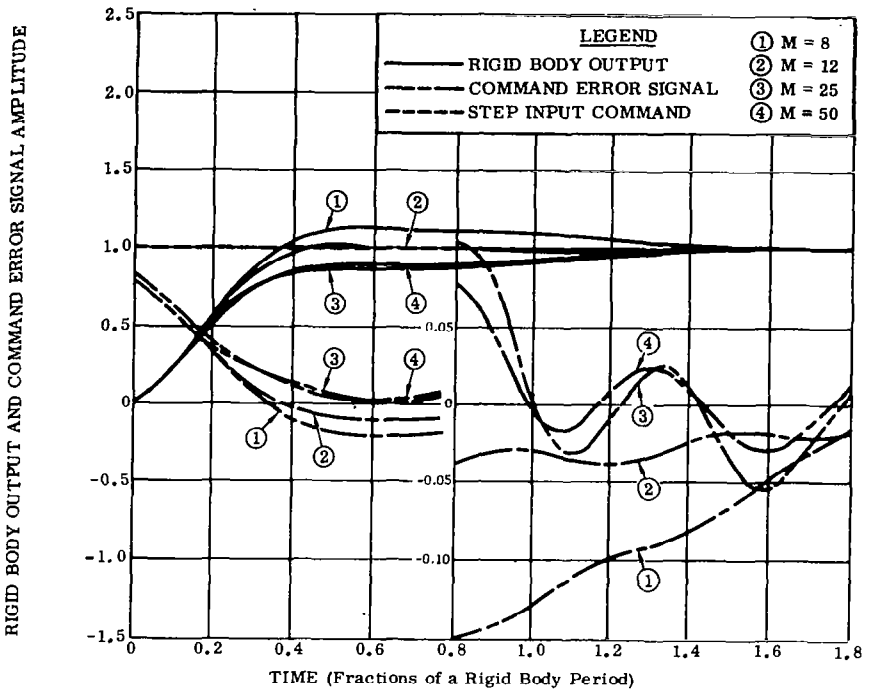

Figure 33. Control System Response with Variation in Sampling Rate Per Rigid Body Cycle

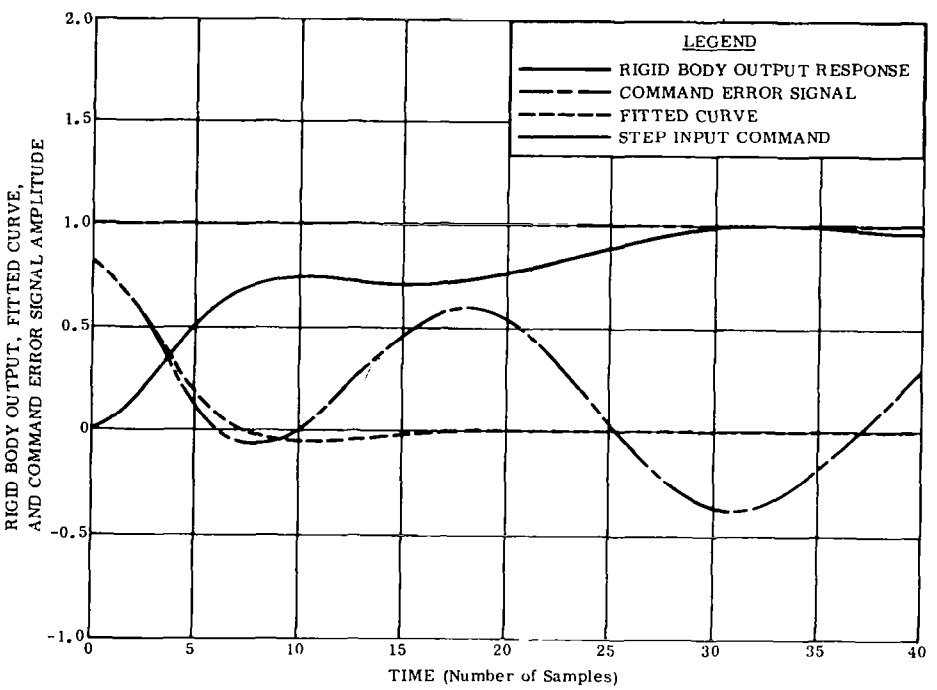

Figure 34. Control System Response with Body Bending Frequency Equal to Rigid Body Frequency

frequency with a 0.05 damping ratio and an initial condition of 0.2 times the amplitude of the command input signal was present in these runs. In Fig. 29 the period of the input is long enough so that the fitted curve is completely determined. In Figs. 30 and 31 the curve fitting process is interrupted by the alternating input. It may be seen that the rigid body output response remains stable and tight. The noticeable increase in the body bending component shown in the command error signal of Fig. 30 at the initiation of several of the new step inputs is attributed to two facts:

a. The curve fitting process does not start until the fourth sample, thus allowing a new unfiltered excitation to the bending mode.

b. The phase relationship between the bending frequency and the input is less favorable to curve fitting as each succeeding step is applied.

Note that the succeeding steps of Fig. 31 do not produce the same trend.

Fig. 32 shows the response to a ramp input. Since the system used here has only one integration in the open loop, a steady-state error will develop in the rigid body output response. This is clearly observed in the figure. Also apparent is the fact that the rigid body output increases smoothly in one cycle (25 samples) to the steady-state condition. This indicates that the digital filter separates the correct "fitted curve" from a "command error." Although the fitted curve goes to zero, a residual error signal is transmitted through the secondary filter so that the modified error signal is not zero and the system continues to follow the ramp command.

The time required to establish a "fitted output" depends strongly on the number of samples used per fitting interval. From the standpoint of economy in the airborne computer it is desirable to reduce the number of samples as much as is possible without deterioration in performance. Fig. 33 shows both the rigid body output response and the command error signal for four runs in which the number of samples per rigid body cycle is varied from 8 to 50. The response curves shown in Fig. 33 all contain a body bending oscillation of twice the closed-loop rigid body frequency and an initial amplitude of 0.2 times the command error signal. The response with both 25 and 50 samples is good, and very little difference may be noted between these runs. A moderate departure in the response may be noted when 12 samples are used, and a substantial departure may be noted when only 8 samples are used.

It may be concluded that the number of samples per closed-loop rigid body cycle can be held to approximately 12 if necessary, although a greater number of samples is desirable if computation time is available in the computer.

The most dramatic feature of the Digital Adaptive Filter is its capability to separate the predominant rigid body mode from the bending mode even when the two are equal in frequency. This condition is illustrated in Fig. 34.

Remark: The Digital Adaptive Filter scheme is an ingenious and powerful method for removing parasitic signals in a control system. It is severely limited (at least as far as application to launch vehicle autopilots is concerned) by the fact that its ability to respond to disturbance (wind) inputs is questionable. In Ref. 6 the combined command and disturbance inputs have been simulated and the performance appears to be adequate. However, no simulation results with a pure disturbance input are shown. As a matter of fact, NASA engineers, with access to an as yet unpublished study on this problem, reported that[2]

> "This method appears to be feasible only when the component of the gimbal input signal, due to the command inputs, dominates the component due to the disturbances, and the commands are of a specified form. Since wind disturbances grossly override command inputs from the guidance system, the digital adaptive filter does not appear to be applicable for launch-vehicle uses."

Thus while the Digital Adaptive Filter system has provided an elegant solution to the main problem, its application to launch vehicle autopilots is frustrated by difficulties that present no problem in conventional approaches. Whether some bright control engineer will be blessed with new insight to revitalize this method remains to be seen.

3.4 NOTCH FILTER METHODS

A simple and highly effective way to gain stabilize the bending modes in a feedback control system is to employ notch filters whose resonant frequencies are set equal to the bending mode frequencies. There are two fundamental difficulties in this approach; namely the bending mode frequencies are not known a priori with sufficient accuracy, and they vary with flight time due to variation in vehicle inertial properties.

It would appear that if one could track the bending mode frequencies automatically during flight and use this information to vary the resonant frequency of a notch filter accordingly, the problem would be solved. This approach has indeed been studied extensively and the methods proposed differ only in the means whereby the bending mode frequencies are identified and in the manner of mechanizing the notch filter. The two most promising techniques are discussed below.

3.4.1 Spectral Identification Filter

Because of the elastic oscillatory motion of the vehicle, the control system sensors (angular displacement, rate, etc.) will contain signals at the bending mode frequencies in addition to those reflecting rigid body motion. The basic principle in the spectral identification method is that if the power spectral density of the sensor

output is measured, there will be peaks at the bending mode frequencies. The problem is then one of mechanizing some scheme whereby these peaks are identified, and using this information to set the notch filter resonant frequency. A schematic of the overall control system configuration is shown in Fig. 35. It is assumed that only the first three bending modes are significant, and therefore three notch filters are used. Note that by using two rate gyros (located at two different points along the vehicle) and subtracting their outputs, a signal is obtained which is free of rigid body information. Thus the input to the spectral filters consists only of bending mode signals. The output of the spectral filters (shown by the dotted lines in Fig. 35) is used to set the resonant frequency of the notch filters. The crucial element in this configuration is the spectral frequency identification system. This will now be examined in some detail.

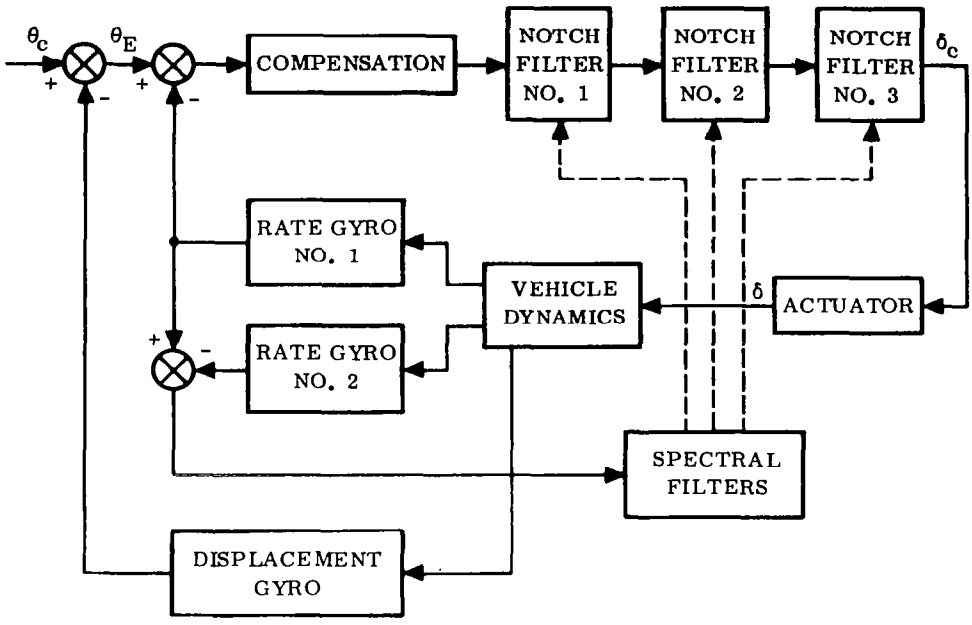

Figure 35. Spectral Identification Adaptive Control System

A typical input to the spectral filter will have the form shown in Fig. 36. This signal is, in general, nonperiodic so it cannot be represented as a summation of terms with discrete frequencies (Fourier series). In fact, f(t) contains components at all frequencies. To obtain a representation of f(t) as a function of frequency, ω, we may proceed as follows.†

Define a function $f_T(t)$ such that

$$f_T(t) = f(t) \ , \quad -\frac{T}{2} < t < \frac{T}{2} \quad = 0 \ \text{ otherwise} \tag{49}$$

† The mathematically sophisticated reader will recognize the following presentation as a heuristic development of the basic results of Fourier Integral theory.

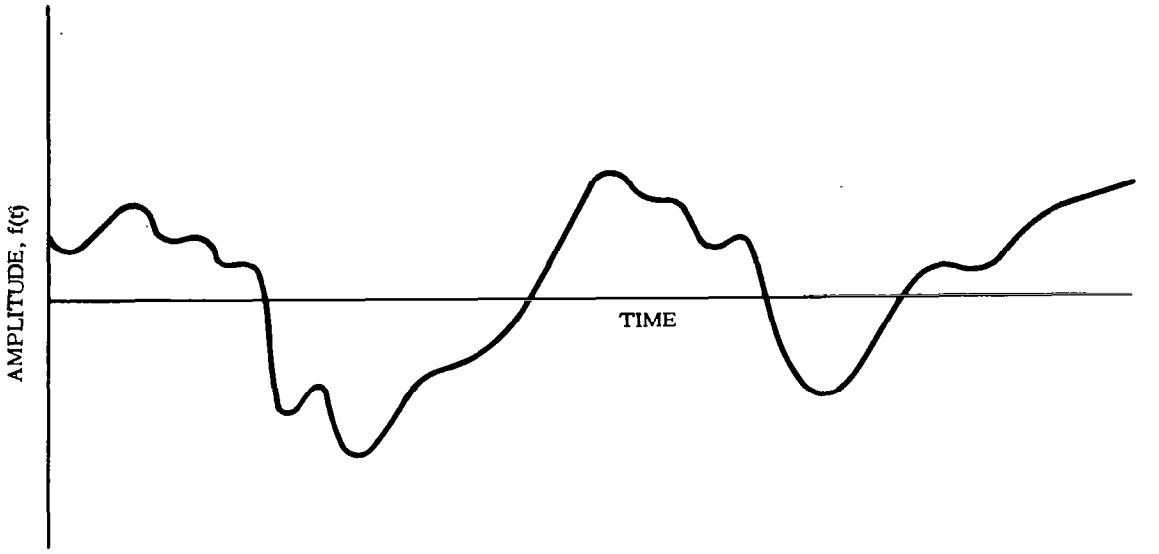

Figure 36. Typical Input to Spectral Filter

This function is illustrated in Fig. 37. If the graph of $f_T(t)$ is repeated every T seconds, we obtain a periodic function of period T, which is expressible as a Fourier series. It would appear plausible that as T is increased without limit, the Fourier series for $f_T(t)$ will approach that of f(t).

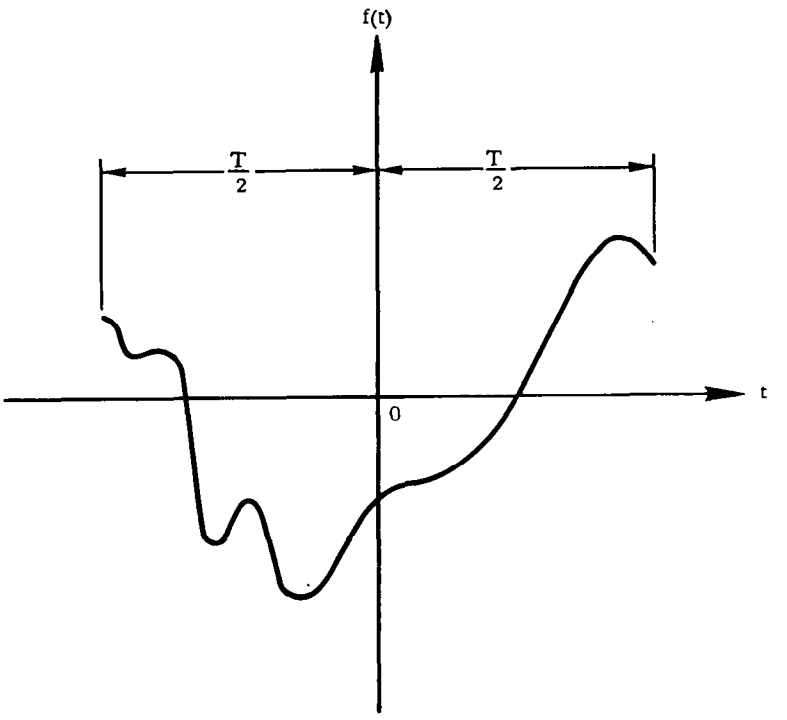

Figure 37. Truncated f(t) Curve

Since $f_T(t)$ has been prolonged as a periodic function, its Fourier series is obtained in the usual way, as follows.

$$f_T(t) = \frac{1}{2} a_0 + \sum_{n=1}^{\infty} \left(a_n \cos \frac{2\pi n}{T} t + b_n \sin \frac{2\pi n}{T} t \right) \tag{50}$$

where

$$a_n = \frac{2}{T} \int_{-\frac{T}{2}}^{\frac{T}{2}} f_T(t) \left(\cos \frac{2\pi n}{T} t \right) dt \tag{51}$$

$$b_n = \frac{2}{T} \int_{-\frac{T}{2}}^{\frac{T}{2}} f_T(t) \left(\sin \frac{2\pi n}{T} t \right) dt \tag{52}$$

If we let

$$A_n = \frac{T}{2} a_n \qquad B_n = \frac{T}{2} b_n$$

$$\omega_n = \frac{2\pi n}{T}$$

then the preceding relations become

$$f_T(t) = \frac{A_0}{T} + \frac{2}{T} \sum_{n=1}^{\infty} \left(A_n \cos \omega_n t + B_n \sin \omega_n t \right) \tag{53}$$

$$A_n = \int_{-\frac{T}{2}}^{\frac{T}{2}} f(t) \cos \omega_n t \, dt \tag{54}$$

$$B_n = \int_{-\frac{T}{2}}^{\frac{T}{2}} f(t) \sin \omega_n t \, dt \tag{55}$$

We now define the quantity

$$\Delta\omega_n = \omega_{n+1} - \omega_n$$

$$= \frac{2\pi(n+1)}{T} - \frac{2\pi n}{T}$$

$$= \frac{2\pi}{T}$$

By substituting this in (53), the latter becomes

$$f_T(t) = \frac{A_0}{T} + \frac{1}{\pi}\sum_{n=1}^{\infty}\left(A_n \cos\omega_n t + B_n \sin\omega_n t\right)\Delta\omega_n \tag{56}$$

However, since $\omega_0 = 0$, we may write

$$\frac{A_0}{T} = \frac{A_0\,\Delta\omega_0}{2\pi}$$

$$= \frac{A_0 \cos\omega_0 t}{2\pi}\,\Delta\omega_0$$

After adding and subtracting $\frac{A_0}{T}$ to Eq. (56) we obtain

$$f_T(t) = -\frac{A_0}{T} + \frac{1}{\pi}\sum_{n=0}^{\infty}\left(A_n \cos\omega_n t + B_n \sin\omega_n t\right)\Delta\omega_n \tag{57}$$

It seems reasonable to suppose that as T approaches infinity, the infinite summation above approaches an integral. This can indeed be established rigorously.† Equation (57) then takes the form

$$f(t) = \int_0^{\infty} A(\omega)\,(\cos\omega t)\,d\omega + \int_0^{\infty} B(\omega)\,(\sin\omega t)\,d\omega \tag{58}$$

†See any standard text on Fourier integrals.

where

$$A(\omega) = \frac{2}{\pi}\int_0^\infty f(t)\ (\cos \omega t)\ dt \tag{59}$$

$$B(\omega) = \frac{2}{\pi}\int_0^\infty f(t)\ (\sin \omega t)\ dt \tag{60}$$

Equation (58) is one form of the Fourier Integral. The functions $A(\omega)$ and $B(\omega)$ are the cosine and sine transforms, or Fourier transforms, of the function f(t).

Note that in a Fourier series we get contributions from integral values of $\frac{\omega t}{2\pi}$. In a Fourier integral there are contributions from every real value of ω.

For present purposes the importance of the representation (58) is that the total squared amplitude of f(t) at the frequency ω_k is

$$A^2\left(\omega_k\right) + B^2\left(\omega_k\right) \tag{61}$$

A spectral filter, tuned to ω_k, is merely a device that computes the quantity (61). In practice, the interval of integration in Eq. (59) and (60) is computed with sufficient accuracy for a time length equivalent to approximately five periods of the spectral tuned frequency ω_k.

For application to a control system configuration of the type shown in Fig. 35, 24 spectral filters were used to span the expected frequency range of the bending modes.[8] Because the spectral filter output amplitudes will be greatest when the tuned frequency of the spectral filter is near a bending frequency, the three tuned frequencies associated with the three spectral filters having the largest amplitudes are used to set the resonant frequencies of the three notch filters.

With 24 spectral filters in the system the rapid computation of the integrals (59) and (60) may impose excessive requirements on the airborne computer. In Ref. 8 the approximate values of $A(\omega)$ and $B(\omega)$ were computed by replacing the sine and cosine functions by a square wave of amplitudes +1 and -1, with the sign change occurring when the respective sine or cosine functions changed sign. This resulted in a significant reduction in computer complexity without markedly impairing system performance. For a thorough analysis of the system the reader is referred to the Autonetics Technical Summary report[8].

Remark: The technical feasibility of the Spectral Identification Adaptive Control system has been established by extensive computer simulation. Applied to a launch vehicle of the Saturn class, the computer requirements are a memory capacity of approximately 2000 words (word length = 16 bits) and a 5-μsec add time.

It has been found that if a bending mode is well stabilized and its excitation is low, then the identification is poor. On the other hand, when the bending mode stability is poor, the bending energy is high and the bending frequencies are well identified by the spectral system. The performance variation is thus in the proper direction.

This same study[8] also noted that the third-mode identification was, in general, poorer than either the first- or the second-mode identification. This was attributed to several possible causes:

a. There is an attenuation of high frequencies due to system lags, and thus the third-mode energy is in general lower than the first- and second-mode energy.

b. The spectral filter accuracy decreases as the number of samples per tuned frequency period decreases, thus the accuracy of the higher-frequency spectral filters is not as high as the lower-frequency spectral filters.

c. The actual frequency being identified is the closed-loop bending frequency, which may shift more radically for the third bending mode.

The general question of how close the lowest bending mode frequency can be to the rigid body frequency without having the notch filter phase lag deteriorate rigid body response to unacceptable proportions, has not been investigated.

3.4.2 Adaptive Tracking Filter

Instead of performing the frequency tracking and filtering functions separately, it is possible to mechanize a device that tracks the bending mode frequency continuously (instead of in discrete fashion as in Section 3.4.2) and sets the notch filter resonant frequency accordingly. This concept has been mechanized in various ways.[9-13]

The principle of operation of one type of frequency sensor may be described with reference to Fig. 38. For simplicity we assume that e_{in} is a sinusoid of the form

$$e_{in} = A \sin (\omega t + \alpha)$$

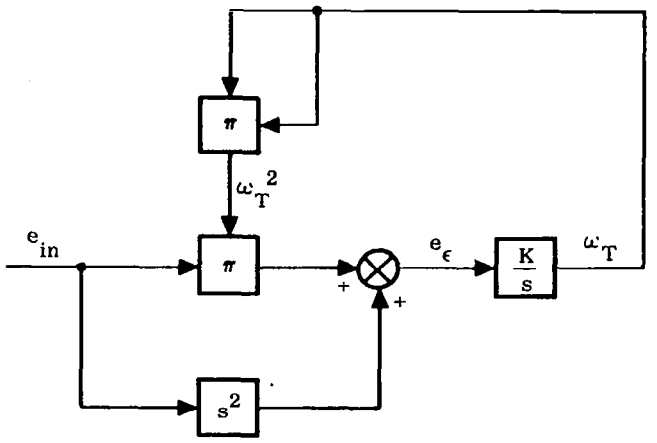

Figure 38. Frequency Sensor Principle of Operation

Consequently it satisfies the equation

$$\ddot{e}_{in} + \omega^2 e_{in} = 0$$

This suggests a type of feedback system of the form shown. If the output of the integrator is initially zero, a nonzero voltage will appear at the output of the summing junction. This in turn produces a voltage at the output of the integrator which causes $e_{in}\,\omega_T^2$ to be nonzero. When the null position is reached ($e_\epsilon = 0$), the output of the integrator, ω_T, is exactly equal to ω, the frequency of the input signal.

Of course the use of pure differentiation renders this scheme quite impractical. A usable form of this principle is shown in Fig. 39. Here the use of a double lag filter in conjunction with the differentiation limits the high-frequency (noise) amplification. An identical lag filter is used in the parallel loop to preserve the phase relationship. In this circuit it is assumed that the input signal e_{in} is composed of several sinusoids. A constant voltage ω_M is summed with the integrator output to assure that only signals whose frequency exceeds ω_M will be sensed. The function of the input filter is to assure that only that sinusoid of lowest frequency (greater than ω_M) is operated upon. This input filter has a transfer function of the form

$$\frac{e_1}{e_{in}} = \frac{\omega_T^2}{s^2 + 2\xi_T\,\omega_T\,s + \omega_T^2}$$

If the integrator output is initially zero, then $\omega_T = \omega_M$, and since e_ϵ is positive, ω_T increases. Denoting by ω_R the lowest frequency in e_{in} greater than ω_M, we see that when $\omega_T = \omega_R$ the output from this filter, denoted by e_2, will contain the

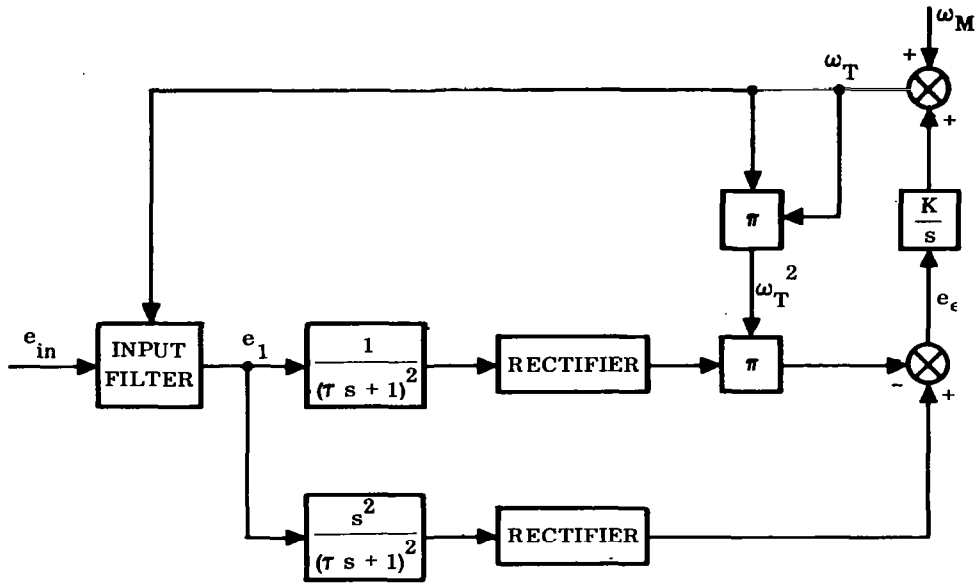

Figure 39. A Practical Frequency Tracker

signal of frequency ω_R highly amplified and all higher frequency signals sharply attenuated. Effectively then, e_1 will contain only the signal of frequency ω_R, and in the null state, ω_T will equal ω_R.

A simplified dynamic analysis of this scheme may be performed to obtain some crude estimates of performance quality. For this purpose we may neglect the influence of the input and double lag filters, in which case it is readily found that ω_T satisfies the equation

$$\dot{\omega}_T = K\left[|\ddot{e}_1| - \omega_T^2 |e_1|\right] \tag{62}$$

If it is assumed that e_1 is a sinusoid of the form

$$e_1 = A \sin \omega t$$

then it follows that

$$\frac{\dot{\omega}_T}{AK\,|\sin \omega t|} + \omega_T^2 = \omega^2 \tag{63}$$

Here A, K, and ω are positive constants. The solution of Eq. (63) is

$$\omega_T = \omega \left[\frac{\frac{\omega_0}{\omega} + \tan\beta}{1 + \frac{\omega_0}{\omega}\tan\beta} \right] \tag{64}$$

where

$$\omega_0 = \omega_T(0)$$

$$\beta = 2\,AK\left(n + \sin^2 \frac{\omega\, t_1}{2}\right)$$

$$t_1 = t - \frac{n\pi}{\omega}$$

$$n = \left\langle \frac{\omega\, t}{\pi} \right\rangle$$

and $\langle\ \rangle$ denotes the maximum integer of the argument; e.g., $\left\langle \frac{23}{4} \right\rangle = 5$.

It is noted that the system is inherently stable (in this simplified version). Furthermore, the manner in which the input signal amplitude, integrator gain, and initial setting of ω_T influence the speed with which ω_T approaches ω is indicated explicitly.

A means whereby the signal frequency is tracked and the notch filter resonant frequency set automatically is shown in the schematic of Fig. 40.

The demodulator is half wave and phase sensitive with a transistor switch performing the demodulation function. To describe the operation, we assume that e_{in} is composed of a single signal of fixed frequency. Now since e_{in}' and e_1 differ in phase only by the contribution of the $(K_T\, s^2 + 1)$ term, we see that e_{in}' is either in phase or 180° out of phase with e_1. Assuming that the resonant frequency of the notch filter is above the frequency of the input signal e_{in}, we note that e_{in}' and e_1 are in phase. Consequently, the demodulator output is positive, which in turn acts to increase K_T, thereby causing the resonant frequency of the notch filter to decrease. If the notch filter resonant frequency is below the input signal frequency, then e_{in}' and e_1 are 180° out of phase and the reverse occurs. When the two frequencies are equal then the phase difference between e_{in}' and e_1 is 90° and the average value of e_c is zero and e_K nulls to a fixed value that is a measure of the input signal frequency.

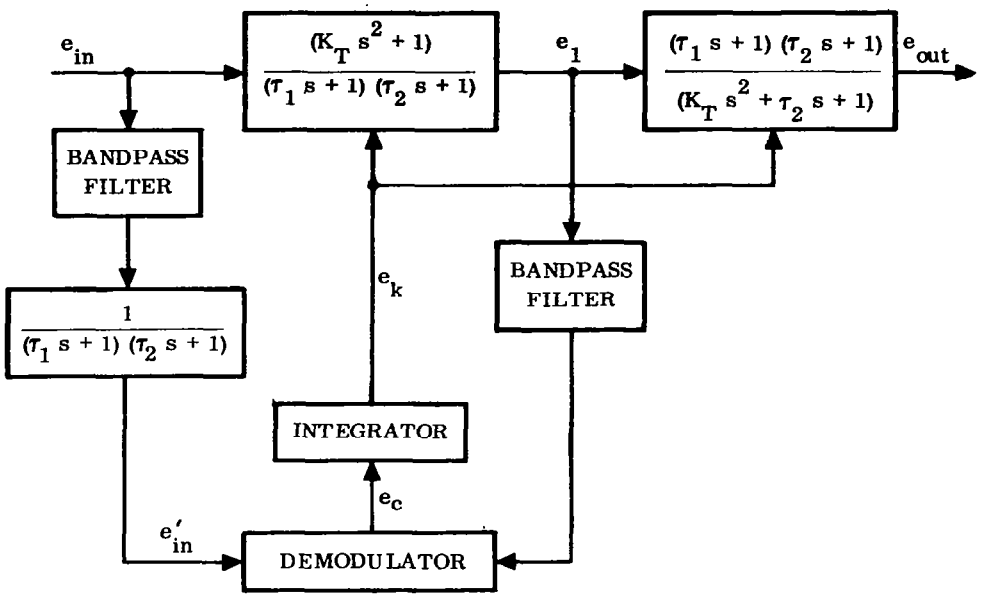

Figure 40. An Adaptive Tracking Notch Filter

It is easy to see that in the steady state, the overall transfer function is

$$\frac{e_1}{e_{in}} = \frac{K_T s^2 + 1}{K_T s^2 + \tau_2 s + 1}$$

where

$$K_T = \frac{1}{\omega_a^2}$$

$\omega_a \equiv$ frequency of input sinusoid, e_{in}

The bandpass filters have the transfer function

$$\frac{\tau_3^2 s^2}{(\tau_3 s + 1)^2}$$

These are designed to attenuate low-frequency (rigid body) signals. As a further precaution against tracking low-frequency signals, a lower limit may be set on the integrator output, thereby preventing the notch filter resonant frequency from tuning to a

rigid body frequency. Another means of ensuring that rigid body signals are not tracked is to feed the difference of two gyro signals into the unit, thereby effectively removing the rigid body content from the frequency tracking input.

Fig. 41 is a detailed schematic of the system shown in Fig. 40. The amplifier gain K was varied by using in the amplifier feedback loop a variable gain potentiometer driven by a servo motor whose input signal was the integrator output. This system, which was built as a breadboard model, is discussed in detail in Refs. 9 and 11. A typical result obtained with this unit is shown in Fig. 42.

The most extensive analysis to date of the tracking notch filter concept and its application to launch vehicle autopilots is the one by Cunningham and Schaeperkotter[14] which was performed in the course of a NASA-funded study. Included in this study were

a. Time required to track the frequency as a function of this frequency.

b. Tracking error.

c. Attainable notch attenuation.

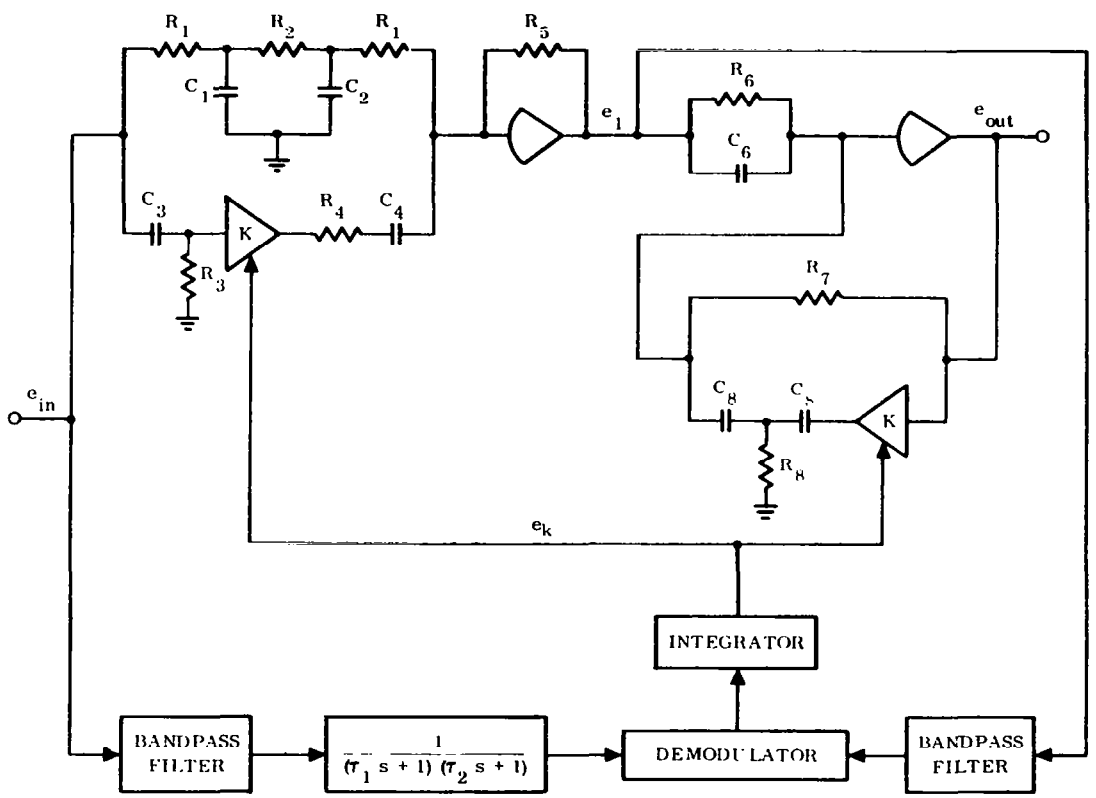

Figure 41. Schematic of Adaptive Tracking Notch Filter

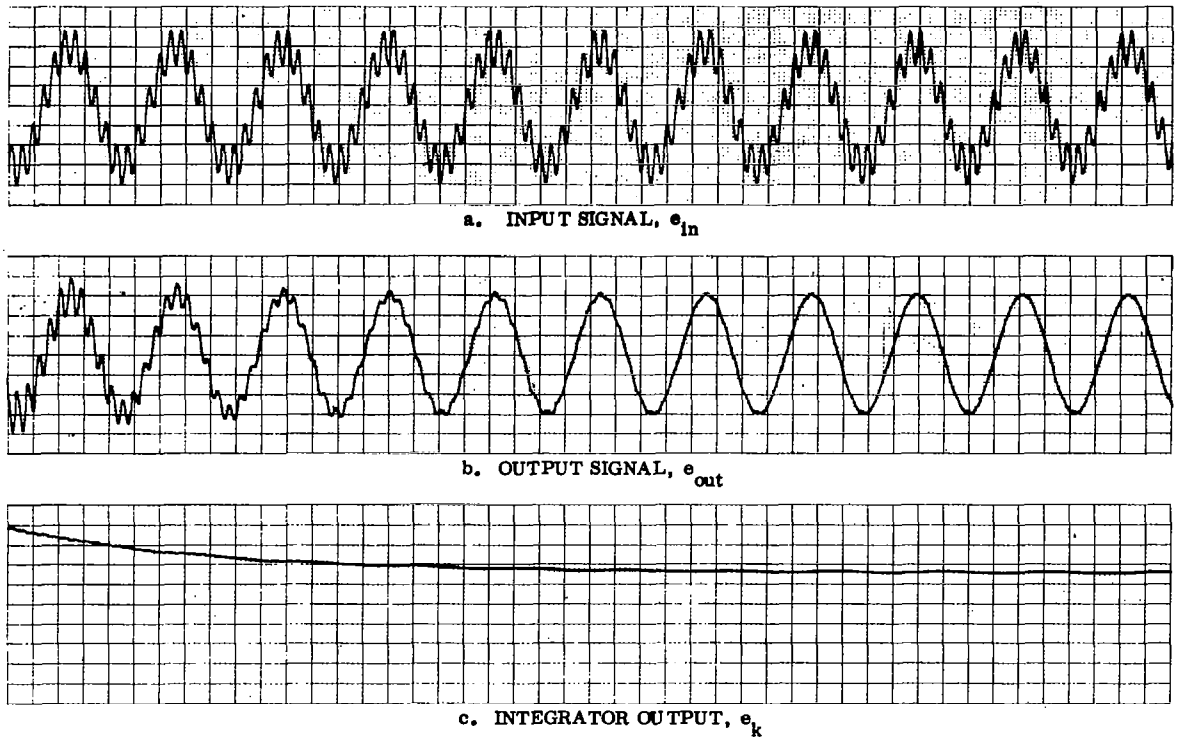

Figure 42. Typical Operation of Adaptive Tracking Filter

d. Demodulator properties.

e. Effect of higher harmonics.

f. Multiple frequency inputs.

The adaptive tracking filter analyzed by Cunningham and Schaeperkotter is shown in Fig. 43. This is a somewhat more generalized version than the types considered thus far, and has the capability for a variety of specialized operations. For a constant ω_p it is readily found that

$$\frac{e_{out}}{e_{in}} = \frac{\lambda_c s^2 + \lambda_b \omega_p s + \lambda_a \omega_p^2}{s^2 + 2\xi_p \omega_p s + \omega_p^2} \tag{65}$$

This has the general form of a complex lag-lead network. The important feature here is that after the bending mode frequency has been tracked, the filter may be used for phase stabilization of the bending mode rather than gain stabilization, which is achieved by the use of a notch filter.

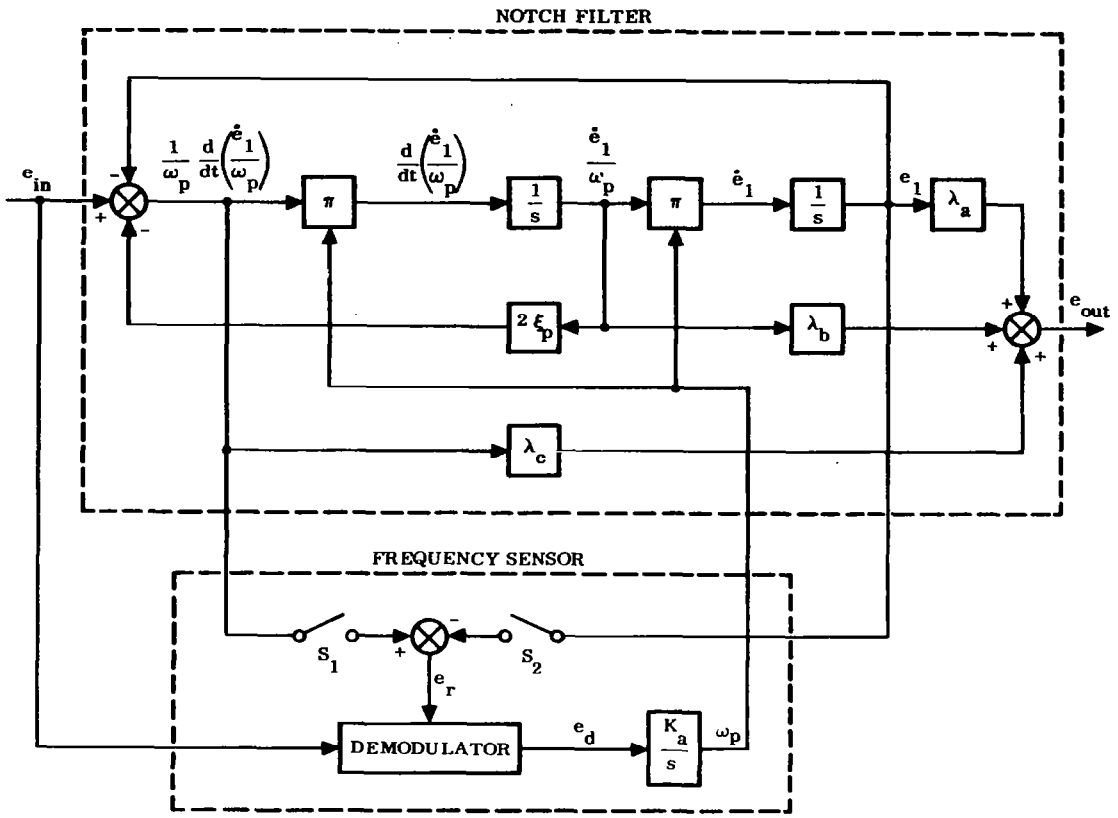

Figure 43. Schematic of Adaptive Tracking Filter

With phase stabilization the control system provides the proper gain and phase characteristics at the bending mode frequency to obtain a closed-loop damping of the mode greater than the open-loop damping. Gain stabilization, on the other hand, provides enough attenuation at the bending mode frequency to ensure system stability regardless of the bending mode phase. Depending on the specific application, one type may exhibit superior features over the other.

To use the configuration of Fig. 43 as a notch filter, we simply put $\lambda_b = 0$, and $\lambda_a = \lambda_c = 1$; viz.

$$\frac{e_{out}}{e_{in}} = \frac{s^2 + \omega_p^2}{s^2 + 2\xi_p \omega_p s + \omega_p^2} \tag{66}$$

Typical frequency response characteristics of the two types are shown in Figs. 44 and 45.

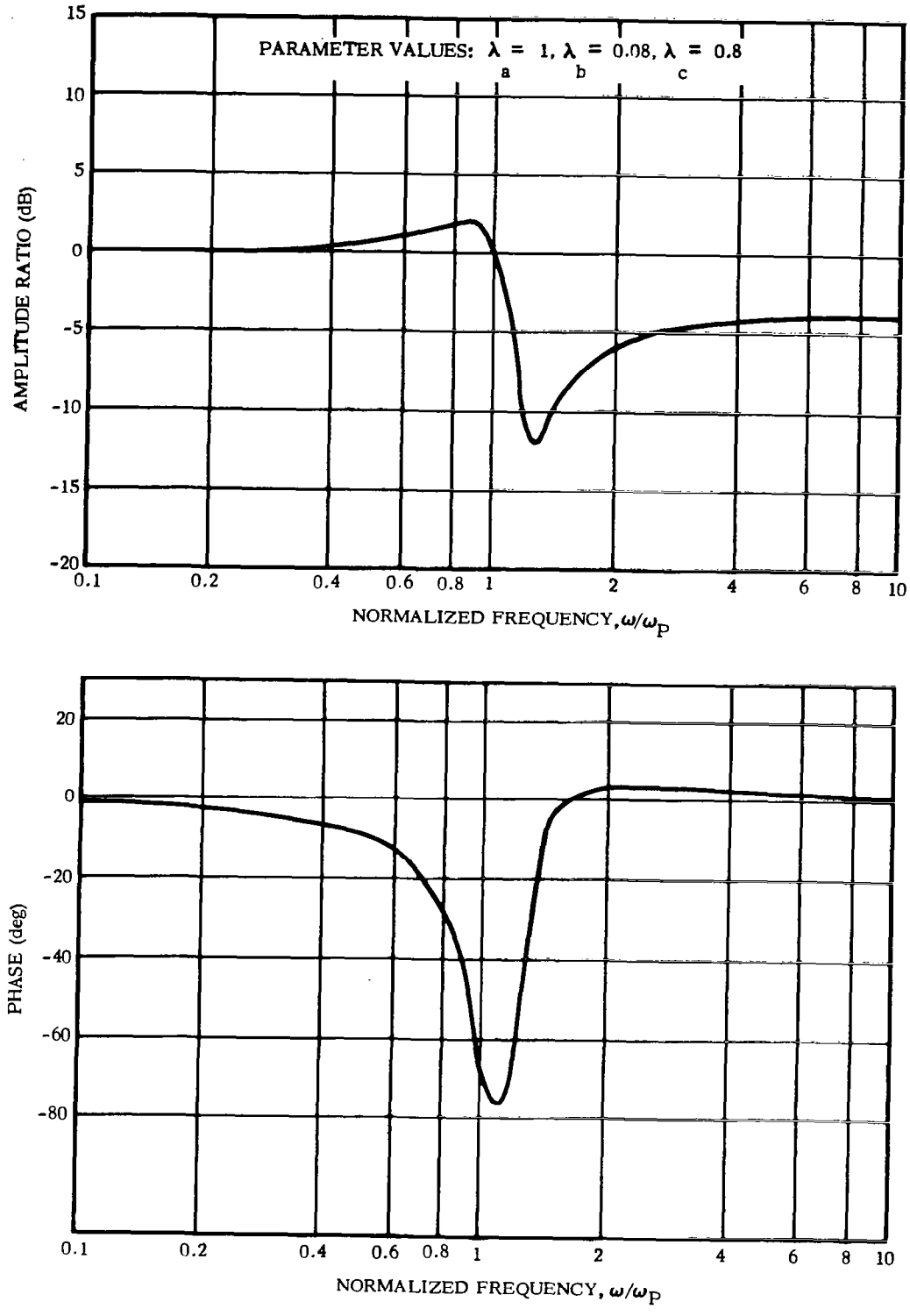

Figure 44. Frequency Response of Lag-Lead Filter, Eq. (65)

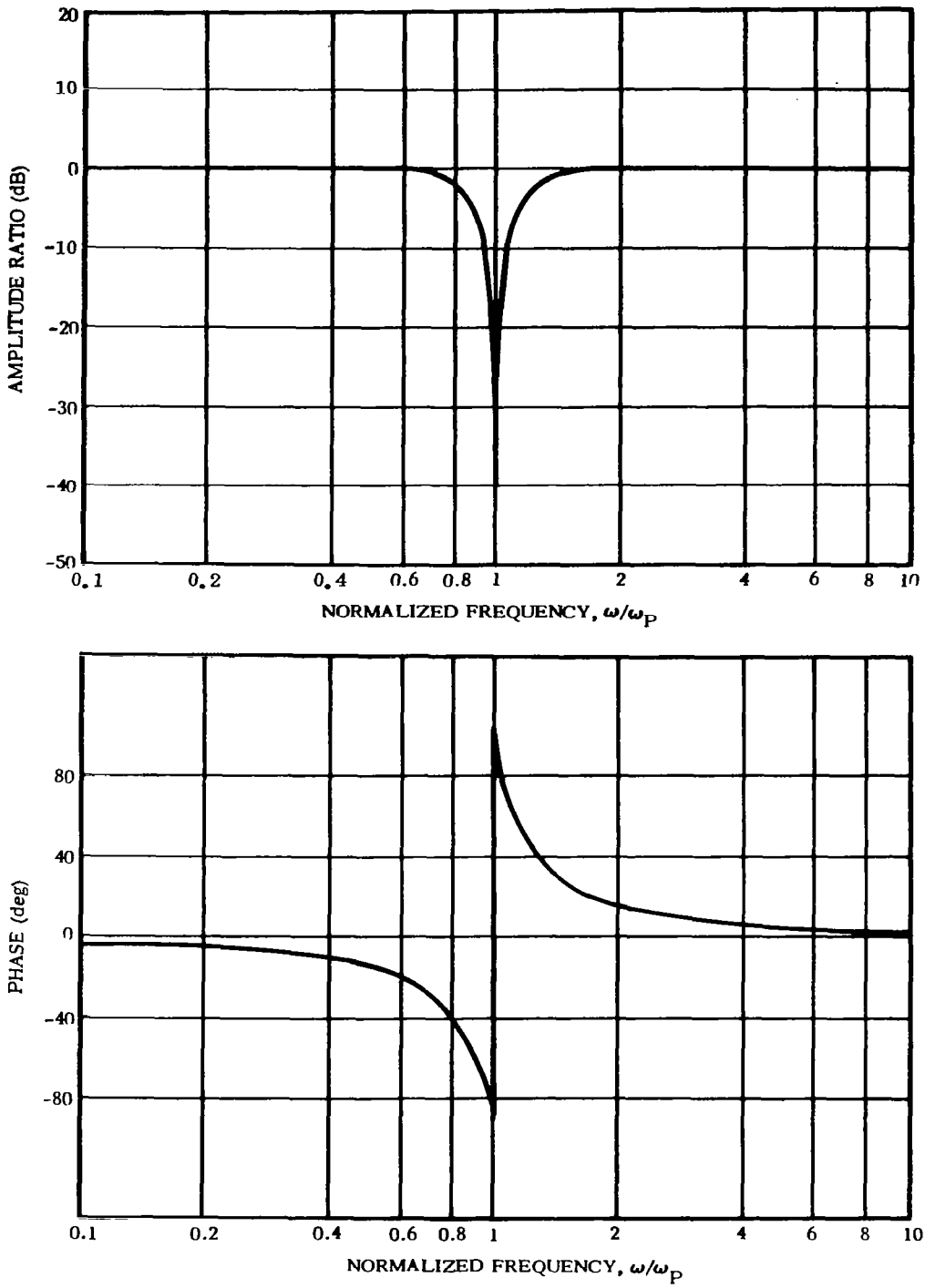

Figure 45. Frequency Response of Notch Filter, Eq. (66)

In the Frequency Sensor portion of Fig. 43 there exists the capability for three types of reference signal e_r for the demodulator, depending on the position of switches S_1 and S_2.

We designate these as follows:

CASE	SWITCH		TYPE
	S_1	S_2	
I	Closed	Open	High Pass
II	Open	Closed	Low Pass
III	Closed	Closed	All Pass

The respective e_r/e_{in} transfer function and frequency response characteristics are shown in Fig. 46. A selection of a particular type is determined by the specific application. For a launch vehicle autopilot the use of case I is indicated since it is desirable to filter out the rigid body and propellant slosh frequencies as much as possible.

It remains to examine the operation of the demodulator. We will investigate three types that are capable of detecting the phase angle between the input and reference signals. These are the multiplier, chopper, and double chopper demodulators.

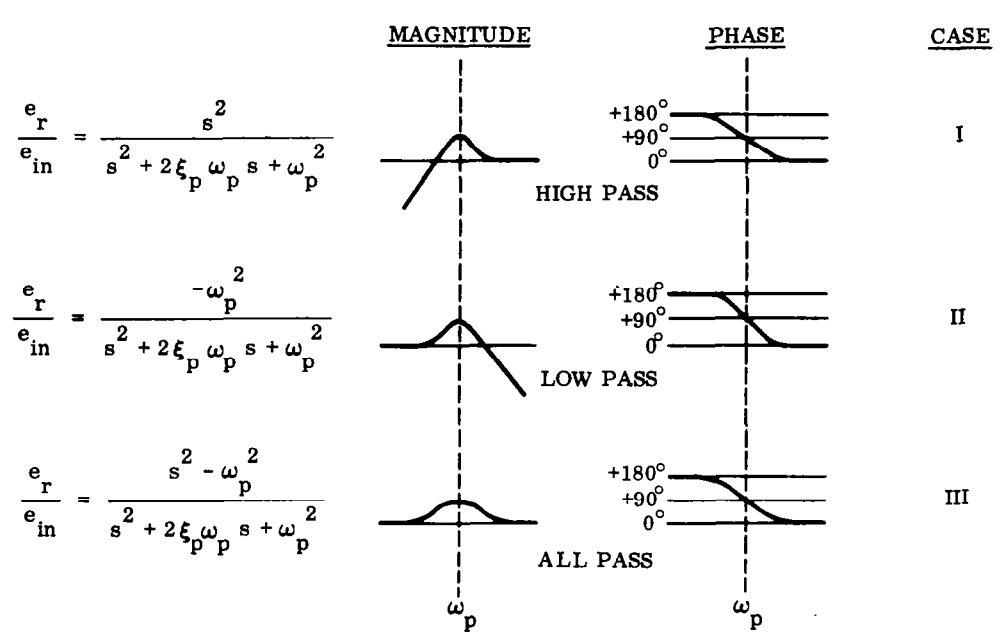

Figure 46. Reference/Input Signal Transfer Functions

For ease of exposition assume that the input signal contains a single frequency; viz.

$$e_{in} = A \sin \omega_a t \tag{67}$$

If $\omega_a > \omega_p$ an examination of Fig. 46 shows that the reference signal e_r leads the input by an angle φ that is between zero and 90 degrees. Therefore we write

$$e_r = C \sin\left(\omega_a t + \varphi\right) \tag{68}$$

$$0 < \varphi < 90^\circ$$

The output for each of the three types of demodulators is shown in Fig. 47. It is apparent that the average value of demodulator output e_d is positive in each case. For the multiplier type we have

$$e_d\Big|_{av} = \frac{1}{2\pi}\int_0^{2\pi} A\,C \sin \omega_a t \sin\left(\omega_a t + \varphi\right) d\left(\omega_a t\right)$$

$$= \frac{1}{2} A\,C \cos \varphi \tag{69}$$

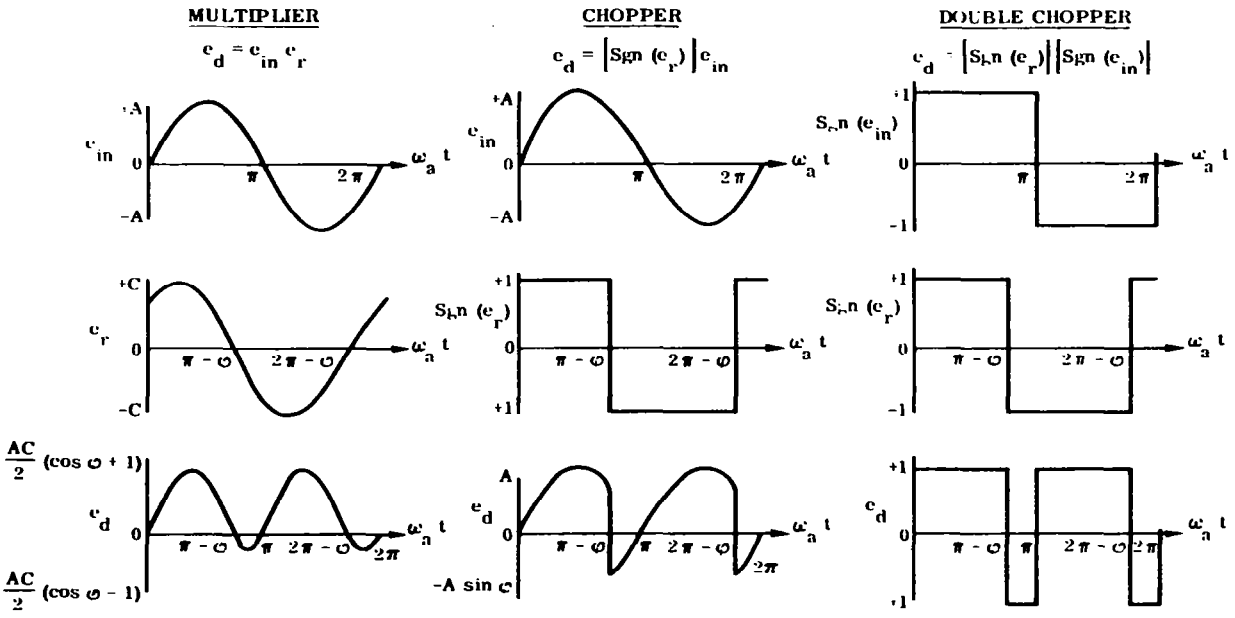

NOTES: 1. $e_{in} = A \sin(\omega_a t)$

2. $e_r = C \sin(\omega_a t + \varphi)$

3. ADAPTIVE TRACKING FILTER FREQUENCY BELOW INPUT FREQUENCY $(0 < \varphi < \frac{\pi}{2})$

Figure 47. Operation of Various Types of Demodulators

When $\omega_p = \omega_a$, that is, when $\varphi = 90^\circ$, we see that the average value of e_d is zero, indicating that in the steady state the resonant frequency of the filter is equal to the frequency of the input signal.

After expressing the output of the chopper demodulator in a Fourier series, the fundamental (d.c.) component is found to be

$$e_d\Big|_{\text{fund.}} = \frac{2A\cos\varphi}{\pi} \tag{70}$$

Similarly, for the double chopper type,

$$e_d\Big|_{\text{fund.}} = 1 - \frac{2\varphi}{\pi} \tag{71}$$

Thus in each case the average output of the demodulator is zero when $\varphi = 90^\circ$. The effect of higher harmonics is investigated in the Cunningham and Schaeperkotter report.

A similar analysis shows that when $\omega_a < \omega_p$ (and therefore e_r leads e_{in} by an angle φ such that $90^\circ < \varphi < 180^\circ$) the system tends to decrease ω_p and lead to the steady-state $\varphi = 90^\circ$ with $\omega_p = \omega_a$.

A schematic of the complete autopilot employing two adaptive tracking filters is shown in Fig. 48. Extensive simulation studies of this system as applied to the Saturn IB vehicle are contained in Ref. 14.

Remark: Many studies have shown that the adaptive tracking filter concept is feasible and practical. Among the objections that may be leveled against it are that the instrumentation is relatively complex and therefore involves a compromise with reliability. There are also lower limits in the ratio of allowable first bending mode to rigid body frequency. Nevertheless this approach is a prime candidate for adaptive control of highly flexible launch vehicles.

3.5 FREQUENCY-INDEPENDENT SIGNAL PROCESSING

The method to be described here is not, strictly speaking, an adaptive technique since it presupposes a knowledge of bending mode data, and all gains and compensation are designed a priori. It is, however, a novel solution to the problem of separating rigid body from bending mode signals, whatever the ratio of the respective frequencies. Unlike passive filtering methods the desired (rigid body) signal is generated free of any phase lag or attenuation and (theoretically) free of all parasitic modes. The method involves the use of "processing functions" and requires that the

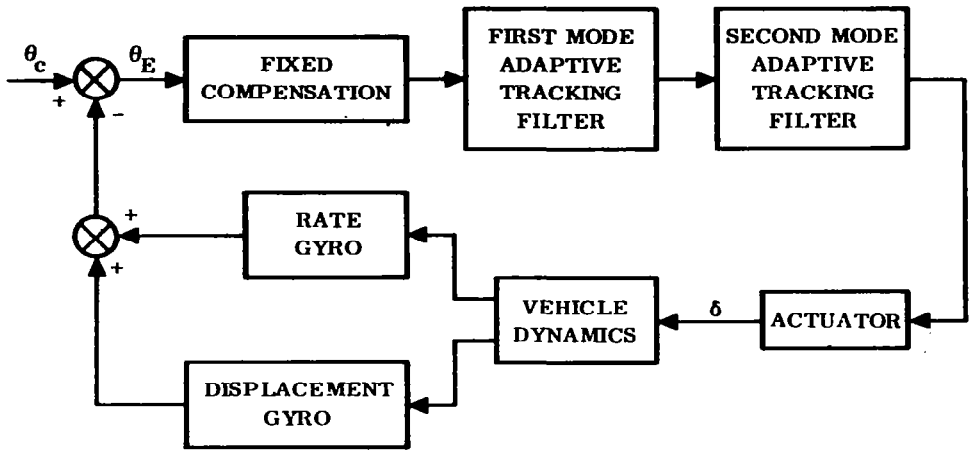

Figure 48. Control System Utilizing Adaptive Tracking Filters

number of sensing elements be equal to the number of modes of motion considered. Rejection of parasitic mode signals is accomplished by making the processing function associated with each sensing element a prescribed function of modal slopes or displacements.

The advantages of this method are its simplicity and the absence of any need for onboard computational capability. Since the modal data are assumed known, the processing functions may be precomputed and no further onboard computations are required. Also, because of the fact that the method does not rely on the relative frequencies of the closed-loop rigid body and elastic modes, the separation and rejection of bending motion are accomplished even in situations where a bending frequency coincides with a closed-loop rigid body frequency.

The main idea is due to Howard[15]. The ensuing discussion essentially parallels his presentation.

According to Eq. (A10) the displacement gyro output is

$$\theta = \theta_R + \sum_i \sigma_G^{(i)} q^{(i)}$$

For notational convenience in the following discussion we will write this as

$$\theta_i = \theta_R + \sum_{j=1}^{n} \sigma_{ij} q^{(i)} \tag{72}$$

where

θ_i ≡ output of displacement gyro located at station i along the vehicle

σ_{ij} ≡ the bending mode slope of the jth bending mode at location i

n ≡ number of bending modes

If there are n+1 gyros at n+1 locations, then from Eq. (72) we have

$$\begin{bmatrix} \theta_1 \\ \theta_2 \\ \vdots \\ \theta_n \\ \theta_{n+1} \end{bmatrix} = \begin{bmatrix} \sigma_{10} & \sigma_{11} & \cdots & \sigma_{1n} \\ \sigma_{20} & \sigma_{21} & \cdots & \sigma_{2n} \\ \vdots & \vdots & & \vdots \\ \sigma_{n0} & \sigma_{n1} & \cdots & \sigma_{nn} \\ \sigma_{n+1,0} & \sigma_{n+1,1} & \cdots & \sigma_{n+1,n} \end{bmatrix} \begin{bmatrix} \theta_R \\ q^{(1)} \\ q^{(2)} \\ \vdots \\ q^{(n)} \end{bmatrix} \tag{73}$$

where

σ_{i0} = 1 for i = 1, 2, ···, n+1

This may be expressed concisely in matrix notation as follows.

$$\Theta = \sigma q \tag{74}$$

Solving for the column vector q,

$$q = \sigma^{-1}\Theta \tag{75}$$

where

$$\sigma^{-1} = \frac{1}{D} \begin{bmatrix} \Sigma_{10} & \Sigma_{20} & \cdots & \Sigma_{n0} & \Sigma_{n+1,0} \\ \Sigma_{11} & \Sigma_{21} & \cdots & \Sigma_{n1} & \Sigma_{n+1,1} \\ \Sigma_{12} & \Sigma_{22} & \cdots & \Sigma_{n2} & \Sigma_{n+1,2} \\ \vdots & \vdots & & \vdots & \vdots \\ \Sigma_{1n} & \Sigma_{2n} & \cdots & \Sigma_{nn} & \Sigma_{n+1,n} \end{bmatrix} \tag{76}$$

$$D = \det[\sigma]$$

and Σ_{ij} is the cofactor of the element σ_{ij} in the matrix σ.

Eq. (75) gives the rigid body rotation θ_R and the n generalized coordinates $q^{(i)}$ as functions of the measured outputs from the n+1 sensors and the known modal data. In particular,

$$\theta_R = \frac{1}{D} \sum_{i=1}^{n+1} \Sigma_{i0} \theta_i \tag{77}$$

If we define

$$P_i(\sigma) = \frac{\Sigma_{i0}}{D} \tag{78}$$

then (77) may be written as

$$\theta_R = \sum_{i=1}^{n+1} P_i(\sigma) \theta_i \tag{79}$$

The quantity $P_i(\sigma)$ is called the attitude processing function, which is a function of the modal data only (assumed known). Consequently, if n bending modes are significant, then the use of n+1 sensors, together with the known attitude processing functions, $P_i(\sigma)$, is sufficient to generate the rigid body rotation signal θ_R free of all bending mode information.

A similar analysis for the rate gyros shows that

$$\dot{\theta}_R = \sum_{i=1}^{n+1} P_i(\sigma) \dot{\theta}_i \tag{80}$$

where $\dot{\theta}_i$ is the output of the rate gyro located at station i, and $P_i(\sigma)$ is as defined by (78).

In the case of n=2, for example (which presupposes that bending modes higher than the second may be neglected), we find that

$$\theta_R = \sum_{i=1}^{3} P_i(\sigma) \theta_i$$

where

$$P_1(\sigma) = \frac{\Sigma_{10}}{D} = \frac{1}{D}\left(\sigma_{21}\,\sigma_{32} - \sigma_{22}\,\sigma_{31}\right)$$

$$P_2(\sigma) = \frac{\Sigma_{20}}{D} = \frac{1}{D}\left(\sigma_{11}\,\sigma_{32} - \sigma_{12}\,\sigma_{31}\right)$$

$$P_3(\sigma) = \frac{\Sigma_{30}}{D} = \frac{1}{D}\left(\sigma_{11}\,\sigma_{22} - \sigma_{12}\,\sigma_{21}\right)$$

$$D = \left(\sigma_{21}\,\sigma_{32} - \sigma_{22}\,\sigma_{31}\right) - \left(\sigma_{11}\,\sigma_{32} - \sigma_{12}\,\sigma_{31}\right) + \left(\sigma_{11}\,\sigma_{22} - \sigma_{12}\,\sigma_{21}\right)$$

and similarly for the rate signals.

We see that the attitude processing functions are "gains" to be used with the gyro outputs (θ_1, θ_2, θ_3) to generate a signal free of bending mode information. The scheme is implemented in the manner shown in Fig. 49.

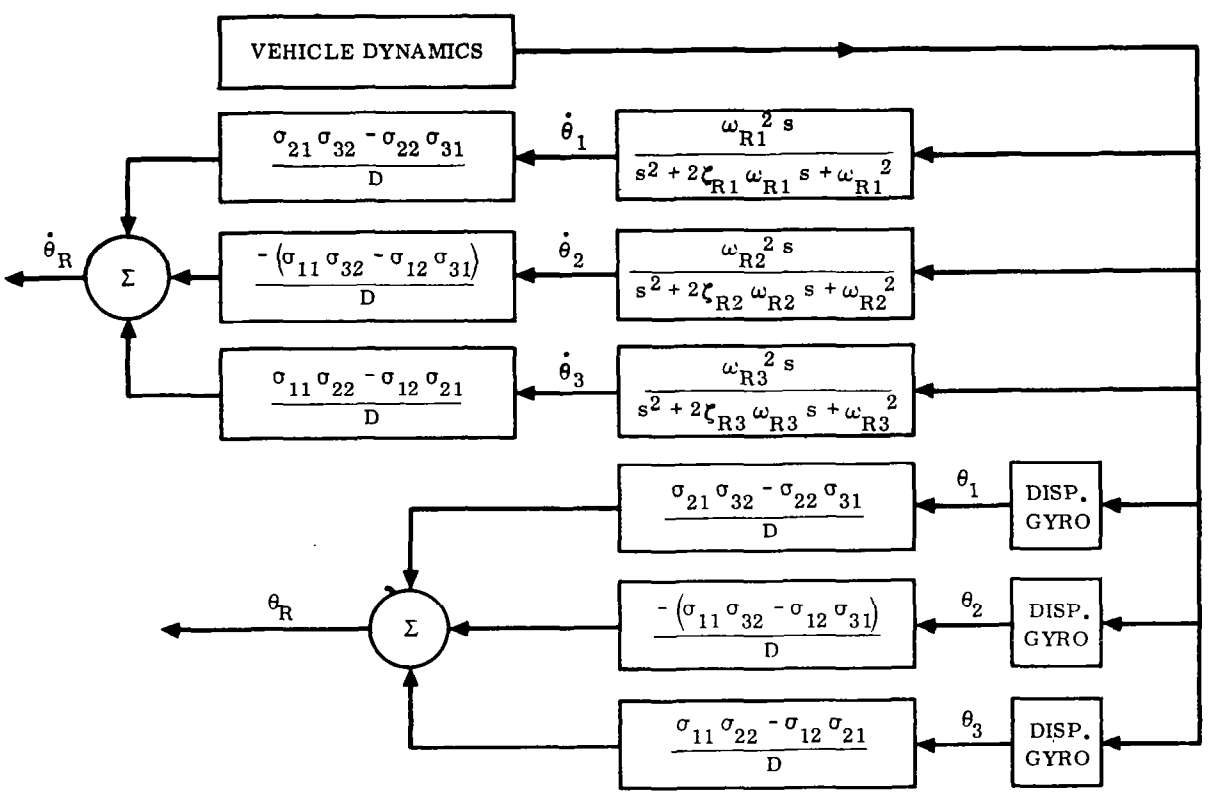

Figure 49. Block Diagram of System for Processing Attitude and Attitude Rate Signals

Remark: Subject to the stipulation that bending mode data are known, the above method is an elegant and attractive means of obtaining a theoretically perfect filtering of bending mode signals, which is in no way affected by the frequency separation between the desired and parasitic signals. Extra sensors are the only additional equipment required and there is no need for "exotic" signal processing.

In application to real vehicles there are two obvious limitations: 1) there are inherent limits in the accuracy of bending mode data, and 2) the bending mode properties vary with flight time due to varying inertial properties of the vehicle as fuel is expended.

Howard's study[15] includes an extensive investigation of the influence of errors in modal data on the closed-loop stability of the system. For a typical launch vehicle it was found that when the amplitude of the rigid body pitch attitude is greater than or equal to the amplitude of the bending motion at the nose of the vehicle, the error in the pitch attitude output will always be less than 16 percent if the modal slope errors do not exceed either +50% or -50%.

An analysis of the influence of modal errors on the stability of the closed-loop system indicated that certain combinations of modal errors tend to degrade stability of at least one of the bending modes, whereas other combinations of modal errors tend to enhance bending mode stability. For modal errors of 10% or less, and those combinations of modal errors that tend to degrade stability, no instability occurred in either mode when the loop was closed with nominal gain. The results indicate, however, that for the nominal range of gain considered, the first bending mode is more sensitive to errors in the modal data than the second and, presumably, higher bending modes.

It has been shown that when the error coefficients are positive, stability is maintained without degradation. This suggests that an attempt be made to bias the nominal value of the modal slopes in such a way as to ensure that the error coefficients are always positive. Examination of the tabulated data for a typical vehicle reveals that it is possible to do this for a range of modal error. This is equivalent to the use of structural feedback to stabilize the bending modes in the presence of errors in the modal data.

As far as the time-varying properties of the modal data are concerned, it would appear that gain switching in the attitude processing functions at preselected intervals would be a plausible solution. However, this must be investigated in detail for each particular vehicle.

4. REFERENCES

1. Greensite, A. — "Attitude Control During Launch," Design Criteria for Control of Space Vehicles, Vol. III, part 1, General Dynamics Convair Report No. GDC-DDE66-028, 5 August 1966.

2. Blair, J. C., Lovingood, J. A., and Geissler, E. D. — "Advanced Control Systems for Launch Vehicles," Astronautics and Aeronautics, August 1966, p. 30 - 39.

3. Lang, G., and Ham, J. M. — "Conditional Feedback Systems, - A New Approach to Feedback Controls," AIEE Trans., Vol. 74, July 1955.

4. Kezer, A., Hofmann, L. G., and Engel, A. G. — "Application of Model Reference Adaptive Control Techniques to Provide Improved Bending Response of Large Flexible Missiles," Sixth Symp. on Ballistic Missile and Space Tech., Academic Press, New York, 1961, p. 113 - 151.

5. Tutt, G. E., and Waymeyer, W. K. — "Model Feedback Applied to Flexible Booster Control," IRE Trans. on Automatic Control, May 1961, p. 135 - 142.

6. Zaborsky, J., Luedde, W. J., and Wendl, M. J. — "Control Through Digital Filtering by Signal Decomposition with Application to Highly Elastic Boosters," IEEE Trans. on Appl. and Ind., March 1964, p. 87 - 98.

7. Zaborsky, J., Luedde, W. J., and Wendl, M. J. — New Flight Control Techniques for a Highly Elastic Booster, ASD TR 61-231, September 1961.

8. Johnson, J. M., Crow, R. K., and Lutes, C. L. — Study of Structural Bending Adaptive Control Techniques for Large Launch Vehicles, Technical Summary Report, Contract No. NAS8-20056 (Autonetics, Inc.), 16 March 1966.

9. Greensite, A. — An Advanced Autopilot for Elastic Booster Vehicles, General Dynamics Convair Report No. ERR-AN-038, February 1961.

10. Smith, G. W. "Synthesis of a Self Adaptive Autopilot for a Large Elastic Booster," IRE Trans. on Automatic Control, Vol. AC-5, No. 3, August 1961, p. 229.

11. Greensite, A. "A Frequency Sensor and Roving Notch Filter for Control System Applications," Proc. Nat'l. Elec. Conf., Vol. 21, 1965, p. 558 - 563.

12. Gaylor, R., Schaeperkoetter, R. L., and Cunningham, D. C. "An Adaptive Tracking Filter for the Stabilization of Bending Modes in Flexible Vehicles," AIAA/JACC Guid. and Contr. Conf., Seattle, 1966, p. 441-447.

13. Hosenthien, H. H., and Borelli, M. T. An Adaptive Tracking Notch Filter for Suppression of Structural Bending Signals of Large Space Vehicles, NASA TM X-53000, 1 October 1963.

14. Cunningham, D. C., and Schaeperkoetter, R. L. Study of Applications of a Tracking Filter to Stabilize Large Flexible Launch Vehicles, Final Technical Report, Contract No. NAS8-20080 (Sperry Inc.), May 1966.

15. Howard, J. C. A Frequency Independent Technique for Extracting the Rigid Body Motion from the Total Motion of a Large Flexible Launch Vehicle, NASA TN D-3109, November 1965.

16. Greensite, A. "Short Period Dynamics," Design Criteria for Control of Space Vehicles, Vol. I, part 1, General Dynamics Convair Report No. GDC-DDE65-055, 1 October 1965.

17. Andeen, R. E. "Self Adaptive Autopilots," Space/Aeronautics, April 1965, p. 46 - 52.

18. Andeen, R. E. "Stabilizing Flexible Vehicles," Astronautics and Aeronautics, August 1964, p. 38 - 44.

19. Stear, E. B. "A Critical Look at Vehicle Control Techniques," Astronautics and Aerospace Eng., August 1963, p. 80 - 83.

20. Smyth, R. K., and Davis, J. C. "A Self Adaptive Control System for a Space Booster of the Saturn Class," Proc. JACC, 1962.

21. Andeen, R. E., and Shipley, P. P. "Digital Adaptive Flight Control System for Aerospace Vehicles," AIAA Journ., Vol. 1, No. 5, May 1963, p. 1105 - 1109.

22. Carney, R. "Design of a Digital Notch Filter with Tracking Requirements," IRE Trans. on Space Elec. and Telemetry, December 1963, p. 109 - 114.

23. Stear, E. B., and Gregory, P. C. "Capabilities and Limitations of Some Adaptive Techniques," Nat'l. Aerospace Elec. Conf., 1962, p. 644 - 660.

24. Smyth, R. K., DuPlessis, R. M., and Mattingly, L. K. "A Digital Self Adaptive Body Bending Filter for Flexible Airframe Control," Nat'l. Aerospace Elec. Conf., 1960, p. 369 - 376.

25. Prince, L. T. Design, Development, and Flight Research of an Experimental Adaptive Control Technique for Advanced Booster Systems, ASD-TDR-62-178, November 1962.

26. Mitchell, R. R. Rapid Identification of the Elastic Mode Frequencies of a Space Booster, General Dynamics Convair Report No. ERR-AN-499, 5 May 1964.

27. Lendaris, G. G. "The Identification of Linear Systems," AIEE Trans. on Appl. & Ind., September 1962, p. 231 - 240.

28. Roy, R., and Jenkins, K. W. Identification and Control of a Flexible Launch Vehicle, NASA CR-551, August 1966.

29. Lee, J. F. "A Digital Adaptive Flight Control System for Flexible Missiles," Seventh Symp. on Ballistic Missile and Space Tech., 1962, p. 115-147.

30. Whitaker, P. H. "Design Capabilities of Model Reference Adaptive Systems," Proc. Nat'l. Elec. Conf., Vol. 18, 1962, p. 241 - 249.

APPENDIX

VEHICLE DYNAMICS

The equations of motion and conventional control techniques for a launch vehicle are described in Refs. 1 and 16. For purposes of completeness, and pertinent to the needs of the present monograph, a simplified summary of the equations that describe the system dynamics are presented below.

$$\ddot{\theta}_R = \mu_c \delta + \mu_\alpha \alpha \tag{A1}$$

$$m\left(\dot{w} - U_0 \dot{\theta}_R\right) = T_c \delta - L_\alpha \alpha \tag{A2}$$

$$\left(s^2 + 2\xi_i \omega_i s + \omega_i^2\right) q^{(i)} = -\frac{T_c}{\mathfrak{M}_i} \delta \tag{A3}$$

$$i = 1, 2, \cdots$$

$$\left(s + K_c\right)\delta = K_c \delta_c \tag{A4}$$

$$s\,\delta_c = K_A\left(s + K_I\right)\theta_E \tag{A5}$$

$$\theta_E = \theta_C - \theta_F \tag{A6}$$

$$\alpha = \frac{w}{U_0} + \alpha_w \tag{A7}$$

$$\alpha_w = -\frac{w_w}{U_0} \tag{A8}$$

Rate gyro output

$$\dot{\theta} = \dot{\theta}_R + \sum_i \sigma_G^{(i)} \dot{q}^{(i)} \tag{A9}$$

Displacement gyro output

$$\theta = \theta_R + \sum_i \sigma_G^{(i)} q^{(i)} \tag{A10}$$

Bending displacement

$$u = \sum_i \varphi^{(i)}(\ell)\, q^{(i)}(t) \tag{A11}$$

The vehicle geometry and sign conventions are shown in Figs. A1 and A2. Typical normalized mode shapes are shown in Fig. A3. Nomenclature is defined as follows:

I = moment of inertia of vehicle about pitch axis

K_A = servoamplifier gain

K_c = engine servo gain

K_I = integrator gain

K_R = rate gyro gain

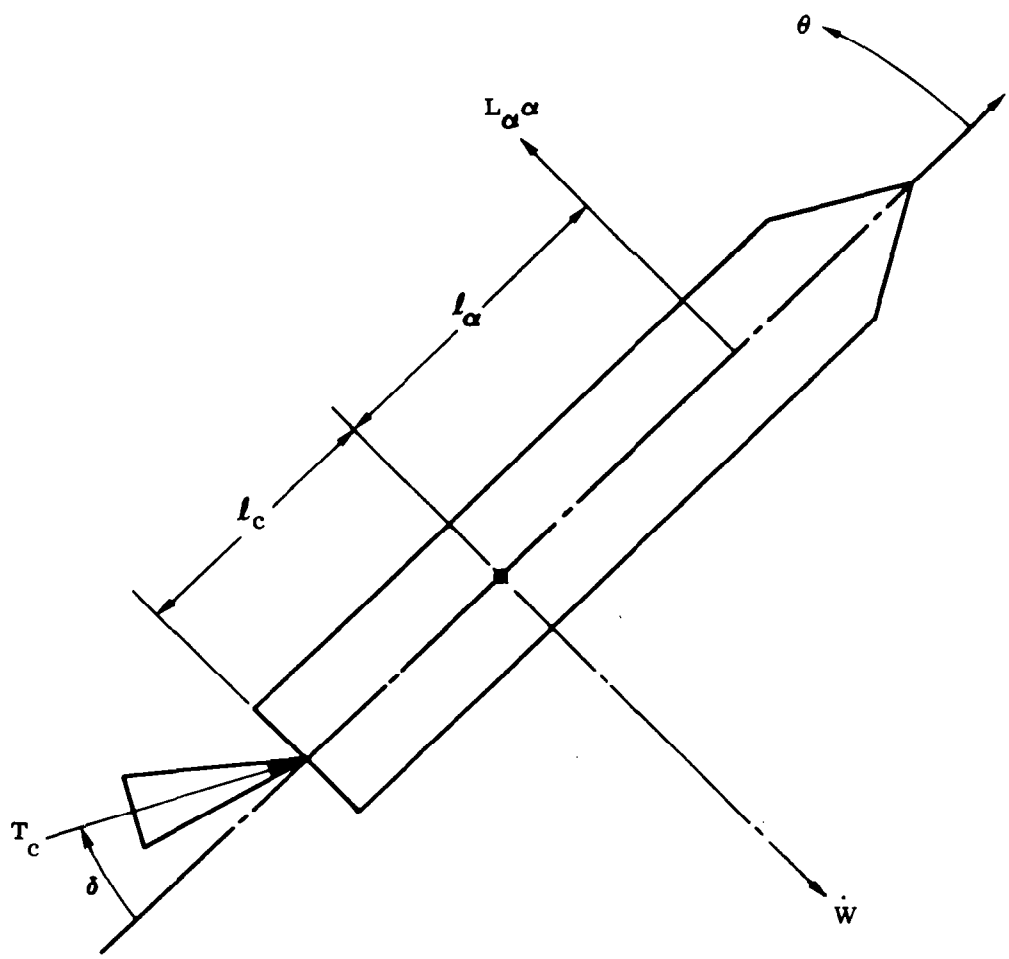

Figure A1. Vehicle Geometry

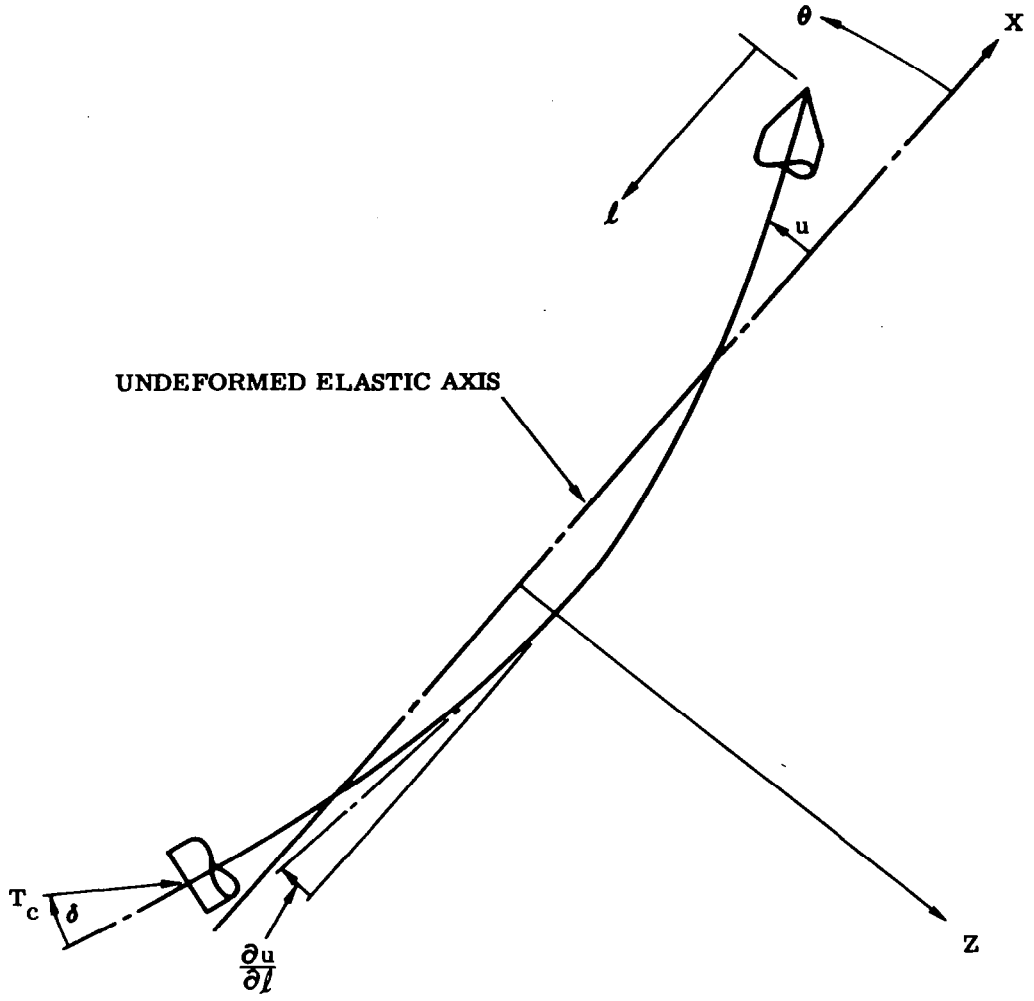

Figure A2. Sign Convention for Bending Parameters

ℓ = length parameter along vehicle; positive in aft direction

ℓ_c = distance from vehicle mass center to engine swivel point

ℓ_α = distance from vehicle mass center to center of pressure

L_α = aerodynamic load per unit angle of attack

m = mass of vehicle

$\mathfrak{M}_i$ = generalized mass of ith bending mode

$q^{(i)}$ = generalized coordinate of ith bending mode

s = Laplace operator

t = time

T_c = control thrust

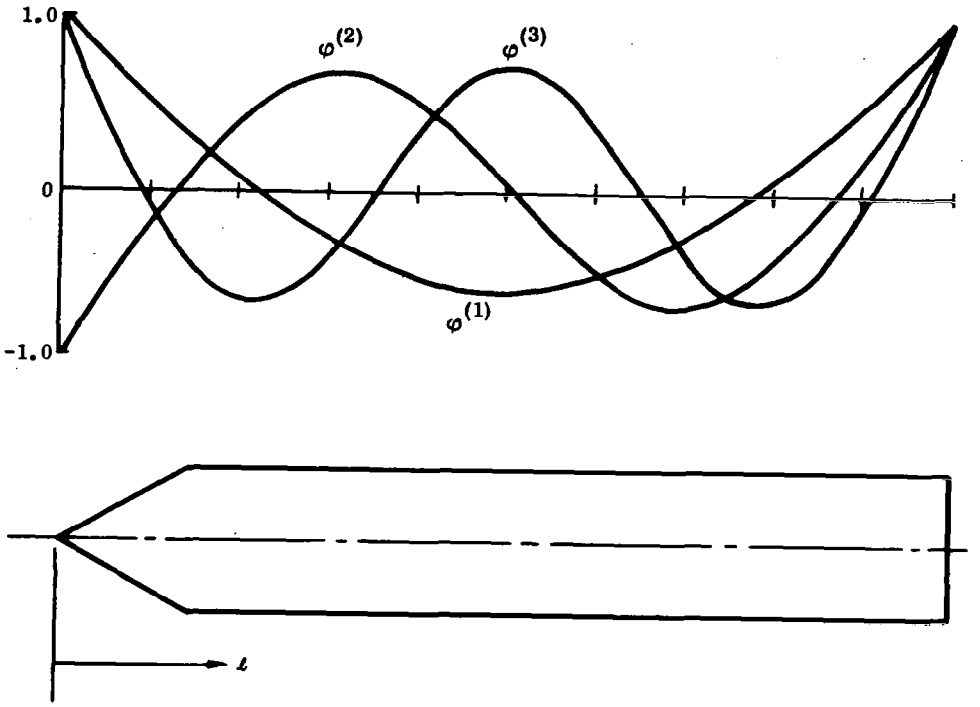

NOTES:

1. $\varphi^{(1)}$ is normalized to unity at engine gimbal point.
2. $\sigma^{(1)} = -\frac{\partial \varphi^{(1)}}{\partial \ell}$.

Figure A3. Typical Normalized Mode Shapes

u = bending deflection

U_0 = forward velocity of vehicle

w = normal velocity of vehicle

α = angle of attack

δ = rocket engine deflection angle

δ_c = command signal to rocket engine

θ_R = rigid body attitude angle

θ_E = error signal

θ_F = feedback signal

θ_c = command angle

μ_c = $T_c \ell_c / I$

μ_α = $L_\alpha \ell_\alpha / I$

$\sigma^{(i)}$ = negative slope of ith bending mode = $-\dfrac{\partial \varphi^{(i)}}{\partial \ell}$

$\sigma_G^{(i)} \equiv \sigma^{(i)}(\ell_G)$ = value of $\sigma^{(i)}$ at gyro location

$\varphi^{(i)}$ = normalized mode shape function for i^{th} bending mode

ξ_i, ω_i = relative damping factor and undamped natural frequency for: i^{th} bending mode

Sloshing and engine inertial effects have been neglected. The engine actuator has been represented by a simple first-order lag and the gyro dynamics have been neglected. This is a valid approximation for studying the lower-frequency elastic modes.

The above model is adequate for exhibiting the salient features of the adaptive methods considered in this monograph.

In studying the stability properties of the system one may also assume that

$$K_I \approx 0$$

and

$$\alpha \approx \theta_R$$

The definition of α given by Eq. (A7) is useful mainly in determining response to wind inputs.

"The aeronautical and space activities of the United States shall be conducted so as to contribute . . . to the expansion of human knowledge of phenomena in the atmosphere and space. The Administration shall provide for the widest practicable and appropriate dissemination of information concerning its activities and the results thereof."

—NATIONAL AERONAUTICS AND SPACE ACT OF 1958

NASA SCIENTIFIC AND TECHNICAL PUBLICATIONS

TECHNICAL REPORTS: Scientific and technical information considered important, complete, and a lasting contribution to existing knowledge.

TECHNICAL NOTES: Information less broad in scope but nevertheless of importance as a contribution to existing knowledge.

TECHNICAL MEMORANDUMS: Information receiving limited distribution because of preliminary data, security classification, or other reasons.

CONTRACTOR REPORTS: Scientific and technical information generated under a NASA contract or grant and considered an important contribution to existing knowledge.

TECHNICAL TRANSLATIONS: Information published in a foreign language considered to merit NASA distribution in English.

SPECIAL PUBLICATIONS: Information derived from or of value to NASA activities. Publications include conference proceedings, monographs, data compilations, handbooks, sourcebooks, and special bibliographies.

TECHNOLOGY UTILIZATION PUBLICATIONS: Information on technology used by NASA that may be of particular interest in commercial and other non-aerospace applications. Publications include Tech Briefs, Technology Utilization Reports and Notes, and Technology Surveys.

Details on the availability of these publications may be obtained from:

SCIENTIFIC AND TECHNICAL INFORMATION DIVISION

NATIONAL AERONAUTICS AND SPACE ADMINISTRATION

Washington, D.C. 20546